Republic of Iraq
Ministry of Higher Education
and Scientific Research
University of Babylon
College of Engineering
Civil Engineering Department

Mitigation Structures for Surface Wave, Case Study, Bahr Annajaf, Center of Iraq

A Thesis

Submitted to the College of Engineering / University of Babylon in Partial Fulfillment of the Requirements for the Degree of Doctor of Philosophy in Engineering / Civil Engineering / Water Recourses

By
Uday Abdul Sahib Mohammed Hassan Alturfi

Supervised By
Prof. Dr. Abdul-Hassan K. Al-Shukur

2023 A.D 1445 A.H

بِسْمِ اللَّهِ الرَّحْمَنِ الرَّحِيمِ

هوَ الَّذِي بَعَثَ فِي الأمِّيِّينَ رَسولا مِنْهمْ يَتْلو عَلَيْهِمْ آيَاتِهِ وَيزَكِّيهِم ْوَيعَلِّمهم الْكِتَابَ وَالْحِكْمَةَ وَإِنْ كَانوا مِنْ قَبْل لَفِي ضَلالٍ مبِينٍ

صدق الله العلي العظيم

{ الآية 2 من سورة الجمعة }

Dedication

To my God

To the prophet of mercy and humanity Mohammed

[Peace be upon him and his progeny]

To my Mother, my Family and Brothers

To my Lovely Wife

To my Friends

UDAY

2023

Supervisor Certification

I certify that this thesis titled " **Mitigation Structures for Surface Wave, Case Study, Bahr Annajaf, Center of Iraq** " which is being submitted by **Uday Abdul Sahib Alturfi** was prepared under my supervision at the University of Babylon as a partial fulfilment of the requirements for the degree of Doctor of Philosophy in Civil Engineering.

Signature:

Name: **Prof. Dr. Abdul-Hassan K. Al-Shukur**

(Supervisor)

Date: / / 2023

In view of the available recommendation, I forward this thesis for debate by the examining committee.

Signature:

Name: **Asst. Prof. Dr. Zaid Hameed Majed**

(Head of Civil Eng. Dept.)

Date: / / 2023

Examining Committee Certificate

We certify that we have read this thesis entitled "***Mitigation Structures for Surface Wave, Case Study, Bahr Annajaf, Center of Iraq***" presented by "***Uday Abdul Sahib Mohammed Hassan Alturfi***" and as an examining committee, we examined the student in its contents and in what is connected with it, and that in our opinion it meets standard of a thesis for the degree of Doctor of philosophy in Engineering / Civil Engineering / Water Resources.

Signature:
Name: ***Prof. Dr. Riyadh Z. Azzubaidi***
(Chairman)
Data: / / 2024

Signature:
Name: ***Asst. Prof. Dr. Riyadh Hamad Mohamed***
(Member)
Data: / / 2024

Signature:
Name: ***Prof. Dr. Nisren J. Al-Mansori***
(Member)
Data: / / 2024

Signature:
Name: ***Prof. Dr. Thair Jabbar Mizhir Alfatlawi***
(Member)
Data: / / 2024

Signature:
Name: ***Asst. Prof. Dr. Mohammed A. Almajeed A. Alabas***
(Member)
Data: / / 2024

Signature:
Name: ***Prof. Dr. Abdul-Hassan K. Al-Shukur***
(Member and Supervisor)
Data: / / 2024

Approved of Head of Department
Signature:
Name: ***Asst. Prof. Dr. Zaid Hameed Majeed***
Data: / / 2024

Approved of the Dean of College
Signature:
Name: ***Prof. Dr. Laith Ali Abdul-Rahaim***
Data: / / 2024

ACKNOWLEDGEMENT

"In the Name of Allah, the Most Gracious, the Most Merciful" Praise to Allah his Majesty before anything and after anything and to the prophet "Mohammed and Ahl-Al-Bait" for the strength, courage, and wisdom that Allah gave me to complete this humble work and lengthy journey.

I would like to express my deepest gratitude and respect to my thesis supervisor **Prof. Dr. Abdul-Hassan Kh. Al Shukur** . I am very grateful for his precious time spent and useful suggestions which provided valuable guidance and important role in the completion of the thesis as well as the moral support continued for the duration of the search, calling God richly rewarded him.

UDAY

2023

Abstract

In the spectrum of waves at sea, the waves induced by winds are the most obvious and usually the most important waves. Given the limited amount of knowledge on the mathematical modelling of the wind induced wave in lake or shallow water depth, considered to this point. The current study adopted a mathematical model to represent the waves generated by the wind in the Najaf sea depression and test the optimal place to choose a mitigation structure to disperse waves energy.

A numerical model based on unstructured mesh is proposed to predicate and visualize wave conditions. MIKE21 spectral model base on mass balance equation had been used as a numerical tool to find the optimal location of mitigation structures to dissipation the wave energy near the neighbor structures. The amount of variation between the simulated wave heights and those calculated using an empirical equation is less than 9%. Three schemes for breakwater were tested to find the optimal location and orientation of breakwater. The results showed that the three schemes used for the breakwater gave varying results, both depending on its location and characteristics. The first scheme gave a covering area approaching 1.19 km^2, and the second scheme gave approximately 0.889 km^2, and third scheme gave a covering area 1.11 km^2. The study showed that the wave heights at the upstream and downstream were measured after the breakwater had been constructed, and they were found to be between 0.35 and 0.7 m. This implies a decrease of around 40% to 60% in comparison to the original heights of 1.25 to 0.9 m. All of these schemes are good to a certain extent in dispersing the energy by breaking the single pattern of the wave at rates that may reach 50% of the height of the arriving wave, the first scenario was the best and most efficient in terms of energy dispersion.

Another part of research, hydraulic performance of the new shape of breakwaters was investigated through a laboratory study supported by a numerical mathematical model CFD to examine the different model shapes cross section depending on the transmissions wave coefficient Ct.

In order to stabilize the incident wave Hi with the same characteristics, waves were defined through the UDF file for CFD model. To investigate the performance of breakwaters base on energy dissipations, different models were tested under various wave condition, water depth, and relative submerged depth. Result of this study are showed that the transmission coefficient is increased with an increase of incident wave high for all type of breakwater model, and for all models of breakwater, transmission wave height (H_t) are increased with an increased relative submerged depth (Hs/Hi). The highest value for energy dissipations (1 - C_t) % are received for zero submerged depth in model of sloped steps model (M2) is 80 %. Ansys Fluent solver are adopted to modelling the transit flow condition with dynamic mesh to represent the flap motion type to generate wave. Numerical beach plays an important role in CFD model to prevent the reflection wave in lee side of breakwater and represent the absorbing shoreline. 240 grid per wave length are selected for mesh independent solution and make an acceptable comparison with an experiment.

Table of Content	
Subject	***Page***

List of Figures

List of Figures

List of Figures

List of Figures

List of Figures

List of Tables

List of Symbol

Symbol	Description
A	Area (L/2)
a	Amplitude Wave (L)
C	Wace Celerity or Speed (L/T)
Ct	Transmission coefficient
$D\omega$	Wave energy dissipation caused by breaking waves
Df	Bottom friction
E	Total Energy of Wave (L)
Fr	Froude Number
g	Acceleration of gravity (M/T^2)
H	Wave Height (L)
Hi	Incident wave (L)
Ht	Transmission wave (L)
H_O	Wave Height in Deep Water (L)
H_{rms}	Signifies the root-mean-square wave height. (L)
hc	Breakwater Height (L)
hs	Submerged depth (L)
K	Wave number
L	Length of wave (L)
P	Pressure field (F/L^2)
u	Velocity component in the X-direction(L/T)
v	Velocity component in the Y-direction(L/T)
w	Velocity component in the Z-direction(L/T)
t	Time (T)
μ	Dynamic Viscosity of water (ML/T2)
ρ	Density (M/L^3)
T	Period of wave (T)
ω	Dissipation per unit turbulence Kinetic Energy (L^2/T^3)
Vt	Turbulent Eddy Viscosity (L^2/T)
Δx	Distance (L)
Re	Reynolds number.
τ	Shear stress ($ML^{-1}T^{-2}$)

Symbol	Description
Kt	Transmission coefficient
η	Water elevation from static water level(L)
K	Wave number
ω	Angular wave frequency(T^{-1})
ζ_	Iribarren Fraction
θ_m	Mean wave direction
η	Water elevation from static water level(L)

Abbreviations

Symbol	Description
CFD	Computational Fluid Dynamic
GEBCO	General Bathymetric Chart of the Oceans and Wet Land
VOF	Volume of fraction
UDF	User Define Function (Fluent. ANSYS)
BISI	British Institute for the Study of Iraq
RANS	Reynolds-Averaged Navier-Stokes
M (1-5)	Model number marked (1-5)
MD (1-5)	Modified model number (1-5)
FDM	Finite Difference Method
FEM	FEM Finite Element Method
FVM	FVM Finite Volume Method
DEM	Digital Elevation Model
SWAT	Soil and Water Assessment Tools
SWL	Sea Water Level

Chapter One

Introduction

Chapter One

Introduction

1.1 Overview

Surface waves, are one of the most important natural phenomena that have been and still interest to researchers in marine science. The study of this subject is not easy at all, due to the complex formation of this phenomenon through the multiplicity of sources (wind, tides, and tsunami) generate waves, as well as the environment that contains them (bathymetry of region, fetch limit, prevailing winds and climate of region). The wind speed and duration are often the primary variables restricting wave development along open coasts. The fetch length is another factor that often limits wave generation for an enclosed body of water, such a small lake, reservoir or estuary, Figure (1.1).

In fact, it is possible to say that it is impossible to obtain a surface of water that is exposed to atmospheric pressure and that there are no waves on its surface. **(Dean and Dalrymple 1991)**

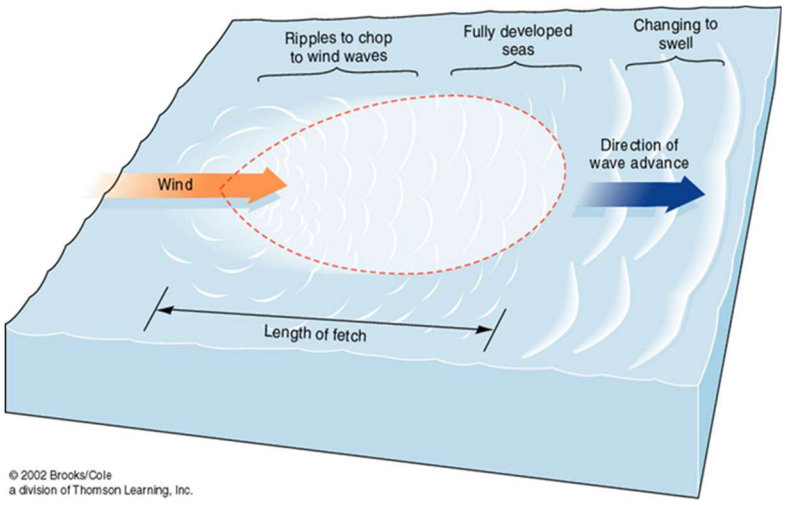

Figure (1.1) Basic definition of wave field **(Garrison, 2014)**

The wave movement may lead to damage to marine installations or buildings and roads adjacent to the borders of the sea or the ocean. Therefore, the boundary between land and water must be studied in deep because of its impact on the basic considerations for designing a facility adjacent to these areas. Because of this, it is challenging to represent system dynamics and phenomena along coasts using numerical models, making accurate wave model implementation necessary, **(Rusu, .2011).**

1.2 Description of Study Area (Depression Najaf-Sea)

One of Iraq's historic low water bodies is the Bahr Annajaf depression, figure (1.2). It is regarded as a natural lake and is situated in the southwest of the Al-Najaf city Centre. Due to influx, precipitation, and seasonal weather changes, that area fluctuated between increases and decreases of water level. The area is classified as a desert where water levels rise throughout the winter owing to increasing rainfall and wind speed in weather station near the region (**Omran, et al., 2014).**

Figure (1.2) Old map to Najaf sea dated back to 1885 (BISI Webinar)

The high-water level in the lake, in addition to the high wind speed recorded by the weather station (Shbicha Station), leads to the generation of waves of heights that may lead to damage to the coastal areas adjacent to the lake.

Figure (1.3), demonstrates some areas that are exposed to the influence of high spectral waves which leads to coastal erosion near Al-Maamel Street that classified as a commercially active area for transporting goods to the city of Najaf.

1.3. Computational Fluid Dynamic Model

Computational Fluid Dynamics **(CFD)** is a powerful tool for modeling the motion of liquids and gases which is used in many different applications, including wave modeling and marina applications. This technology was first used to model offshore waves in the 1980s. The aim was to improve our understanding of the interaction between water and air, and the effects interaction of waves on marine structures. CFD technology has been widely used in the marine and coastline to improve design performance and increase safety at near sea structures.

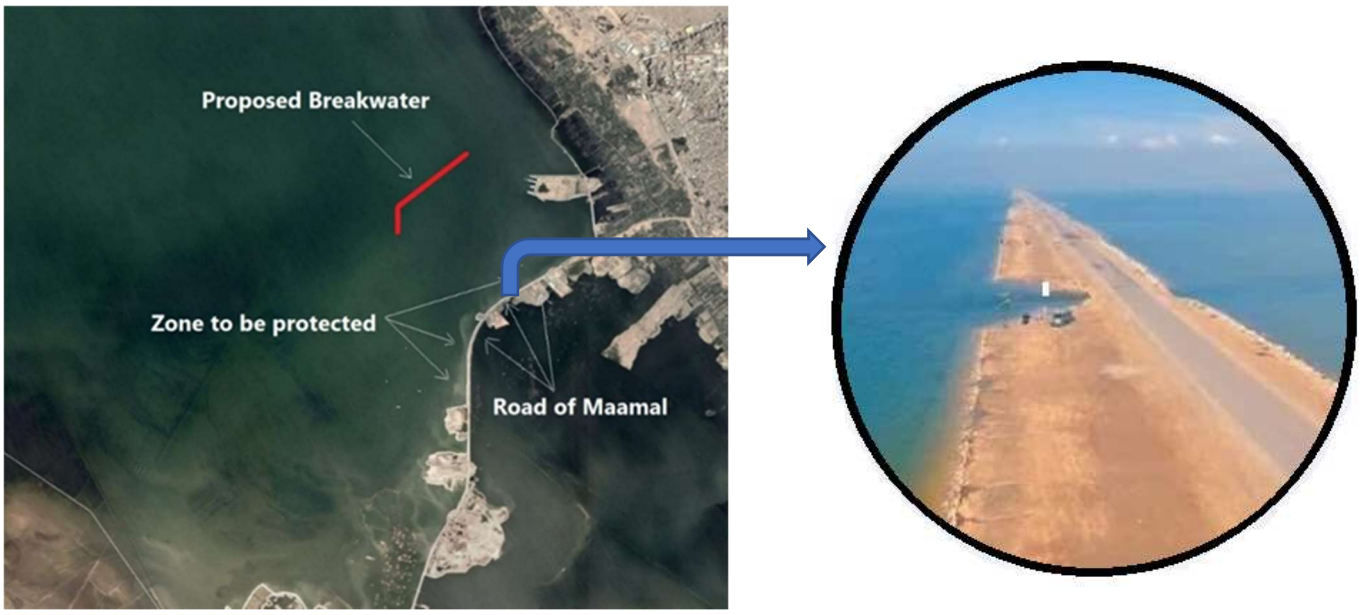

Figure (1.3) Selected region in study area shows damage causes by wind wave

In the current study, the CFD technique was adopted to model and analyze a mathematical model for study area (full-scale model) depression of Najaf sea, with reliance on bathymetry and winds field data for a period of not less than 30 years. Weather data close to the study area were collected from Shbicha gauge station.

The worst possible scenarios were represented by the highest wind speed (Return Period 10, 25, 50 years) recorded in order to design a mitigation structure (breakwater) that is able to dissipated the highest significant wave it could happen even once in 50 years. Physical model was prepared to examine the different breakwater cross section an addition to the adapted new shape (modified slopped steps breakwater).

1.4 Objective of Present Work:

The study intends to achieve the following main goal:

- Propose the optimum location of Breakwater according to many schemes tested based on worst conditions of spectral wave.

This objective is achieved through the following finding:

1. Build a mathematical full-scale model of depression Najaf-sea to study the wind induced waves for different conditions based on computational fluid dynamic model.
2. Build a Bathymetric map for study area and validated through measured data
3. Examine the CFD model through prepared experimental work for different cross section of breakwater.
4. Propose a new shape or compound Breakwater (modified slopped steps) model to investigate the performance on dissipations of wave energy in land side of Breakwater.

1.5 Assumption and Limitations

Some of limitations and assumption are adopted in present work:

- Spectral wind wave is the major sources for wave propagate of study reach
- Breakwater proposed with crest level identical with mean sea level
- The model is based on the solution of the 2-dimensional incompressible Reynolds averaged Navier-Stokes equations, subject to the assumptions of Boussinesq and of a hydrostatic pressure.
- Depth-induced breaking occurs when waves propagate into very shallow areas.

1.6 Methodology of thesis

The current thesis is organized into a total of seven chapters, with the introductory chapter being the first. **Chapter two** includes theories and literature review concern about wind induced wave modeling bases on wave transmission coefficients. **Chapter three** introduces experimental work to examine the performance of different breakwater shapes and validation of CFD model. **Chapter four** introduces of CFD modelling used in the current study (MIKE21 for large scale model and ANSYS Fluent for experimental simulation). **Chapter five** discusses the results of experimental and CFD model. **Chapter six** describes the study area (case study) depression of Annajaf sea and demonstrated the numerical model for implantation of case study for different scheme of breakwater location and proposes cross section. **Chapter seven** present the conclusions concern about wave water model and future work recommendations.

Chapter Two

Wave Principles and Literature Review

Chapter Two

Wave Principles and Literature Review

2.1 Introduction

In this part of study, the theoretical bases governing water wave, their types, and the causes of their occurrence will be discussed in a simplified manner. Since the topic is related to waves and their impact on the environment that incubates them. It is necessary to clearly refer to energy dispersal facilities (mitigation structures of various types) and touch on new methods in this topic and indicate what is important and needs to be studied deeply.

The other part of this chapter, will deal with the previous historical studies of the wave modeling, and on the other hand, will deal with the studies that concerned the calculation of the transmission Coefficient (C_t) of waves as an important criterion for determining the efficiency of dispersion installations of various types and functions of mitigation structures.

2.2 Waves

Waves represent a significant natural phenomenon that exerts its influence on coastal region. According to **(Krogstad and Arntsen ,2003)**, waves are characterized by variations in water elevation across both space and time, Figure (2.1).

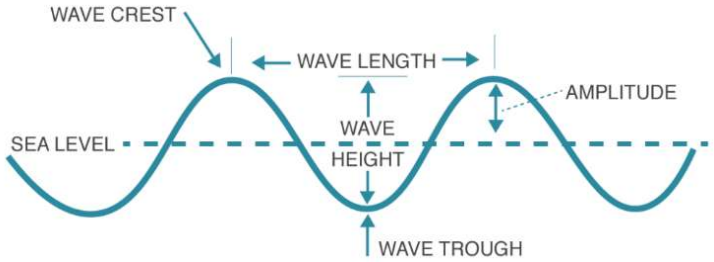

Figure (2.1) Basic parameters of wave, **Lin, P. (2008)**

Linear wave theory is the most basic method of explaining waves. According to **(Krogstad and Arntsen ,2003)**, linear wave theory involves a reduction in complexity where by waves are represented in a sinusoidal form, Equation (2.1).

$$\eta = \eta(x,t) = \frac{H}{2} cos(kx - \omega t) \quad \ldots\ldots\ldots\ldots (2.1)$$

Where: H represent height of wave, L length of wave, k employs the wave number, ω is the angular wave frequency, η is the water elevation from static water level, t represent time, and x employs the distance. Figure (2.2) shows liner wave parameters

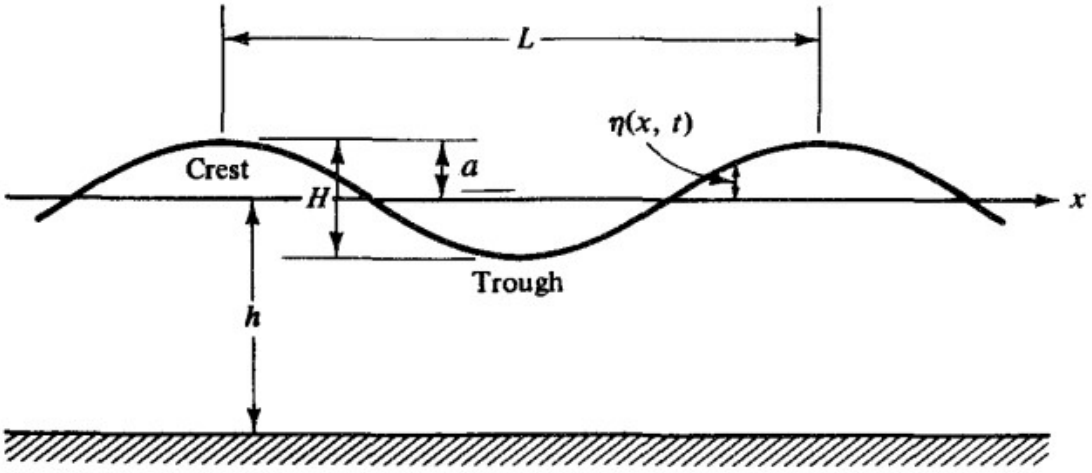

Figure (2.2) liner wave parameters **(Rafael et al ,2014)**

There are many distinct kinds of waves, including wind, tidal, tsunami, and other sorts. These waves are produced by several physical processes. Wind waves are the most prevalent form and are the wind created during a storm. Wind blowing across a region causes these kinds of waves to form. Fetch extent, speed of spectral winds, and duration represented the most effected factors that developed this type of wave characteristics, **(Kamphuis, 2020)**.

2.2.1 Wind Induced-Waves

Surface gravity waves, sometimes referred to as wind-generated waves, arise from the interaction between wind and the momentum of the water surface. According to **Roelvink and Reniers (2012)**, this momentum results from wind-induced pressure fluctuations on the water's surface. The conversion of wind energy into wave energy occurs as a result of the wind's influence. When the wind disappears, the waves will continue in their motion until they strike an obstruction or reach a region of reduced water depth, finally culminating in their arrival to the shoreline., Figure (2.3).

Wind induced-waves may reach huge size. The warship USS Ramapo observed significant wave activity during her Pacific Ocean trip in 1935, with wave heights reaching a reported value of 34 meters, **(Garrison,2014).**

2.2.2 Waves in deep and shallow water

Waves in the deep water are typically characterized by their irregularity and encompass a diverse range of height, lengths, and wave periods. Waves propagating in water with a depth that exceeds fifty percent their wavelength are often referred to as deep water waves, Figure (2.4).

The circumstances vary when it comes to wind-generated waves in proximity to the shoreline. The close closeness to the ocean floor causes the orbits of water molecules in shallow water waves to become more flattened. The water located just above the bottom lacks the ability to circulate in a circular trajectory, being limited to only forward and backward movements. Shallow-water waves refer to waves that occur in water with a depth less than 1/20 of their original wavelength, **(Garrison,2014).**

In a broad sense, it may be seen that wave energy tends to propagate at a more rapid rate across water when the wavelength is longer. The connection for deep-water waves may be expressed using the following formula:

$$C = L/T \qquad \text{…….…….. (2.2)}$$

C: Refer to wave speed (L/T), length of wave L, and T is time, or period (seconds).

The velocity of shallow-water waves may be mathematically expressed using an alternative equation.

$$C = \sqrt{gd} \quad \text{or} \quad C = 3.1\sqrt{d} \qquad \text{……. (2.3)}$$

Where: C is speed (in meters per second), g is the acceleration due to gravity, and d is the depth of the water (in meters) where wave is happening. **Lin, P. (2008)**

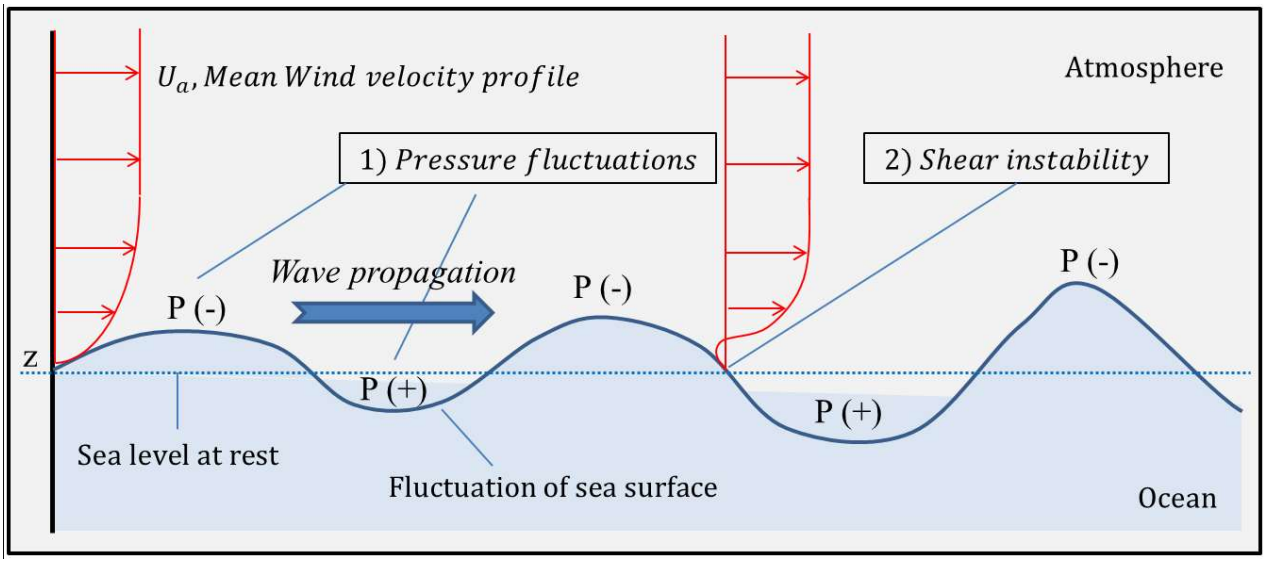

Figure (2.3) Pressure fluctuations of sea water surface. **Lin, P. (2008)**

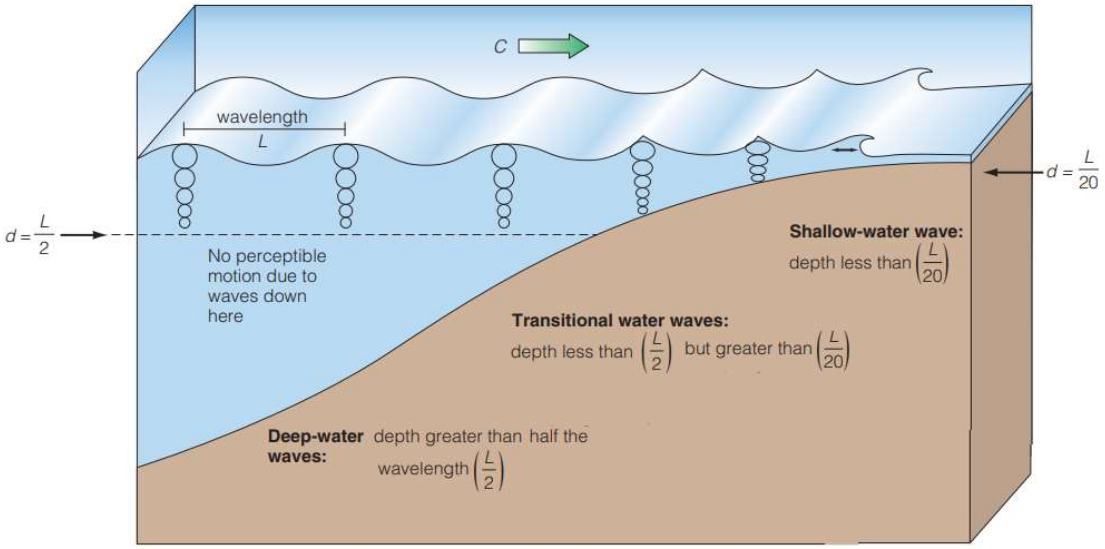

Figure (2.4) Classification of waves progressive depends on depth of water (**Garrison,2014**).

2.2.3 Factor developing wind waves

Three elements impact wind wave growth, energy transmission from air to sea requires the wind to be quicker than the wave crests, hence wind wave growth depends on wind speed, wind duration represent another factor. The fetch is the third component which represent the distance that the wind blows without changing direction, Figure (2.5).

2.2.4 Wind wave in closed region (Lakes)

As mentioned previously, the waves generated in open region are mainly controlled by the wind speed and its duration. As for closed region such as lakes and depressions, some considerations must present wave progressive that are restricted by length of fitch (L), Figure (2.6)

According to **Pickrill ,** findings in **1985**, it can be inferred that limited fetch environments have the ability to produce waves that are small, possess a short period and low energy. These waves are typically steeper and more erosive in nature. Due to their constrictive size, lakes are also unable to develop swell waves as there is not enough space for wave dispersion to occur across**. (Mathewson,2011)**

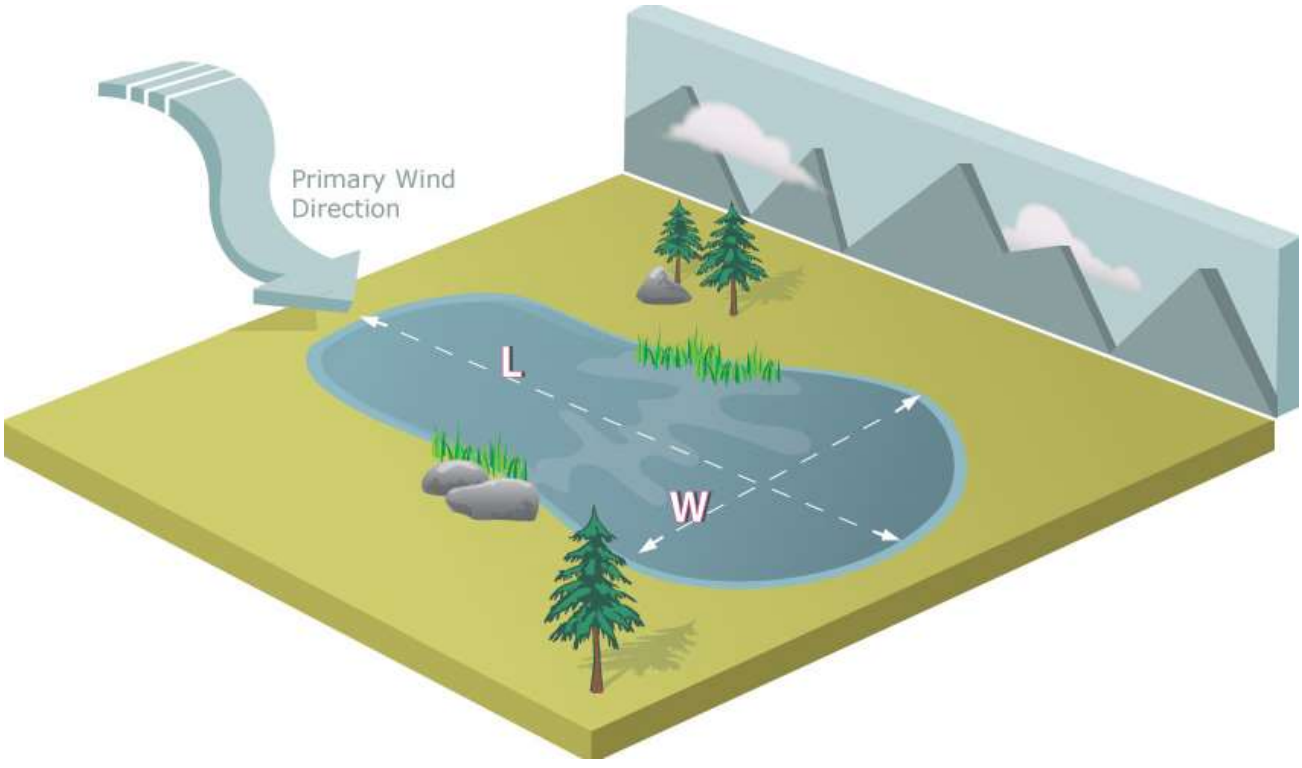

Figure (2.6) Sketch to visualized fetch length and direction in lake **(Garrison,2014).**

2.2.5 Seiche Phenomenon

The Seiche phenomenon was first studied in Switzerland's Lake Geneva by 18th-century researchers curious about the fluctuation of water levels near the extremities of elongated and narrow lakes in response to windstorms occurs periodically. The wave in question is often referred to as a standing wave due to its vertical oscillation without any noticeable horizontal displacement. The following **Figure (2.7)**, represent a graph of a seiche in Lake Erie. Strong westerly winds in November 2003 caused a Seiche with more than 4 meters (13 feet) of difference in water level from Toledo on the western end of the lake to Buffalo on the eastern end. **(Garrison,2014).**

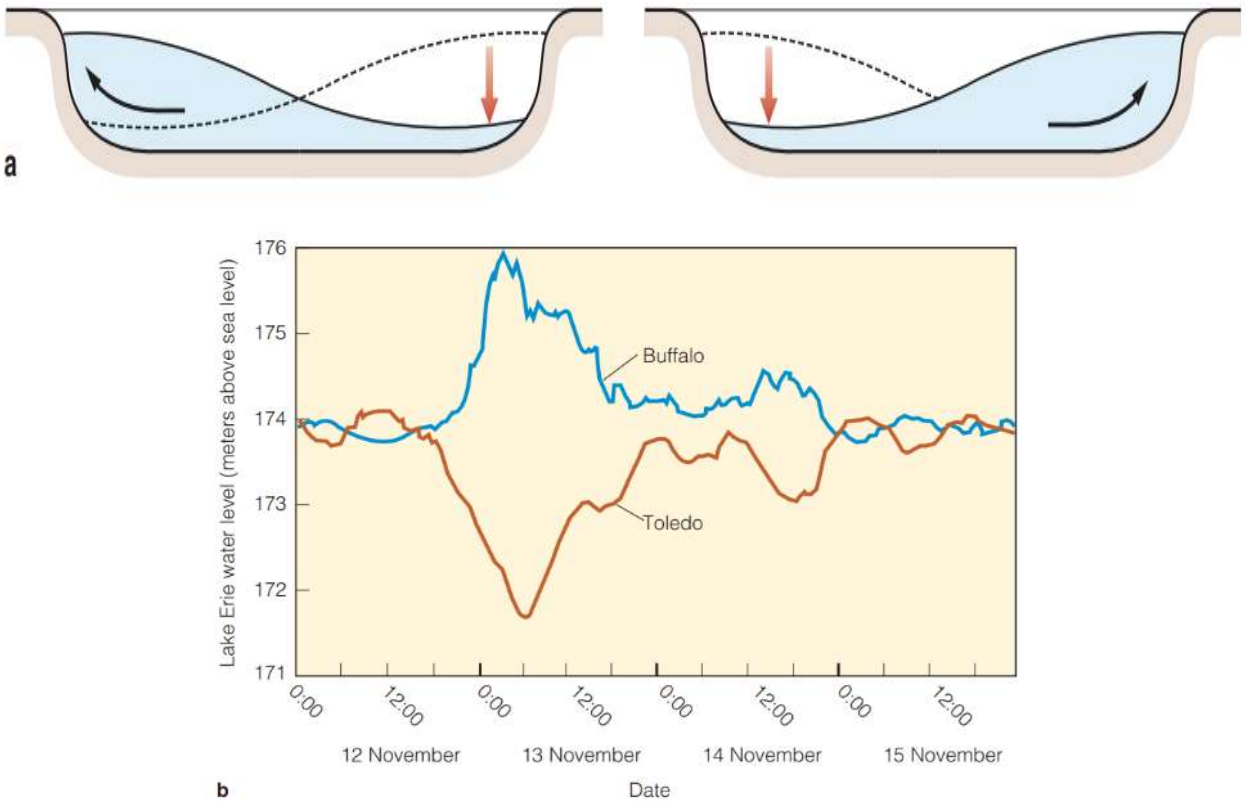

Figure (2.7) Water level fluctuation in Lake Erie cause by Seiche phenomenon. **Garrison, (2014).**

2.2.6 Spectral Description

Reliance on deterministic wave data representation, spectral description of wave climate is adopted. Spectral description uses statistical factors to indicate sea condition in a place. Upon observing an irregular sea, it can be observed that it is comprised of multiple sinusoidal waves exhibiting varying wave heights and wave periods. **(Krogstad and Arntsen, 2003).**

Equation (2.4) represents the water surface elevation resulting from the superposition of sinusoidal waves. The amplitude of each wave is represented by a_n, while wave parameters K_n and $\boldsymbol{\omega_n}$ are dependent on their respective period and wavelength.

$$\boldsymbol{\eta(x,t) = \sum_{i=1}^{N} a_n \cos\left(\omega_n t_{-k_n x-\emptyset n}\right)} \quad \ldots\ldots. (2.4)$$

The equation (2.4) can presented in term of energy in equation (2.5) below

$$\boldsymbol{E = \rho g \ _{Var}(\eta) = \int_k \psi(k)\, d^2 k} \quad \ldots\ldots (2.5)$$

The determination of the wave spectrum necessitates the consideration of the wave energy E, which is denoted as in equation (2.5). The variables in the equation are as follows: ρ denotes the density of water, g represents the force of gravity, η signifies the surface elevation, and Ψ pertains to the density of waves that correspond to different values of k, where k is equal to 2π/L. The aforementioned equation is attributed to, (**Krogstad and Arntsen 2003).**

The energy spectrum can be determined by Equation (2.5), wherein the energy is a function of the frequency. The frequency of a wave is influenced upon both its wavelength and amplitude. Long and high amplitude waves are associated with

lower frequencies, whereas short and small amplitude waves are associated with higher frequency concentration in the spectrum.

2.2.7 Wave Energy

Wave energy is a significant factor that affects coastal environments. Coastal processes are a result of the energy generated by waves and the cumulative impact of wave energy on the shoreline.

Equations 2.6 and 2.7, as presented by **Kamphuis (2010)** , Roelvink **and Reniers (2012)** respectively refer to the energy conservation equation and its application in the context of waves.

$$\Delta \cdot (ECg) = 0 \quad \text{..... (2.6)}$$

$$\frac{\partial E_\omega}{\partial t} + \frac{\partial}{\partial x}(E_\omega C_\omega \cos(\theta m)) + \frac{\partial}{\partial y}(E_\omega Cg \sin(\theta_m)) = -D_\omega - D_f \quad \text{..... (2.7)}$$

$$E_\omega = \frac{1}{8}\rho g H_{rms}^2 \quad \text{..... (2.8)}$$

Equation (2.7) is related to the wave energy, denoted as $E\omega$, and its dependence on H_{rms} as demonstrated in Equation (2.8). The energy velocity is represented by Cg, while θ_m denotes the mean wave direction. Additionally, $D\omega$ signifies the wave energy dissipation caused by breaking waves, and Df represents the bottom friction. The energy, $E\omega$, is expressed in Equation (2.8), where ρ denotes the water density, g represents gravity, and H_{rms} signifies the root-mean-square wave height.

2.2.8 Wave Transformation

The waves that develop from an offshore location exhibit weakly non-linear behavior and can be adequately characterized using linear wave theory due to their weakly non-linear nature. When waves are subject to nonlinear properties, alternative theories must be employed and the characteristics of the waves undergo

modification. This phenomenon is commonly referred to as wave transformation. The equations of wave transformation demonstrate changes in the behavior of waves, which can be attributed to the principle of energy conservation in waves **(Kamphuis, 2010).** The principle of energy conservation is involved in modifying the direction of waves as described by the wave propagation equation presented in equation (2.8).

$$\nabla \times k = 0 \quad \text{..... (2.9)}$$

$$\nabla \cdot (ECg) = 0 \quad \text{..... (2.10)}$$

K: represent wave number vector, which specifies the direction of the waves.

E: represents the energy flux, while Cg, which is equivalent to the product of n and C, Here, n represents the group velocity parameter, while C signifies the velocity of propagation.

Equations 2.9 and 2.10 facilitate the derivation of distinct wave transformations.

$$E = \frac{1}{8}\rho g H^2 \quad \text{..... (2.11)}$$

Figure (2.8) demonstrate the orbital motion of water particles in transition zone, and five stages are used to described the wave transformation according to (Garrison,2014):

1: referee to the phenomenon of wave swell is detected to the ocean floor when the depth of the water is less than half of the wavelength.

2: referee to the crests of waves are observed to become peaked due to the concentration of the wave's energy in a reduced water depth.

3: The circular wave motion is subject to a constraint due to its interaction with the ocean floor, which results in a reduction of its velocity. However, the waves

following it continue to propagate at their initial speed. Consequently, the wavelength undergoes a reduction, while the period remains constant.

4: The wave is nearing the critical ratio of 1:7 between its height and wavelength.

5: The phenomenon of wave breaking occurs at a critical point where the proportion of wave height to water depth reaches approximately 3:4.

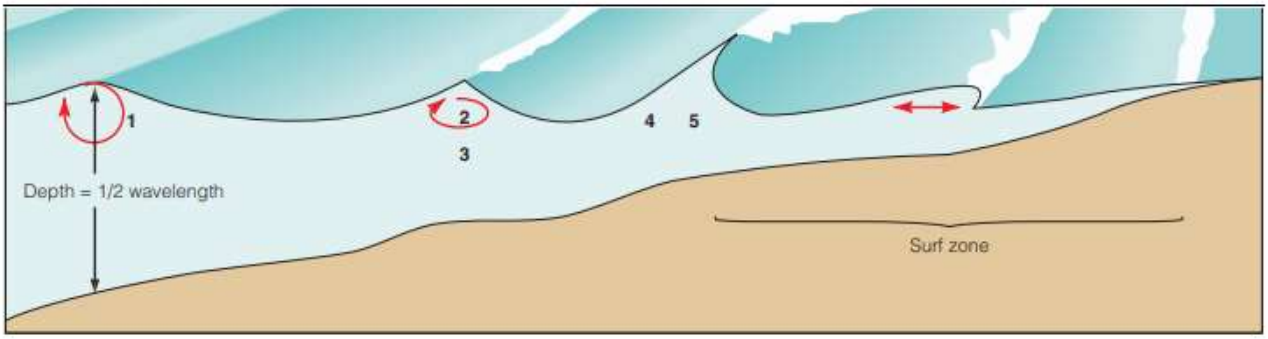

Figure (2.8) Wave transformation, **(.** the color red indicates the motion of water particle. **(Garrison,2014)**

2.2.9 Shoaling

Shoaling refers to the phenomenon in which the amplitude of waves rises when they encounter shallower water depths. The connection between wave height and sea depth is described by the shoaling equation (2.12), which is derived from the conservation of energy equation (2.11).

$$\frac{H_2}{H_1} = \sqrt{\frac{n_1}{n_2}\frac{c_1}{c_2}} \qquad \ldots\ldots\ldots (2.12)$$

2.2.10 Wave Refraction

Refraction refers to the alteration in the direction of waves as they approach the shoreline. When waves impinge against the coastline at an oblique angle, the

phenomenon of refraction occurs simultaneously with shoaling. The interaction between the waves and the ocean floor causes a modification in the direction of the wave crest, resulting in a more direct approach towards the shoreline. The phenomenon that occurs is that as waves propagate towards a shallow region, their velocity diminishes due to the dissipation of energy resulting from interaction with the seabed. The bending of the wave crest results in its alignment parallel to the contours of the bottom.

Equation (2.13) represented the refraction wave parameters, where n represent the group velocity parameters and C is velocity of propagation

$$\frac{H_2}{H1} = \sqrt{\frac{n_1}{n2}\frac{c_1}{c_2}}\sqrt{\frac{b_1}{b_2}} \qquad \ldots\ldots\ldots (2.13)$$

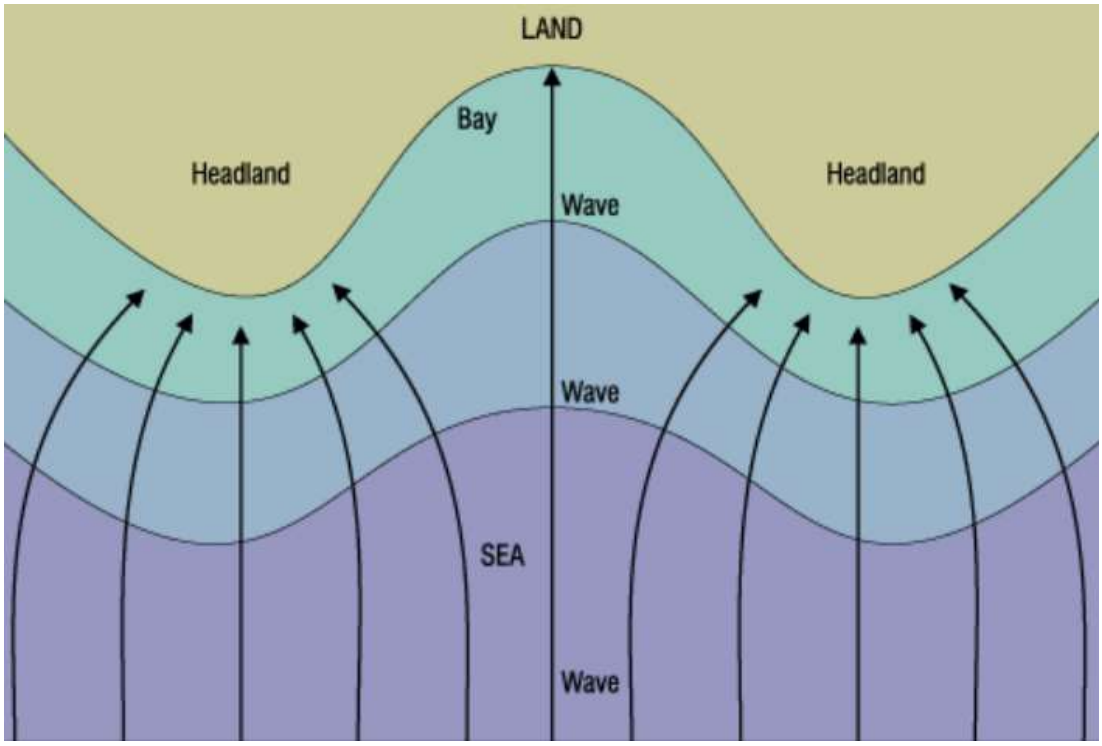

Figure (2.9) Parameters of wave refraction, **Garrison, (2014)**

2.2.11 Waves Breaking

The shoaling effect leads to an increase in wave height as waves propagate into shallow water. Ultimately, the waves will attain the threshold steepness and start the process of breaking.

The process of wave breaking initiates the conversion of wave energy into turbulence and water movement. The breaking waves exhibit various forms of breaking, including surging, collapsing, plunging, and spilling. **Galvin (2016)**

Equation (2.14), describes the breaking circumstances.

$$\frac{Hb}{Lb} = 0.14\, tan\, h\left(\frac{2\pi\, d_b}{L_b}\right) \qquad \ldots\ldots. (2.14)$$

Where: H_b is the height breaking wave, L_b is the length breaking wave and d_b is the water depth for the corresponding wave height and wavelength".

2.2.12 Transmission Coefficients (Ct)

One of the most important physical expressions that can be relied on in the process of evaluating the performance of the Breakwater in dispersion of energy is the Transmission coefficients, which represents the ratio between the value of the transient wave **Ht** and the incident wave **Hi** as shown in the figure (2.10) and equation (2.15).

$$Ct = \frac{\mathrm{Ht}}{\mathrm{Hi}} \qquad \ldots\ldots\ldots (2.15)$$

Where: H_i represented incident wave height, H_t represented transmission wave height and Ct transmission coefficient.

Many researchers in this field considered that the use of this expression can be adopted in assessing the performance of the breakwater for energy dispersion.

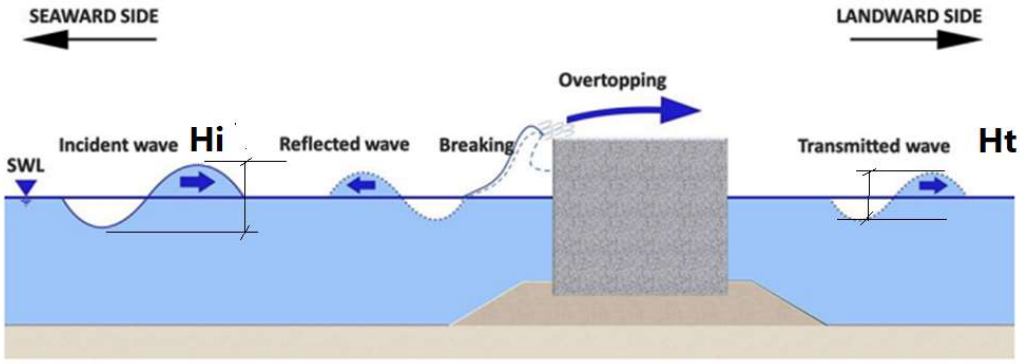

Figure (2.10) Transmission coefficient of wave parameters, Galvin **(2016)**

2.2.13 Iribarren Number

Among the most significant term when studying coastal engineering and determinants of wave breaking is the **Iribarren Fraction,** which is known as the self-similarity-Parameter. **Battjies (1974),** gives a mathematical expression (2.15) to a relation that gives an impression of the behavior of the wave before it starts breaking.

$$\zeta_0 = \frac{tan\,\alpha}{\sqrt{s_0}} \qquad \ldots\ldots (2.15)$$

2.3 Shallow Water Equations

One of the most important equations that describe the behavior of the wave in coastal areas or areas where the water depth begins to recede is the shallow water equation, this equation is derived from the famous Navier Stock Equation. Its applied for two-dimensional or three-dimensional problems and is considered one of the partial differential equations that describe the behavior of a free surface fluid flow taking into account turbulence, velocity and pressure. The following equation (2.15), (2.16), (2.17) demonstrated the equation of shallow water:

$$\frac{\partial \rho u}{\partial t} + u\frac{\partial \rho u}{\partial x} + v\frac{\partial \rho u}{\partial y} + w\frac{\partial \rho u}{\partial z} - fcor\rho v = \left(\frac{\partial \sigma xx}{\partial x} + \frac{\partial \tau xy}{\partial y} + \frac{\partial \tau xz}{\partial z} - \frac{\partial p}{\partial x}\right) \quad \ldots\ldots (2.15)$$

$$\frac{\partial \rho v}{\partial t} + u\frac{\partial \rho v}{\partial x} + v\frac{\partial \rho v}{\partial y} + w\frac{\partial \rho v}{\partial z} + fcor\rho u = \left(\frac{\partial \sigma y}{\partial x} + \frac{\partial \tau yy}{\partial y} + \frac{\partial \tau yx}{\partial z} - \frac{\partial p}{\partial y}\right) \quad \ldots\ldots (2.16)$$

$$\frac{\partial \rho w}{\partial t} + u\frac{\partial \rho w}{\partial x} + v\frac{\partial \rho w}{\partial y} + w\frac{\partial \rho w}{\partial z} = \left(\frac{\partial \sigma yx}{\partial x} + \frac{\partial \tau yy}{\partial y} + \frac{\partial \tau yx}{\partial z} - \frac{\partial \rho}{\partial y}\right) - \rho g \quad \ldots\ldots (2.17)$$

Equation (2.18) represent mass balance.

$$\frac{\partial \rho}{\partial t} + \frac{\partial \rho u}{\partial x} + \frac{\partial \rho v}{\partial y} + \frac{\partial Pu}{\partial z} = 0 \quad \ldots\ldots (2.18)$$

x, y, and z represent velocity in cartesian coordinate system denoted as u, v, and w. ρ, σ denoted the water density, normal stress respectively. τ denoted shear stress related to the viscosity, p is the pressure and force is the Coriolis force. Figure (2.11) shows three-dimensional fluid element with all forces applied.

The four-equation mention are vailed for three dimensional and two-dimensional flow and applied for solved hydrodynamic coastal zone using numerical modeling analysis. **Lin, P. (2008)**

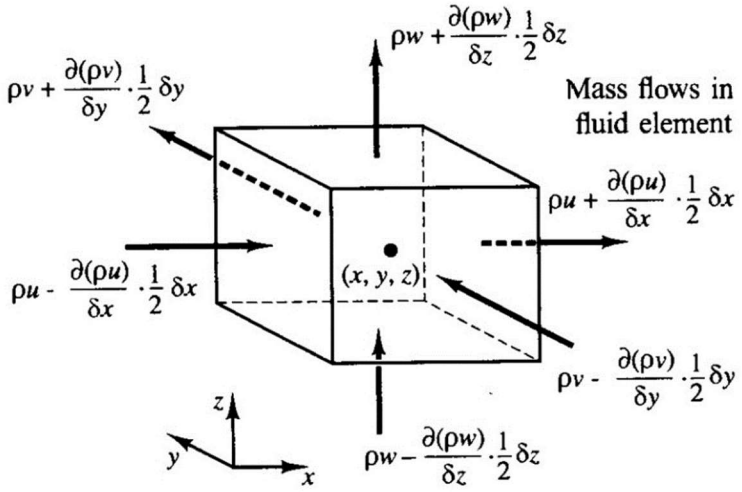

Figure (2.11) Three-dimensional element with all forces, **Lin P. (2008)**

2.4 Theory of Stokes Wave

The proposal of water particles moving in circular orbits as waves pass through them was put forth by Sir George Gabriel Stokes in 1847. According to this theory the crests of waves become gradually sharper and flatter as their amplitude increases or their water depth decreases. Although liner wave theory become inacceptable for described the wave characteristic or less accurate to described wave. Another description, the Stoke wave theory is a mathematical model that describes the behavior of ocean waves.

Le Mehautes (1976) study, an examination was conducted to assess the validity of multiple theories pertaining to periodic water waves. Figure (2.12) demonstrated the different theories described the wave height according to water depth. The region colored in light blue represents the range within which conidial wave theory is applicable. Similarly, the light-yellow area corresponds to the range of validity for Airy wave theory. The dashed blue lines serve as boundaries indicating the necessary order for Stokes' wave theory. The light-gray shading represents this range extension.

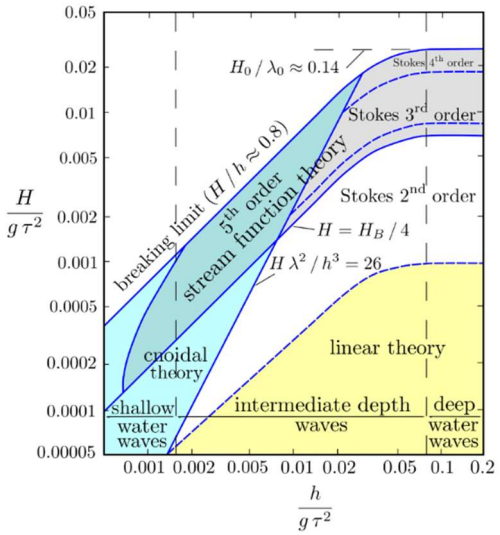

Figure (2.12) Validity of water wave theories . **Garrison ,(2014).**

2.5 Numerical Wave Modeling

Numerical wave modeling is a methodology employed to replicate the dynamics of oceanic waves through the utilization of mathematical equations and computer-based simulations. The process entails decomposing the intricate behavior of ocean waves into more manageable constituents that can be represented and analyzed through numerical techniques.

2.5.1.1 Spectral Wave Modeling (MIKE 21) DHI

Wave climates at offshore and coastal places may be estimated with the help of DHI (Denmark Hydraulic Institute), Water and Environment's MIKE 21 SW spectral wind-wave model. It promotes the development, degradation, and modification of wind-generated waves and swells in offshore and coastal regions. Because exact wave load estimates are critical for both safety and economic reasons, it is extensively used in the construction of offshore, coastal, and portal buildings.

The three primary computational procedures for computing wave fields are the energy balance equation, the mild slope equation, and the Boussinesq equation. Because of the physical assumptions made, each approach has a limited applicability range. An effective mathematical model for describing the motion and distortion of coastal waves is the Mild slope equation. Nevertheless, it is not appropriate for complicated settings with quick topographical changes because of its challenging analytical solution, demanding processing needs, and absence of white wave loss and wind energy input.

The Boussinesq equation include that in calculation: refractions, shallow water deformations, diffractions, and reflections of waves, nevertheless, it is restricted by the depth of the water and requires a lot of labor to compute, which is why it is only helpful for calculating wave behavior over very small regions.

The wave spectrum model MIKE21 SW, which is based on a mass conservation of wave action, can handle a variety of situations, including wind waves, nonlinear waves interactions, whitecaps loss, friction loss cause by bottom, wave breaking, and reflections and diffractions, shallow water deformations, (**DHI, M. 2017).**

The MIKE21 SW model uses central differentiation in constrained volumes for discretization. Depending on the technical and geographic conditions, both unstructured and structured grids may be used concurrently. The model may automatically adapt its time step based on the stability situation. Several sequence explicit methods and a stepwise integral in time are used in this model to calculate wave transport. The migration equation for wave density is solved to describe the dynamic mechanics of gravity waves. Since the wave density spectrum varies with time (t) and space (x, y), it is a function of two-phase parameters. The two-phase parameters in this model are the relative wave frequency ω and the wave direction (in degrees). The basic equation is as follow:

$$\frac{\partial N}{\partial t} + \nabla.(\mathrm{v}N) = \frac{S}{\sigma} \qquad \ldots\ldots\ldots (2.19)$$

Where: S is the source term (J), t is time (s), v is the wave group's propagation velocity in the four-dimensional phase, and N is the energy wave (J). **Xiang, et al. (2019)**

2.5.1.2 Wave Energy Transient Condition:

When considering the link between the wave energy spectral density E (σ, θ) and the wave action density N (σ, θ), $^{\partial N}/_{\delta t}$ reflects the change of wave energy with regard to time.

$$N(\sigma, \theta) = \frac{E(\sigma,\theta)}{\sigma} \qquad \ldots\ldots\ldots (2.20)$$

The relationship between the absolute and relative wave frequencies is seen in the equation (2.21). In the discretized linear equation, their connection may be represented as follows:

$$\sigma = \sqrt{gk\tanh(kd)} = \omega - k.U \quad \ldots\ldots. (2.21)$$

where k is the wave number, $k = 2\pi/L$, U is the flow velocity vector, and g is the acceleration of gravity, **Xiang, et al. (2019)**.

2.5.1.3 Frequency wave energy

With regard to the geo-domain, frequency domain, and direction domain, wave energy changes are represented by the $\nabla.(vN)$. The major causes of changes in the frequency domain are variations in the water depth and flow rate. The fractions caused by the water depth and flow speed are represented as changes in the direction domain:

$$v = \left(c_x \cdot c_y \cdot c_\sigma \cdot c_\theta\right) \quad \ldots\ldots\ldots. (2.22)$$

Where: c_σ is the variation in the frequency caused by changes in the level of water and flow speed (Hz/s); c_θ is the fraction caused by the changes in level of water and flow; and c_x and c_y are changes in the wave propagation in the x and y directions, respectively (measured in m/s).

$$c_x = \frac{dx}{dt} = \frac{1}{2}\left[1 + \frac{2k\,d}{\sin h(2kd)}\right] \cdot \frac{\sigma k_x}{k^2} + U_x \quad \ldots\ldots\ldots (2.23)$$

$$c_y = \frac{dy}{dt} = \frac{1}{2}\left[1 + \frac{2k\,d}{\sin h(2kd)}\right] \cdot \frac{\sigma k_y}{k^2} + U_y \quad \ldots\ldots\ldots (2.24)$$

$$c_\sigma = \frac{d\sigma}{dt} = \frac{\partial\sigma}{\partial d}\left(\frac{\partial d}{\partial t} + U.\nabla d\right) - c_g k.\frac{\partial U}{\partial S} \quad \ldots\ldots\ldots. (2.25)$$

$$c_\theta = \frac{d\theta}{dt} = -\frac{1}{K}\left(\frac{\partial\sigma}{\partial t}\,\frac{\partial d}{\partial m} + k.\frac{\partial U}{\partial m}\right) \quad \ldots\ldots\ldots (2.26)$$

Where: s represents the direction coordinate, m: perpendicular coordinate to s, U_x and U_y are the components of U, k_x and k_y are the components of k, Cg is the magnitude of the group velocity. **Xiang, et al. (2019)**

2.5.1.4 Source function:

The energy conservation equation, which is shown as a spectral density, uses S as the source function. According to Water and Environment DHI (2016), it is the superposed form of the source functions of a range of physical phenomena:

$$S = s_{in} + s_{nl} + s_{d_s.} + s_{bot} + s_{surf} \quad \text{..... (2.27)}$$

Where :S_{in} is the energy supplied by the wind (J), S_{nl} is the energy lost as a result of nonlinear wave interactions (J), S_{ds} is the energy lost as a result of whitecaps (J), S_{bot} is the energy lost as a result of bottom frictions (J), and S_{surf} is the energy lost as a result of wave breaking as a result of changes in water depth (J).

2.5.2 Ansys Fluent Model

In the current work, the Volume of Fluid (VOF) formulation in FLUENT is used to create the two-dimensional numerical model. The nonlinear and free surface flow motion of the wave is formulated using the Navier-Stokes Equation (2.28) and the continuity equation (2.29). The water is assumed to be an incompressible Newtonian fluid whose density is constant across time.

$$\rho\left(\frac{\partial w}{\partial t} + w\nabla w\right) = -\nabla_P + \nabla\mu(\nabla w) + F \quad \text{..... (2.28)}$$

$$\frac{\partial u}{\partial x} + \frac{\partial u}{\partial y} = 0 \quad \text{..... (2.29)}$$

So basically, you've got w for fluid velocity, u and v for velocity in the x and y directions, p for fluid pressure, Z for fluid density, and μ for dynamic fluid

viscosity. So, in equation (2.28), the left part in equation represent forces that make things move; the second part represent pressure and other forces; the third part is about how sticky the fluid is; and the fourth part is about any outside forces acting on the fluid.

2.6 Literature Review for Mitigation Structure (Breakwater)

Energy dispersal structure or Breakwater are constructed near coasts and land-water areas, acting as a means of mitigating and reducing the impact of wind waves by breaking and bouncing waves. These breakers are classified according to many variables, including shape, material and function.

The Al-Faw port breakwater is a unique of the examples of Rubel mound stone breakwaters implemented in Iraq, which was built in order to mitigate the impact of surface waves caused by wind and tides and to create a suitable environment for port work, figure (2.11) shows the Al-Faw port breakwater.

Figure (2.11) Al-Faw port Breakwater

In this part of research, a briefly review on the most important numerical and experimental studies on the use of breakwaters as a means of dispersing energy of wave incident. Historical studies on mitigation structures, also known as submerged breakwaters, have indicated that these structures influence a wide range of physical processes. Some factors, such as structural design, sloping ground stability, scour, wave transmission, and flow pattern are extremely important. The transmission coefficient (C_t), which measures the ratio of the passing wave to the incident wave, is one of the most successful methods for designing a breakwater. Many researchers have focused their attention on the study of submerged breakwaters due to the importance of these structures in coastal protection.

In fact, the failure of mitigation structures leads us to re-evaluate the design of these installations. In the port of **Rumoi in 1920** there was a failure of the sliding type of the caisson breakwaters as described by **Ito, and Henry. (1996).** Many researchers attributed this failure to the composite type breakwater , which was designed on the basis of designs developed by Japanese engineers .As a result of the difference in the design culture between the engineer in Europe and the Japanese engineers , the essence of the difference is that Japanese engineers believe that the use of a composite breakwater, especially the vertical top only has the ability to resist the impact of the wave and due to its weight . Reported that a lot of designers want to employ vertical breakwaters once again, their popularity had declined due to their repeated tragic failures in the **1930s.**

Stucky and Bonnard (1937) using a two-dimensional structure in the shape of a trapezium and carried out the first known experiment in the physical realm to investigate wave transmission related to submerged breakwaters**.**

The **Beach Erosion Board** (1940) continued their research in more thorough 2D geometrical detail. Rectangular breakwaters were studied by **Morison (1949)** and **Johnson et al. (1951)**.

Longer period waves were often less impacted by breakwater crest width and height, according to **Johnson et al. (1951)**, who also demonstrated superior energy dissipation of steeper waves with a broader barrier.

In the study conducted by **Stoker in 1957**, a theoretical solution was derived for the transmission of waves across a stationary horizontal plate. This solution was based on the principles of Airy wave theory. formulation (2.30) was formulated to describe the suggested transmission coefficient equation.

$$k_t = \frac{H_t}{Hi} = \frac{1}{\left[1+\left(\frac{\pi B}{L}\right)^2\right]^{0.5}} \quad \text{..... (2.30)}$$

Where: H_i, H_t, K_t Represented incident wave, transmission wave, transmission coefficient respectively. L and B represented the length of wave, breakwater length (m) respectively.

Numerous researches have been undertaken to investigate the box culvert-type slotted breakwater, which was first introduced by **Jarlan, (1961)** coated from **Nur Yuwono, et al (2022).** These studies have mostly concentrated on exploring various variations and configurations of this breakwater design.

Dick and Brebner (1968), performed tests on submerged breakwaters. The studies were done with a water level of 60 cm, and the height of submergence ranged from 4cm to 20 cm. Upon plotting the transmission coefficient, it was seen that the Kt exhibited an upward trend as the depth of submergence increased. Additionally, it was observed that the transmission coefficient also increased with an increase in the (h/d) ratio, while keeping the (L/B) ratio constant.

For several types of breakwaters structures, **Abdul Khader and Rai (1980)** calculated the coefficient of transmission K_t, or the ratio of transmitted to incident wave height. They came to the conclusion that, when compared to other varieties of submerged breakwaters, rectangular breakwaters are the most efficient in dissipating energy.

J.D. Mettam et al. (1982) conducted an assessment of the prevailing design philosophy pertaining to breakwaters. They identified the limitations associated with this approach and provided recommendations for including considerations of safety in order to enhance the design. The authors also propose the substitution of the practice of assessing stability by testing against extreme events occurring once in 50 or 100 years with the use of a design wave that carries a chance of surpassing no more than 5% during the lifespan of the structure. Many designers extensively depend on hydraulic model testing since the current design formulas are insufficient in assessing the system's safety margin against failure.

The U.S. Army Corps of Engineers (1984) conducted a study in which they presented a variety of empirical equations generated from wave tank recorded data. The experiments conducted as part of this study included testing on submerged breakwaters, which provided insights into wave energy. The results indicated that increasing the submergence height of the breakwaters resulted in a decrease in wave energy. Equation (2.31) demonstrated the transmission coefficient equation proposed by **(Hanson .J and Jensen.2004)**

$$k_t = -0.4\frac{R_C}{H_i} + 0 \cdot 8\left(\frac{B}{H_i}\right)^{-0\cdot 31}(1 - e^{-0.5}) \quad \ldots\ldots\ldots\ldots (2.31)$$

Many researchers have dealt with transmission coefficient Kt and some of them, Dougelass and Krolaak (2008), Dick and Brebner (1968), Seabrook and Hall (1998) Calabrese (2003), Tajziehchi (2006), Liao, et al. (2013), **Ilaria** (2016).

Alshaikhli (2022), demonstrated a mathematical and experimental analysis of several forms of an inclined rubble mound breakwater. to examine the design of mound breakwaters in order to ascertain the breaking wave behavior, including transmission coefficient and energy dissipation. Most of the mentioned researchers have shown that the wave dispersion coefficient varies within the limits (40 % to 75%) and is controlled by the wave properties.

The velocity field and vortex formation around the submerged breakwaters were researched by **Hsu et al. (2000; 2004)** and **Chang et al. (2001; 2005). Young and Testik (2009; 2011)** investigated the reflection and diffraction of waves from underneath breakwaters. Experimental research on wave breaking and energy loss over porous structure submerged breakwater was conducted by **Liao et al. (2013).**

El Saie (2014) , conducted a laboratory study that included three types of breakwater , vertical, rubble mound , and pile breakwater to protect the shoreline .The researcher touched upon the use of multiple values of the wave height and the submerged part of the breaker to investigate the values of the energy dispersion coefficient according to each of the three types .The results of this study are shown in the following figure, which shows that the values of the energy dispersion coefficient ranges from (20% to 80 %) of the incident wave value. Figure (2.12) shows the variation of transmission coefficient for three different model.

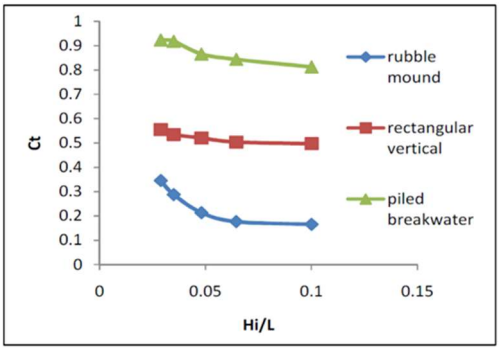

Figure (2.12) Transmission coefficient for three type breakwater **El Saie (2014)**

Hajivalie et al. (2015) investigated the impact of vertical breakwater size on transmission coefficient and vortex production around the breakwaters using a RANS equation based computational model in conjunction with a conventional k-model. Conclusion that extending the breakwater width would not significantly improve wave energy dissipation by the breakwater unless it is wider than a specific rate, which may vary depending on the relative submergence depth. Researcher clarify that at this particular breadth, the vertical submerged breakwater is not subject to wave breaking. This discovery casts doubt on earlier predictions that the vertical breakwater may dissipate more wave energy than other submerged breakwater shapes, such as trapezoidal and semicircular, in every situation.

A. V. Mahalingaiah et al. (2015) provided a comprehensive explanation of the design process for a rubble mound breakwater. They illustrated this technique by presenting a case study of breakwaters planned for the establishment of a fisheries port in Majali, Karnataka. Empirical formulas, such as the Hudson formula and the Van der Meer formula, are often used in the initial design phase to estimate the unit weight of armor materials. This is crucial since armor plays a significant role in ensuring the stability of buildings. The majority of these formulas include factors such as wave height, density of the armor units, and the angle of the breakwater slope.

Hajivalie et al (2018), made a laboratory study on rectangular-shaped models of a semi-submersible breakwater. The study included different shapes of the breaker as well as different heights to clarify the extent of the impact of The Shape of the origin on the values of the energy dispersion coefficient. The height of the model is 0.25 meters and the width vary between (0.3, 0.9, 0.6). The researcher's findings were that the transient wave coefficient decreases with increasing the width of the breaker.

Al-Sheikali in (2022), presented a laboratory study and a mathematical model using the FLOW 3D model, this study included many aspects. Use different physical models of a steps and non-steps breakwater. One of the outputs of this study is that the steps breakwater has a higher efficiency in energy dispersion compared to a regular Surface breakwater by obtaining results for the value of the dispersion coefficient of the wave. The other part of this study, the researcher made a physical model of the Al-FAW port breakwater in Basra, Iraq. The results of this study recommended the use of steps breakwater instead of regular. Figure (2.14) present some results of this study

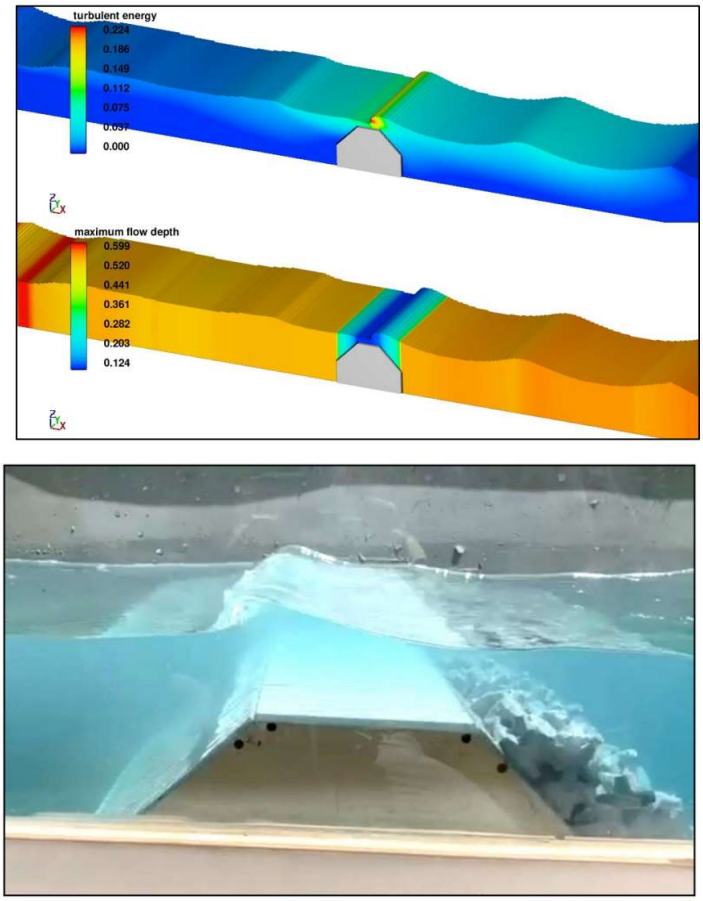

Figure (2.14) Results of flow3d model and experimental, Al-Sheikali, (2022)

2.7 literature Review Large-Scale Wave Modelling

For decades, researchers have been working on numerical wave water modelling. The earliest numerical models for wave water modelling were established in the 1960s and 1970s, although their computing capacity was restricted at the time. Throughout the 1980s and 1990s, as computers got more powerful, numerical models for wave water modelling became increasingly advanced.

One of the earliest numerical models for wave water modeling was the Mild Slope Equation (MSE) model, which was developed in the 1960s. The MSE model is a linear model that is used to simulate waves in shallow water, such as nearshore areas. The model presents that water depth is much smaller than the wavelength of the waves. in the 1970s, researchers began to develop more sophisticated numerical models for wave water modeling.

The Boussinesq Equation (BE) model was one of the most significant of these models. This model is a nonlinear model that is used to simulate waves in both shallow and deep water. The model considers the effects of wave breaking and wave dispersion in its calculations.

In the 1980s and 1990s, numerical models for wave water modeling continued to evolve. Researchers began to develop models that could simulate the interaction between waves and currents, as well as the effects of sediment transport. One of the most important of these models was the **SWAN** (Simulating Waves Nearshore) model, which was developed in the Netherlands in the 1990s. The SWAN model is a sophisticated numerical model that can simulate wave propagation, wave breaking, and sediment transport in coastal areas. (Wang. et al .2015)

One example of a modern numerical model for wave water modeling is MIKE21SW, developed by DHI in Denmark. **MIKE21SW** is a three-dimensional

model that can simulate wave propagation, wave breaking, and wave runup in coastal areas. The model considers how tides, currents, wind, and bathymetry affect wave behavior. **(DHI, M. 2017)**. Many studies anterior possible to remember that used modern numerical model:

WAVEWATCH III was used by **Li et al. (2014)** in order to provide wave prediction for the Bohai Sea of China. **Bi et al. (2015)** used WAVEWATCH III to carry out a simulated examination of the waves that are found in the Pacific Ocean. **Yang and Zhang (2013)** used SWAN to simulate wind wave activity in Bohai Bay from 1989 to 2008 and analyze wave probability**. Ayat (2013)** used the MIKE21 SW model to simulate waves in the East Mediterranean and Aegean waters and analyze wave energy in the relevant waters. To comprehend the effects of man-made structures like mudflats and breakwater on shoreline changes, **Noujas et al. (2017)** used the MIKE21 SW model to study the Indian southwest coastal waves.

Goda and Suzui (1976), The study included conducting a series of experiments using irregular waves to simulate the behavior of seawalls, both with and without the presence of concrete block mounds for protection. The researchers put out a set of twelve diagrams based on their experimental findings. These diagrams facilitate the rapid estimate of the overtopping rate of seawalls across various water depths, ranging from offshore to shoreline locations.

Hara et al. (1991) employed numerical study to investigate the performance of wave breaking behavior in impermeable conventional breakwaters. Through regression analyses, the researchers posited that the breaking wave phenomenon is not solely influenced by the bed slope and wave steepness, as indicated by the Iribarren number. Instead, they found that it also depends on the height of the breakwater (hc) and the width of its crest (B). Consequently, the researchers

proposed modifications to the Iribarren number in order to account for submerged breakwaters.

Liu et al. (1999), introduces a numerical model that may be used to simulate the interaction between waves and porous materials. The Finite Volume Model employs the free-surface-capturing approach in conjunction with a novel Cartesian cut cell treatment to compute the two-phase flows occurring outside a porous structure. This computation is based on the Navier-Stokes equations. Meanwhile, the flow within the porous structure is characterized by Navier-Stokes type model equations. The numerical model utilizes a computational domain to simulate the phenomenon of a breaking wave overtopping a caisson breakwater. The breakwater is safeguarded by a layer of armor units. The findings indicate that the use of a porous amour layer has shown to be successful in mitigating the occurrence of overtopping in the caisson breakwater.

The study conducted by **Sakakiyama and Liu (2001)** focused on the examination of wave behavior and turbulence flows occurring in the vicinity of a caisson breakwater. During the conducted trials, the breakwater structure was equipped with wave-absorbing blocks and reinforced by a debris pile. The researchers reached the conclusion that a wave breaking mechanism and the presence of an armour layer both contribute to the generation of substantial turbulence. The turbulence created in the vicinity of the caisson breakwater was noticed, resulting in significant implications for wave impacts and the scouring phenomenon occurring in the area directly in front of the breakwater.

Suh et al. (2007) introduced a new approach based on the work of Kim (1998) to address the issue of single row vertical slotted barriers with square piles. The authors assert that the proposed methodologies found in existing literature for wave transmission prediction have a tendency to underestimate wave transmission values

within the lower ranges of wave steepness. The proposed solution incorporates a combination of principles from basic fluid mechanics and empirical formulations, resulting in a hybrid approach. The authors propose that the novel methodology yields superior outcomes, and advocate for the integration of empirical formulae with fundamental principles in the field of fluid mechanics. According to the authors, the hybrid approach may also be used for circular pile breakwaters.

Noujas et al. (2017) conducted a study focuses on a coastline length along India's southern SW coast where Sundar and Sanna siraj (2006) suggested using an existing barrier and groins field to manage severe erosion. Prior to the development of the intended groins field, two groins were first built as a pilot program in 2008–2009 to validate the net littoral drift of this area and for a preliminary evaluation of the Groins performance. With the two groins in place, the coastline location was periodically monitored from 2009 to 2014. Using field measurements from 2010–2011, a shoreline evolution model for the research area was built up, calibrated, and verified.

Yan Xiang et al, (2019), proposed a numerical solution for model presented by **MIKE21** SW to simulation the wind induced wave in shallow reservoirs in Cangzhou City, Hebei Province, China. This study focused on the use of artificial islands as a means of dispersing energy by adding more than one proposed scenario for the location of virtual islands or their area. The results showed that the use of artificial islands reduces the value of wave height by approximately 10% - 30%, percent of sign wave height, figure (2.15) shows some of result conducted by this study.

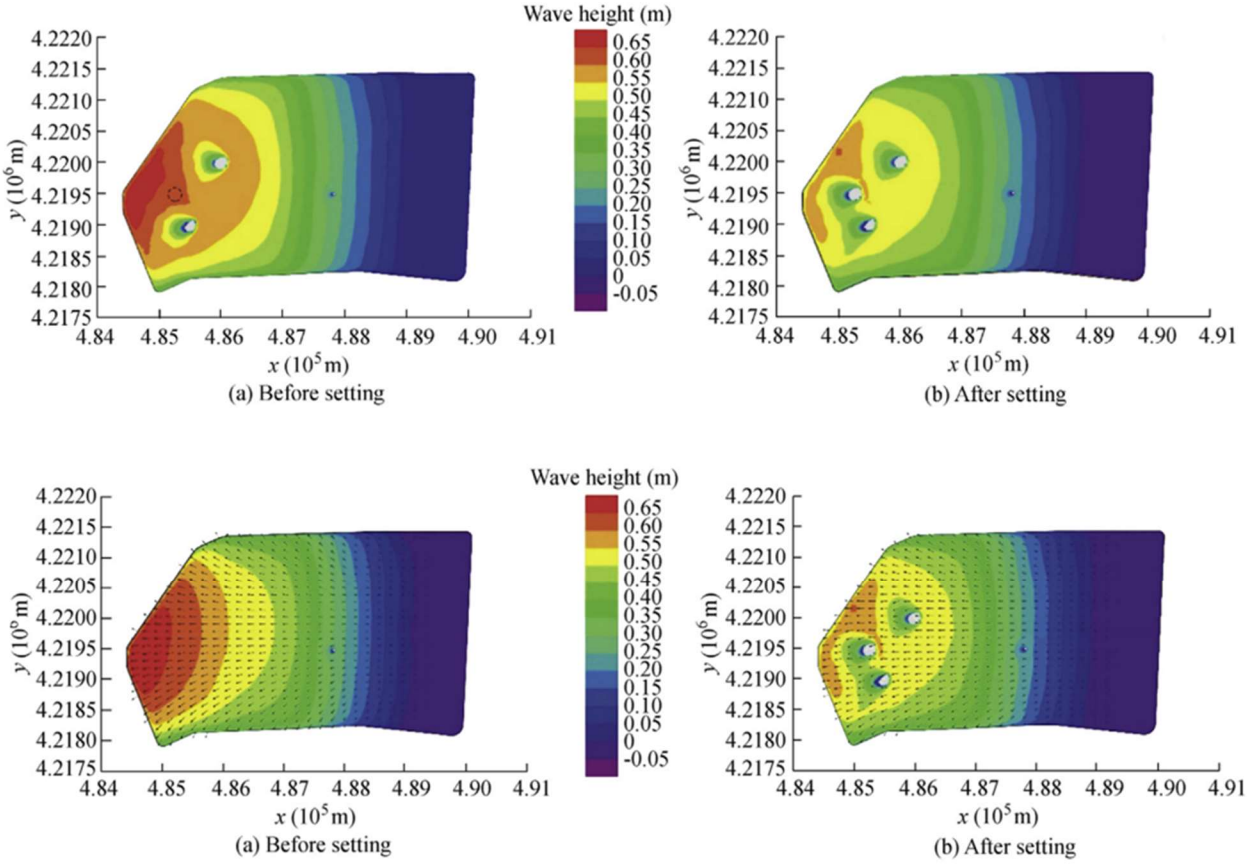

Figure (2.15) MIKE12 SW Results of sign wave height, **Yan Xiang et al, (2019)**

Ho Gou et al (2020), used the MIKE21 Spetral Waves (SW) and MIKE21 Boussinesq Waves (BW) wave models are combined in this work to be used together for a joint application (SW-BW nested model). In this study, the researchers made a mathematical model of Zhoushan-based Yanwo Island in China, which included two models, one to represent the waves caused by the wind and another model that tests a set of scenarios that suggest a location for the breaker in order to mitigate the impact of rising waves in the region. Figure (2.16) shows Daishan Island and proposed breakwater location. Results of this study are showed in Figure (2.17), it can be seen that the difference between the sign wave height distribution before and after project of breakwater.

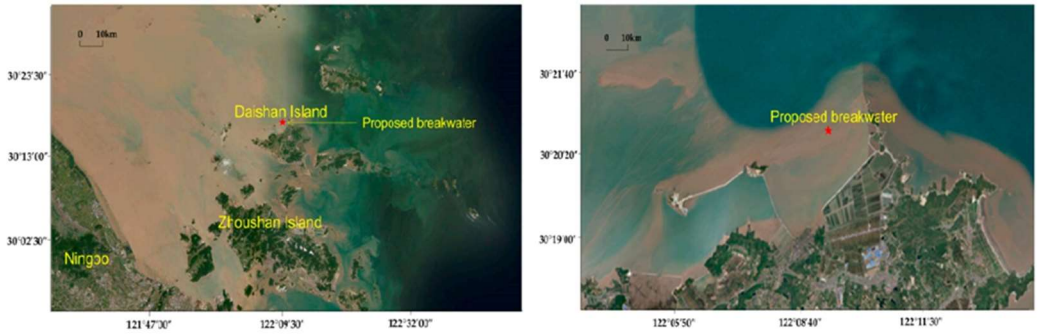

Figure (2.16) Daishan Island and proposed breakwater location

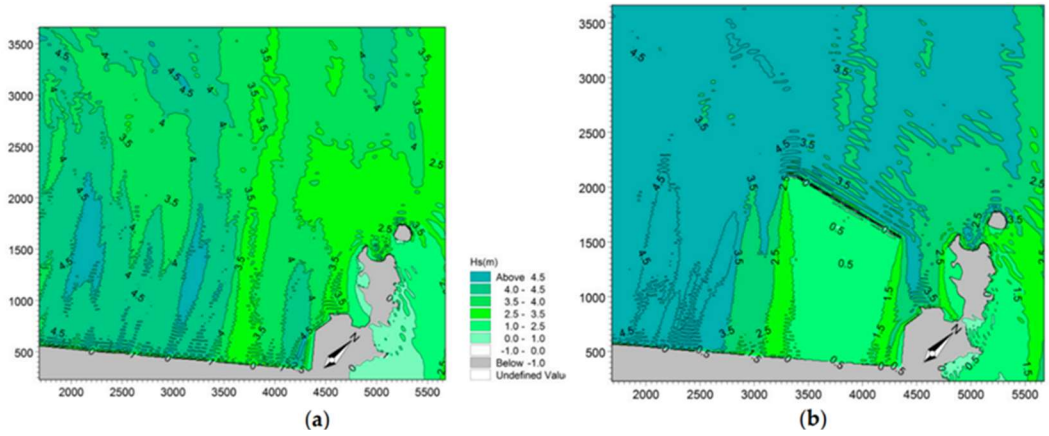

Figure (2.17) Sign wave height before and after project of breakwater

Azharul Hoque et al (2020), implemented a mathematical model using (SWAN) to represented a full-scale simulation of the Canadian Beaufort Sea. this study focuses on simulated four storms by (SWAN model). The model simulations conducted inside the shallow water depth region additionally take into account the influence of bottom friction and depth induced effect interactions. As a result, found that wave simulations that incorporate a white capping formulation dependent on local spectral steepness yield superior results compared to simulations that rely on mean spectral steepness. However, the inclusion of a bottom friction term and triad mechanisms in the current study did not result in any significant improvement in the simulations. Figure (2.18) shows some results of spectral wave model.

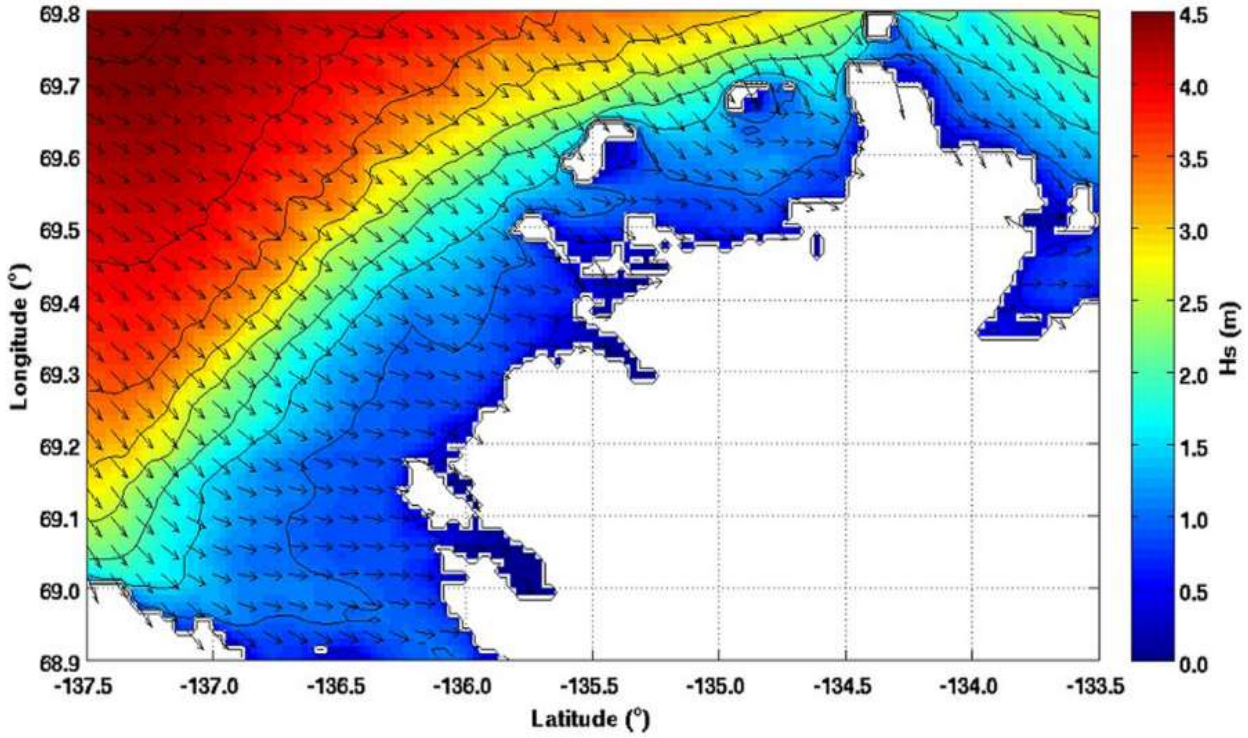

Figure (2.18) Wave height Hs according to storm simulation at (17 September 1985). Beaufort Sea

Gomes, A. et al (2020), findings of using a comprehensive tool (CFD) to examine the performance of a perforated semicircular mitigation structures with a foundation built on a rubble mound shape were presented in this article. The model was tested against experimental findings to determine the critical weight required to prevent sliding while accounting for the impacts of water depth and various wave types. The effectiveness of the breakwater to diffuse wave energy is compared between the perforated and non-perforated option. Figure (2.19) Shows energy dissipation for two cases, perforated, non-perforated model.

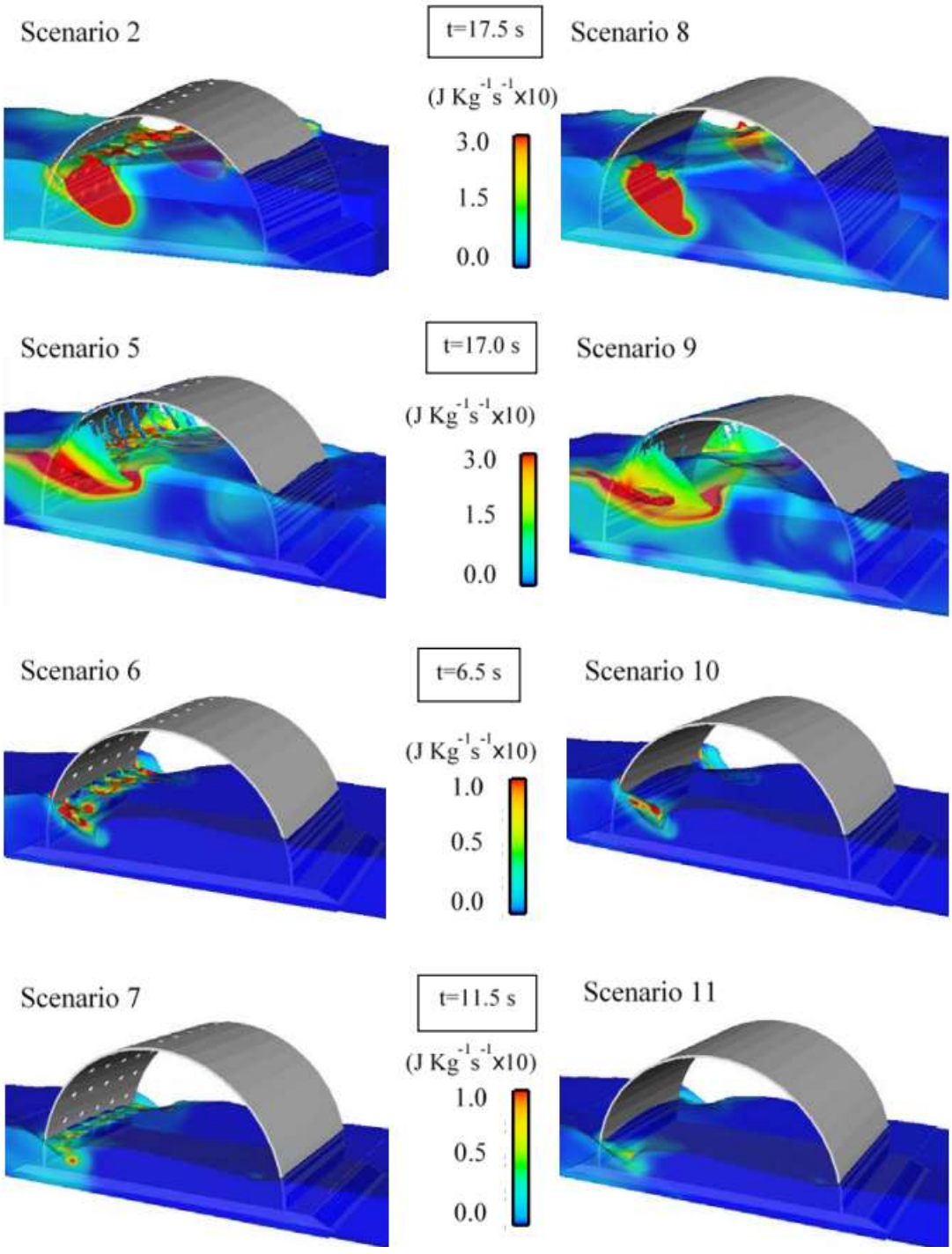

Figure (2.19) Energy dispersion, (left) perforated model, (right) non- perforated model (**Gomes, A. et al (2020).**

Yuwono, N, and Sriyana I (2022), conducted a study concerned about slotted box-culvert mitigation structures to investigated the transmissions coefficients of the model according to different wave characteristic parameters. This context bases on experimental work for different physical model. The results indicate that there is a decrease in the transmission coefficient (C_t) when the (h_L/d) decreases, while an increase in the (B/L) and (H/L) values, where B length and H height. The C_t coefficients has an upward trend when relative wave height, relative wave length, and B/L grow, but afterwards experiences a decline once it reaches its maximum value, which corresponds to the optimal H × B/L.

Research produced by **Al-Sheikali (2022)**, and **Ho Gou et al (2020)**, the closest studies to the subject of our study in terms of laboratory work and the\mathematical model used

Summing up the studies and previous researchers, the region (depression of Annajaf sea) adopted in this study has not been studied by any researcher in with regards of wind induced wave previously. And, the shape of breakwater that will be studied (sloped steps on sides and top) was a completely new shape that has not been touched upon previously. Also, the phenomenon of waves propagated as a result of wind in a closed region was studied, which is one of the topics that are considered very important from the climate changes that have begun to appear during recent year in the study area.

Novelty of current study it can summarized as:

- Study of wind induced wave in close region **(Lake of Annajaf)** based on worst case combination of maximum lakes levels and highest wind speed recorded

Chapter Three

Experimental Work

Chapter Three

Experimental Work

3.1 Introduction

The complex behavior of the waves as well as the interference with the breakwater, leads to study it in the laboratory to understand the behavior of the wave and the breakwater together by making physical models of multiple shapes. As mentioned in chapter two, the cross section of the breakwater is very important in determining the value of the transmissions wave coefficient and wave reflection, in addition to other factors related to the wave characteristics.

In this chapter, a laboratory flume will be employed in order to generate waves with variable specifications and also add the idea of wave absorption at the back of the flume to eliminate the reflection wave in downstream side of breakwater.

3.2 Experiment Set-up Specifications

3.2.1 Wave Flume

The hydraulic laboratory of the Faculty of Engineering, University of Kufa-Iraq, has a 3D-wave flume where the physical model studies are conducted. Didacta Italia manufactured the flume to investigate the hydrodynamic characteristics of open surface streams in channels with different angles of inclination. The wave generator used in the experiment is a top-hinged paddle design capable of creating predictable single sign waves. The waves propagated by the wave paddle run through thin vertical sheets of stainless steel to provide free smooth waves. The wave flume contains active wave absorption that may take in the test to reflected wave. The channel is composed of tempered glass, section 0.3 m x 0.45 m, length 15 m.

flume include with wave maker submerged blade type, an electric motor with a variable speed serves as its controller, Figure (3.1), Figure (3.2).

Figure (3.1) hydraulic flume in lab

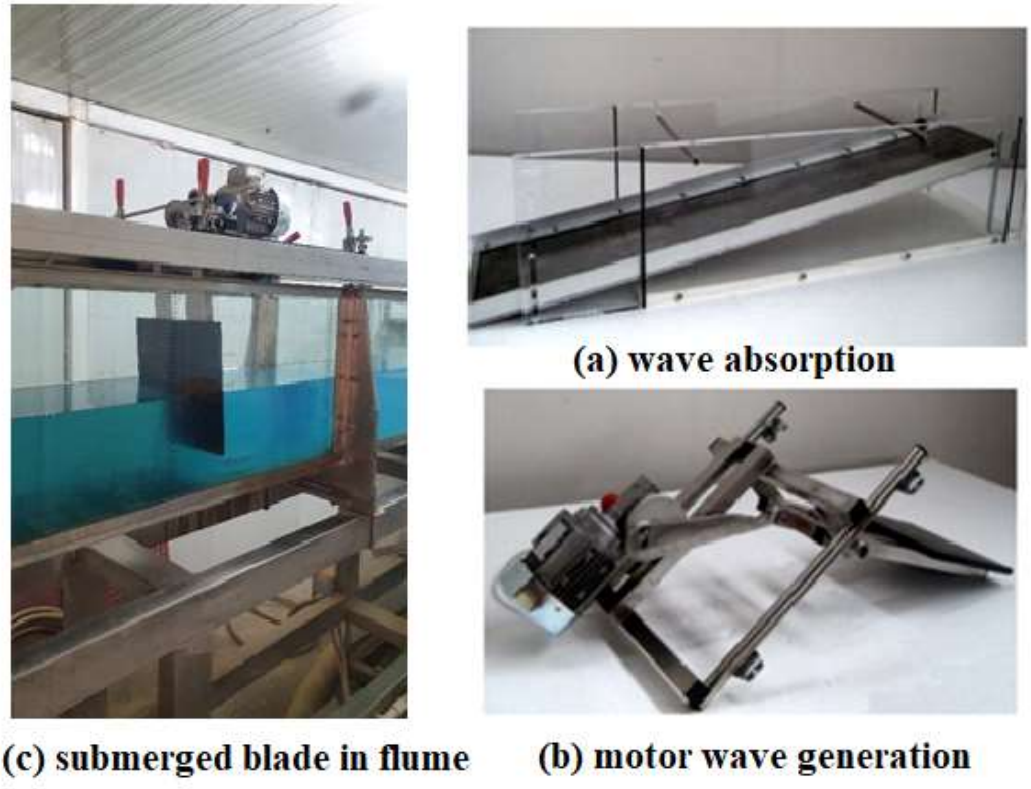

Figure (3.2) Some of device fixed in flume

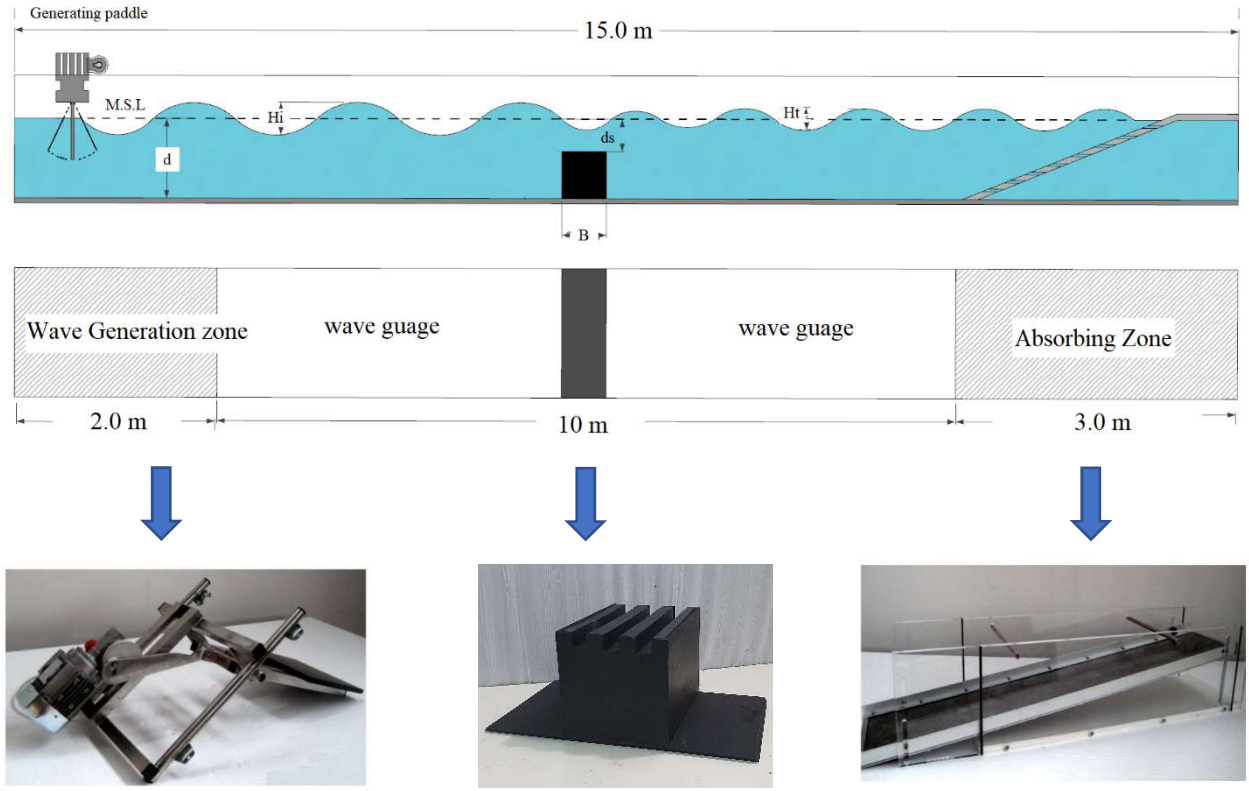

Fig (3.3) Flume with step-up of wavemaker, breakwater model, absorbing device

Wave generated by wave maker of the submerged blade type, and it is operated by an electric motor with variable speed. It enables one to see the form of the waves as they travel through a channel. Specification of wave tank flume: Ratio-motor: speed ratio 1:30, max speed 47 rpm, absorbed power: 0.12 kW. Inverter for revolution speed regulation, Figure (3.3) shows the wave generator and absorbing beach in flume.

3.2.2 Wave tank modelling

Discussing of an experimental research employing various methods of surface wave generation on a tank (piston and flap type wavemaker) is one of the goals of this study. For various boundary conditions, some computer simulations of these processes have been created. The wave tank is roughly represented in **Figure (3.4)**.

3.2.3 Wavemaker Theory

A wavemaker produces waves by oscillating a mechanical component within the wavemaker. The two kinds of wavemakers that are often distinguished are flap and piston. For experiments in shallow water, a piston-type wavemaker is utilized. Modelling buildings along the shore, harbour, etc. uses this form of generator because the piston motion limits the particle orbital motion to an ellipse. Galvin puts up a straightforward wavemaker idea in 1964. The particle orbital motion in a wavemaker of the flap type decreases with depth and becomes insignificant at the bottom, as showing in figure (3.4), **Ringe, S. (2020).**

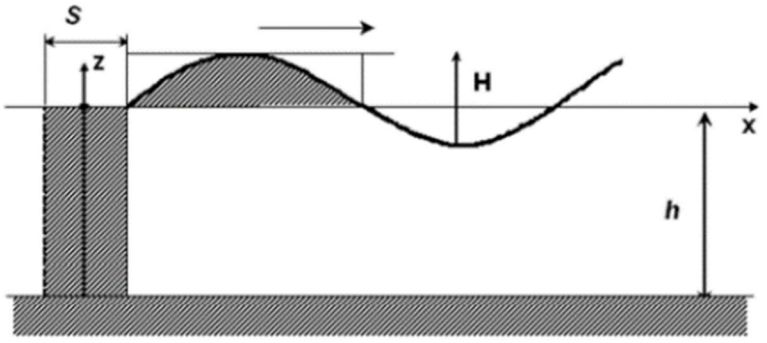

a. Piston type wavemaker

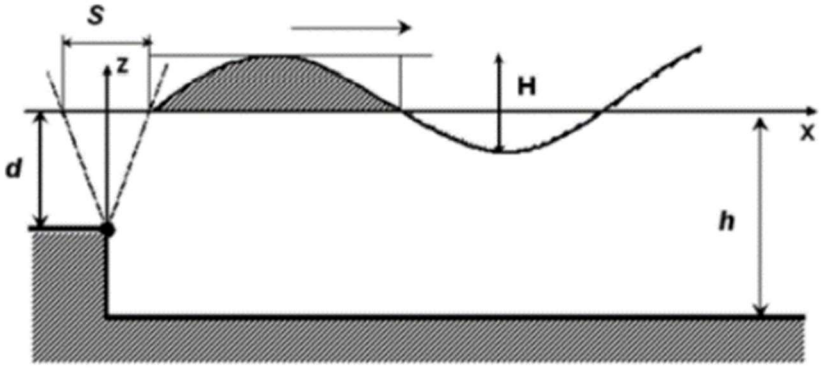

b. Flap type wavemaker

Figure. (3.4) wave maker type according to mechanics of movement, **Ringe, S. (2020).**

According to Galvin's hypothesis for flap-type wavemakers, when the piston has a stroke of S with depth h, the volume of water displaced will be S h. A wave crest's water volume may be calculated using the formula of equation (3.1), **(R. G. Dean and R. A. Dalrymple.1991)**

$$\int_0^{\frac{\lambda}{2}} \left(\frac{H}{2}\right) \sin kx\, dx = \frac{H}{k} \quad \text{..... (3.1)}$$

consideration the volumes into both sides, the following expression become as.

$$SH = \frac{H}{k} = \frac{H}{2}\left(\frac{\lambda}{2}\right)\frac{2}{\pi} \quad \text{..... (3.2)}$$

In Figure (3.4), the shaded area corresponds to the factor 2/ π. The straight forward wavemaker hypothesis for a piston is as follows equation (3.3):

$$\left(\frac{H}{s}\right) = kh \quad \text{..... (3.3)}$$

Where: H/S stands for the shallow water-appropriate height to stroke ratio (shallow water condition kh < π/10). The wavemaker theory is complete when boundary conditions are taken into account, and the following formula for wave height to stroke is derived, **Ringe, S (2020)**.

$$\frac{H}{s} = \frac{2(\cos 2k_p h - 1)}{\sinh 2kph + 2\ _p h} \quad \text{..... (3.4)}$$

H; represent height of wave: and the progressive wave number is denoted by k_p

In the present study, according to the flume experimental flap type wavemakers are generally used for investigating and generating water waves, as showing in figure (3.5). When the flap connected device wavemaker is hinged at the base of flume, the expression is:

$$\left(\frac{H}{S}\right) = \frac{kh}{2} \quad \text{..... (3.5)}$$

The stroke number to wave height ratio of the flap type wavemaker changes to equation **(3.6),** when boundary circumstances are taken into account.

$$\frac{H}{s} = 4\left(\frac{sinh\, kph}{\overline{k_P h}}\right)\frac{k_p h\, sin\, hkPh - cosh\, kph +}{sin\, h2\ _p h + 2k_P h} \qquad \ldots\ldots. (3.6)$$

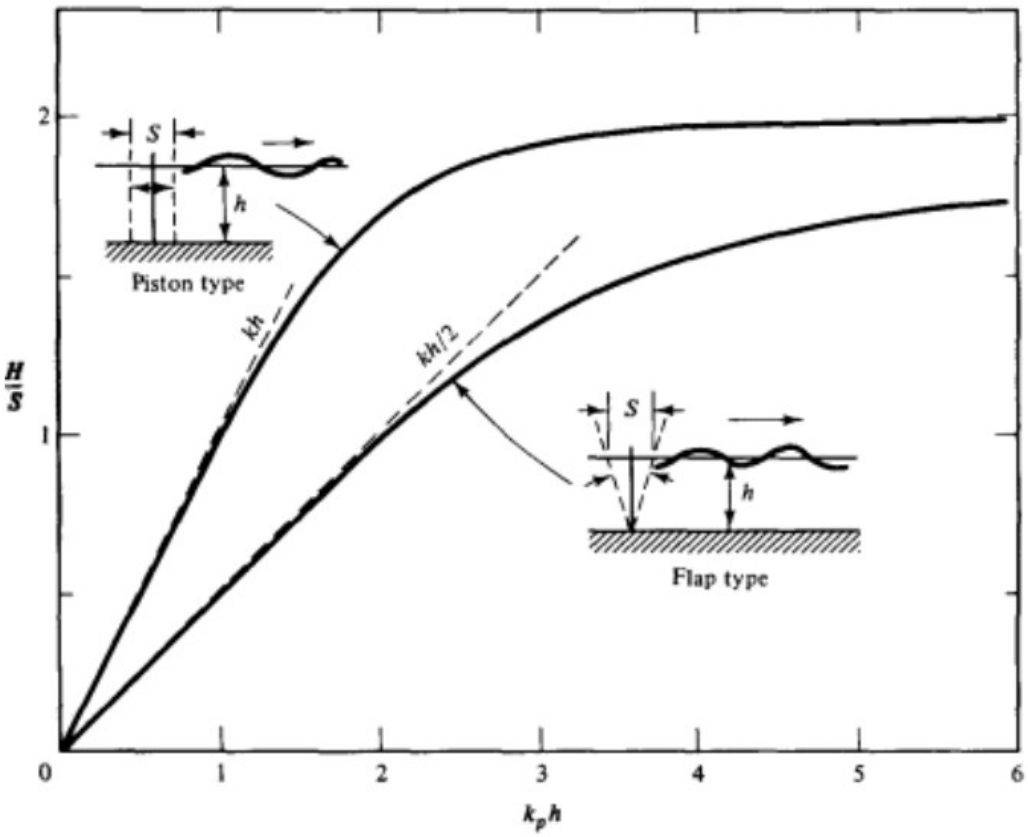

Figure (3.5) flap type wavemaker relation H/S and *Kp* h according to (R. G. Dean and R. A. Dalrymple.1991)

3.3 Model set-up and geometry

The model studies were primarily used to understand how the transmission coefficient varies with regard to regular wave conditions such as: shape of breakwater: incident wave height: wave steepness, transmission coefficient for each type. Figure (3.6) represent the model installed in flume and all parameters for breakwater and wave conditions.

Where: H = Wave height, H_i = Incident wave height, H_t = Transmission wave, h= Static water level SWL, Hs = Submerge depth, L_B = Length of breakwater, and H_B= height breakwater.

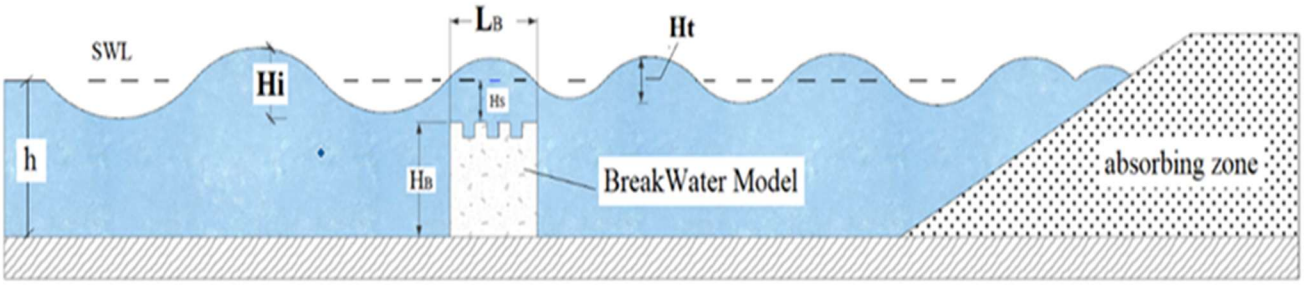

Figure (3.6) Sketch demonstrate breakwater model and wave specification parameters.

3.4. Hydraulic Parameters of Breakwater:

Five model are used to test the wave transmission coefficient, these models are organized according to the shape of cross section as shown in Figures (3.7), (3.8),(3.9),(3.10),(3.11) and (3.12) . These models are manufactured from moisture-resistant plastic materials using machinery 3D printing for very fine details.

Table (3.1), demonstrates the hydraulic characteristics that characterized the physical model, breakwater shape, and wave conditions. Each experiment test being repeated three times to get the average of each run, so that the total number of experiments was 150 tests as shown in table (3.1). During experiments, the incident waves are measured using wave measurement device at a distance approximately of one wave length L. The wave transmission coefficient (Ht) is measured at the lee side of breakwater. As the beginning of wave generation, a regular wave propagated in the flume using a user define function (UDF) with the movement of the flap-type paddle, the formation of waves is started under hydrostatic circumstances (water at

rest) of the flume. The liquid face is given a static pressure as a starting condition, and the VOF model are used to describes the free surface profile.

Table (3.1) Breakwater model assignment and experimental test specifications

Model breakwater	Symbols	Submerged Depth (H_s) (cm)	incident wave elevations (H_i)(cm)	Motor Speed Ratio max speed 47 RPM
Rubble mound	M1	0, 4, 8, 12, 15	10, 12,15	20, 30 and 47
Sloped with steps	M2			
Rectangular	M3			
Rectangular with steps	M4			
Rectangular narrow	M5			

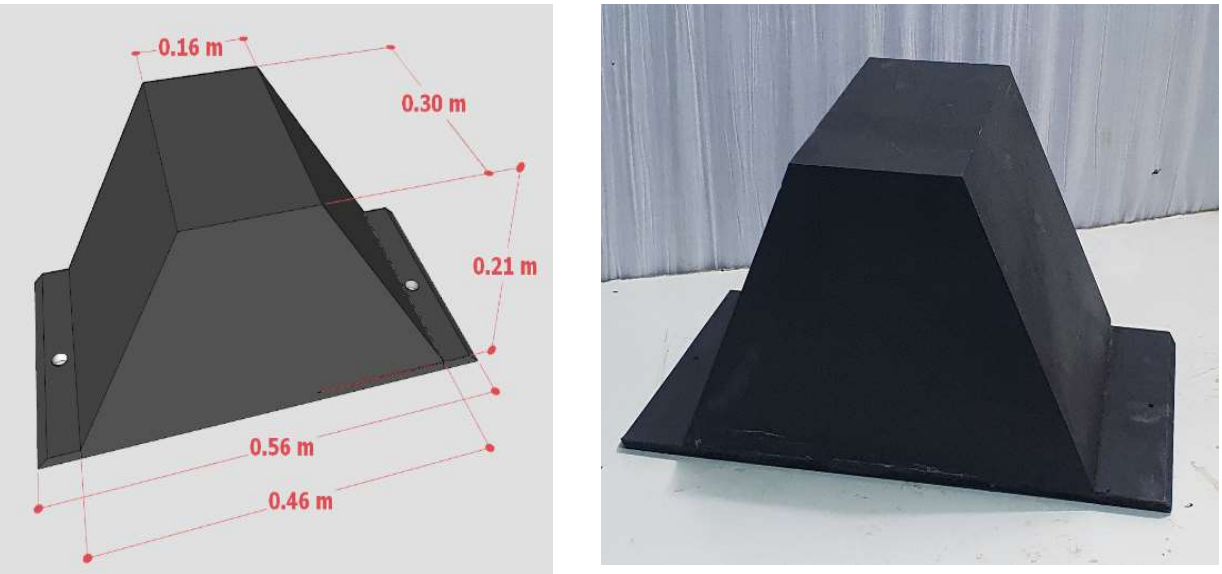

Figure (3.7) Rubble mound (model Symbol M1)

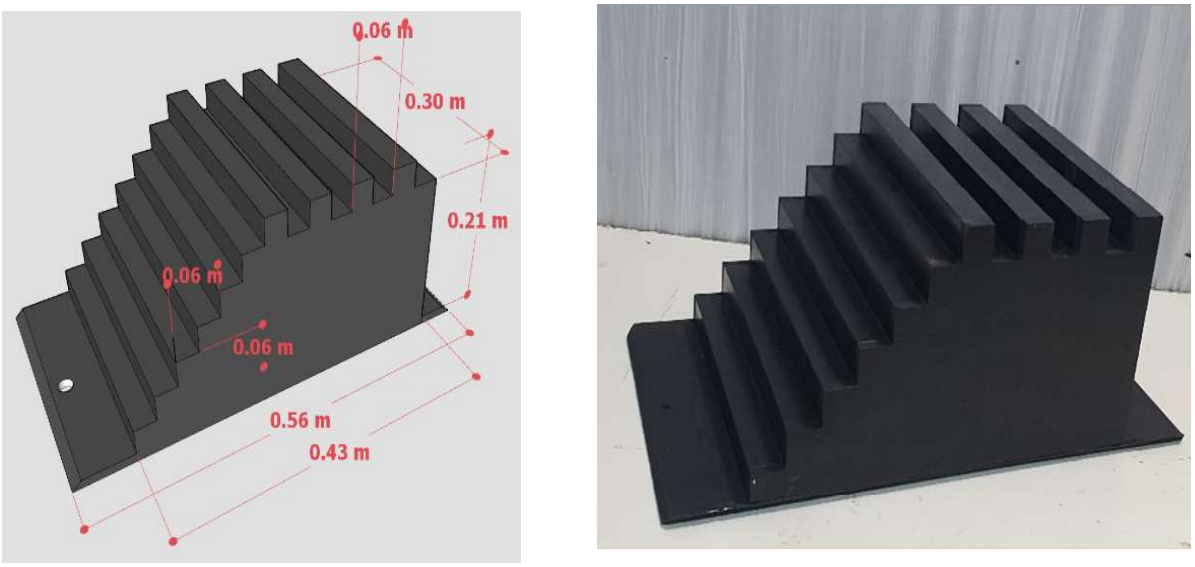

Figure (3.8) Sloped with steps (model Symbol M2)

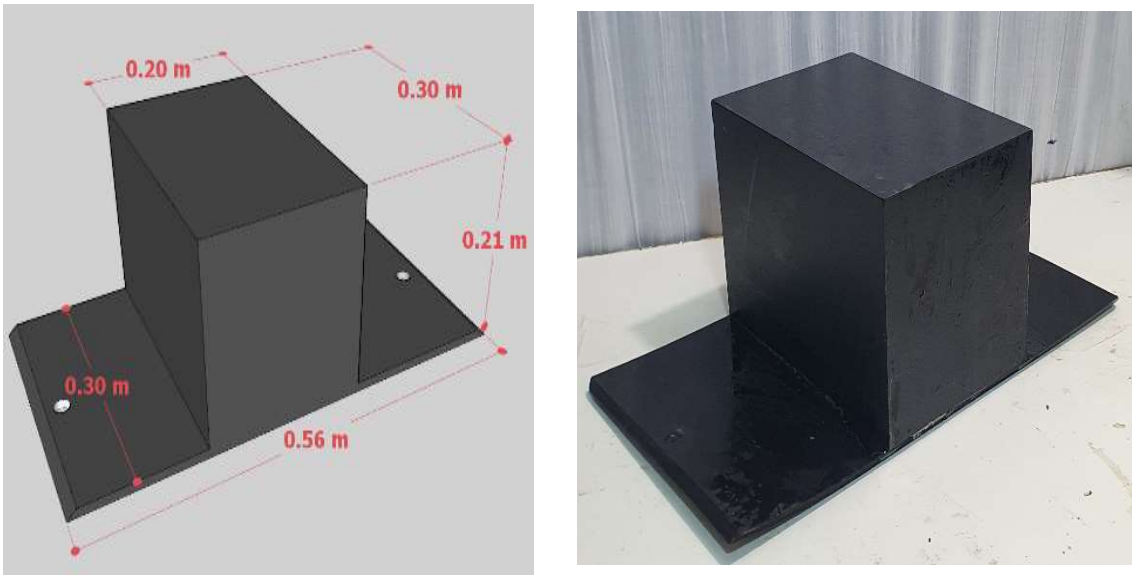

Figure (3.9) Rectangular (model Symbol M3)

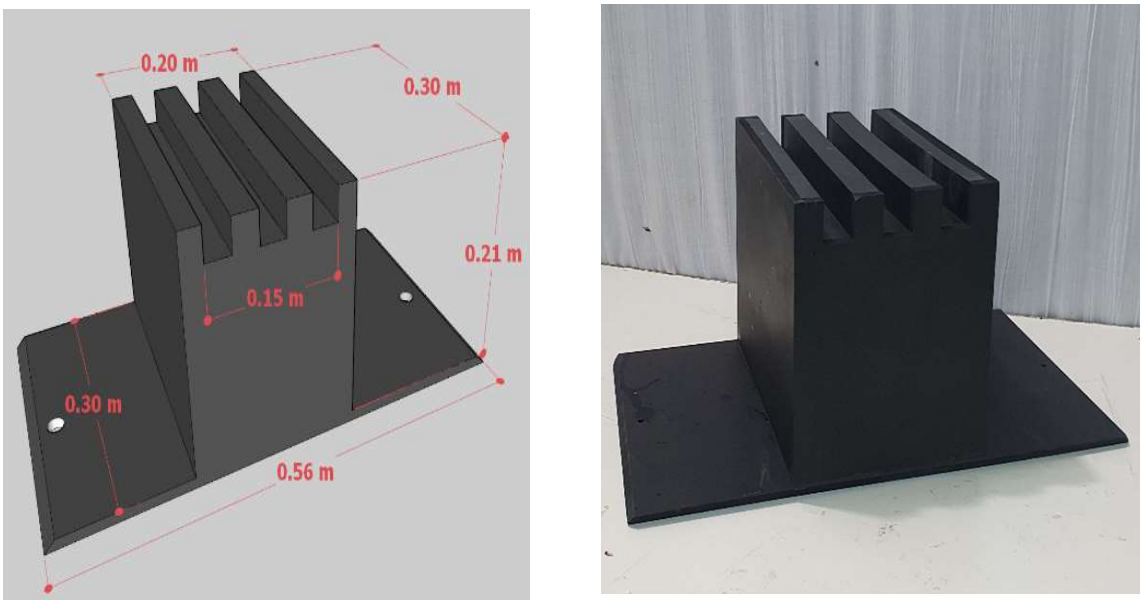

Figure (3.10) Rectangular with steps (model Symbol M4)

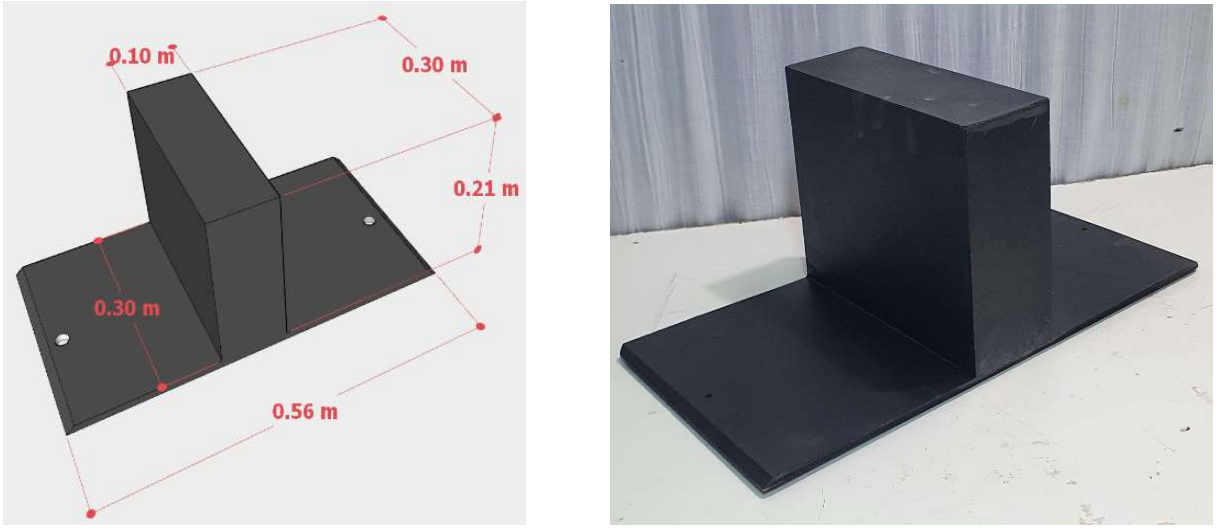

Figure (3.11) Rectangular narrow (model Symbol M5)

3.5 Constrain of Mode Dimensions

Hughes (1993) demonstrated that achieving precise similarity in model research is unachievable. In the context of large-scale models, it is observed that the prototype and the model exhibit more similarity, hence mitigating the influence of scale effects and the inaccuracies arising from the scaling of factors such as fluid density and viscosity. Nevertheless, it is crucial to acknowledge the significance of the economic benefits associated with small-scale models. Additionally, there are instances when the laboratory setting may be inadequate for conducting large-scale simulations. For instance, it is possible that the flumes may not have sufficient capacity to accommodate device like a wave generator. Therefore, min size models are chosen to align with the laboratory settings. Hence, in order to determine the optimal mode of scale, one must carefully evaluate the merits and drawbacks associated with both big and min-size models.

The constraints provided by the laboratory environment force the use of Fr and geometric similarities in breakwater model investigations. As a result, the model size is determined based on the following parameters.

- The experiment flume is capable of investigating the maximum water depths (45 cm).
- Motors Operation limits of the wave generator: (0. 5 Hz < Frequency < 0.783 Hz) or (30 RPM < Frequency < 47 RPM)
- Wave absorbing are adopted at distance 6 m in the downstream of breakwater
- According to the restricted width and height of flume the breakwater model height not exceeded 0.35 m

3.6 Equipment of measuring wave characteristic

The utilization of point gauges of wave hight or level measuring techniques enables the manual and precise measurement of the wave high in upstream and downstream side. The accompanying accessory is provided in its entirety with a single plain needle and a double needle. The illustration depicted in figure (3.12) displays a point gauge and its corresponding measurement system.

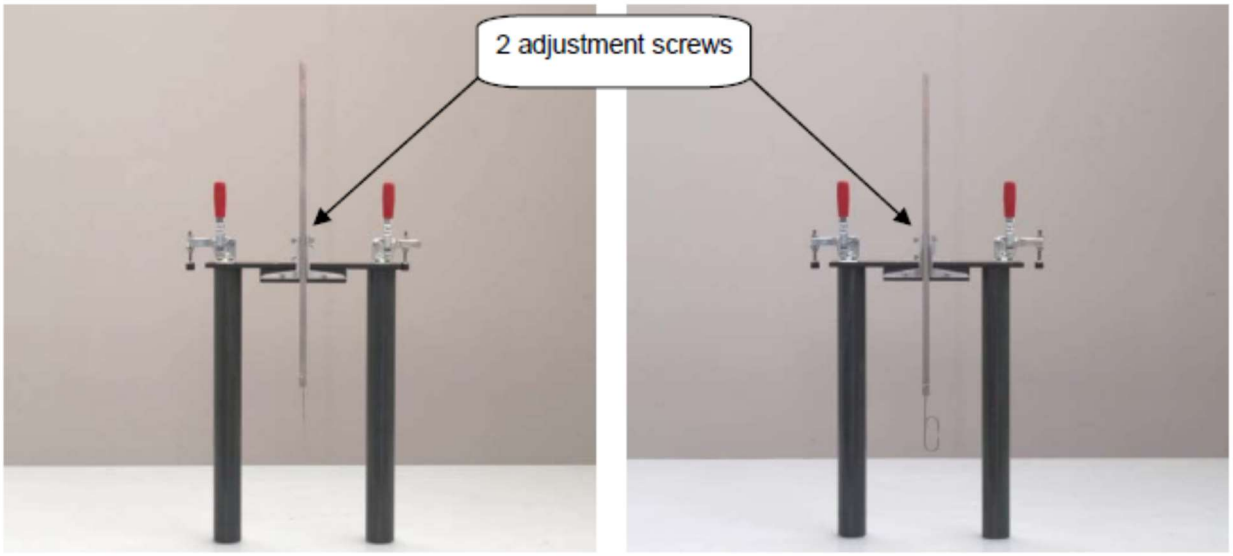

Figure (3.12) Piont gage used to mesured wave high

3.7 Experimental Procedure:

In the following steps, represented of each examination carried out in the laboratory to calculate the energy dissipations or transmission coefficient Ct of mitigation structures.

1. Installed the breakwater model and fixed in bottom of flume by hidden bolt
2. Installed the absorbing wave equipment in downstream side.
3. Start the pump to fill the flume to stall water level required (SWL)

4. Fixed the motor of wave generation with blade in upstream side
5. Set the motor speed to control the wave high required RPM
6. Measured the wave high in upstream breakwater and in downstream side.
7. Repeated the measurement : Three measurements were made for each experiment to ensure high accuracy and avoid error.

The following figures presented some of snap shot of experimental work in lab.

Figure (3.13) Wave propagated

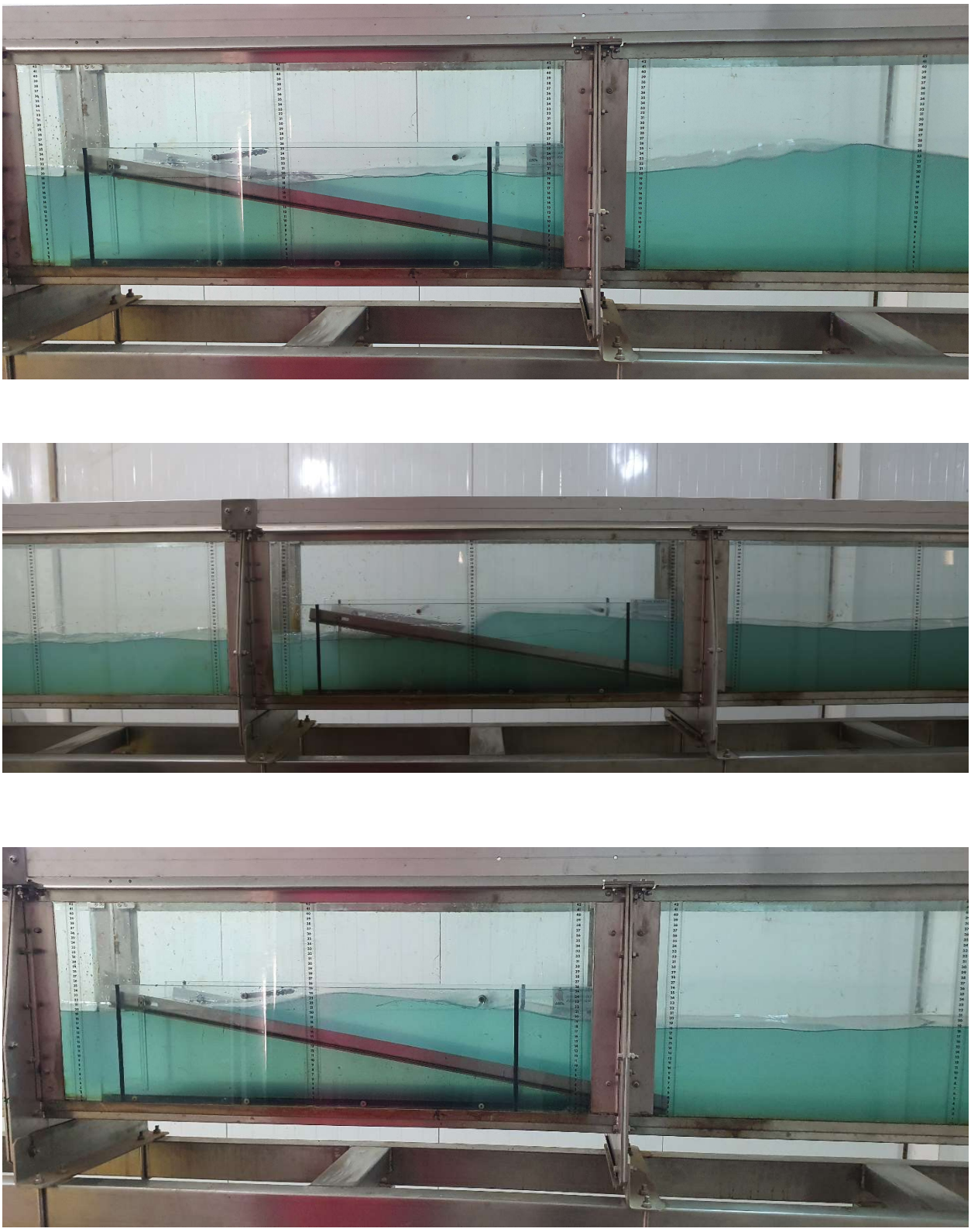

Figure (3.14) Wave runup over artificial absorbing zone

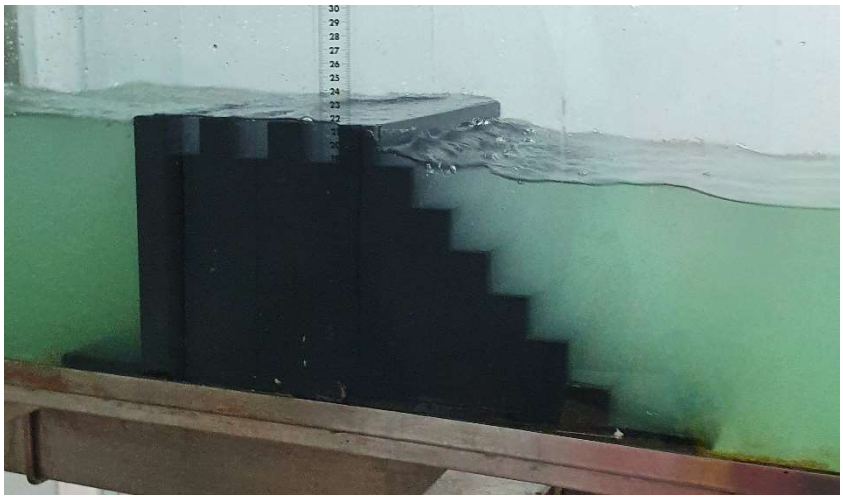

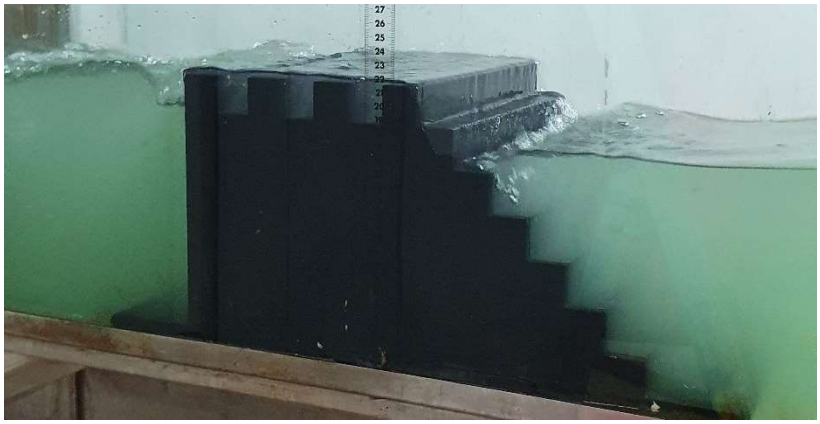

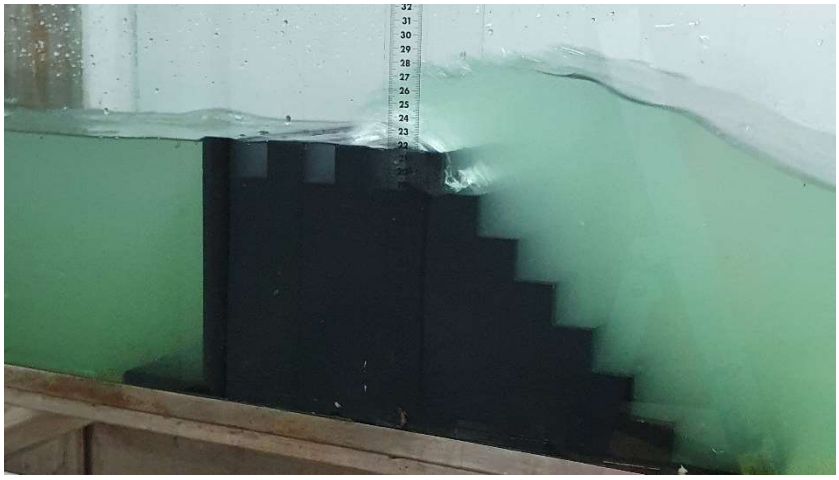

Figure (3.15) wave breaking near model M1

Chapter Four

Computational Fluid Dynamic

Chapter Four

Computational Fluid Dynamic

4.1 Introduction

This part of the research, intends to clarify and answer some of the questions concern about the Computational Fluid Dynamic **(CFD)**. Which is considered one of the most important cognitive sciences and the basis for modeling and simulation of fluid flow and in the specialty of hydraulic structures and Marine Science.

The field of Computational Fluid Dynamics **(CFD)** involves the utilisation of mathematical and physical problem formulation techniques, to simulate fluid engineering systems, numerical techniques such as discretization techniques, solvers, and grid generations are used. The procedure is depicted in Figure (4.1), Pre-processing, processing, and post-processing comprise **CFD**. The pre-processing stage is when the computational grid is built and the modelling objectives are established. The solver is launched in the second phase after setting the numerical models and boundary conditions. Solver continues to run until convergence is achieved. The post-processing phase, which begins at the solver's termination, involves reviewing the findings.

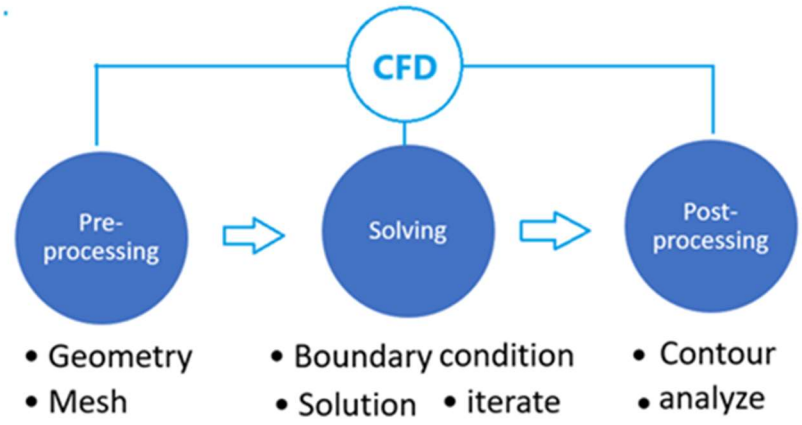

Figure (4.1) The CFD processing in three stages (Ansys. Fluent user guide)

The first step in CFD is to identify the optimal mathematical model for the issue, which is followed by the designation of the computational area of interest. Almost all commercial numerical solution programs begin with the early and crucial step of computational domain discretization, Figure (4.2) demonstrates the most steps in model by CFD **(ANSYS 17.2).**

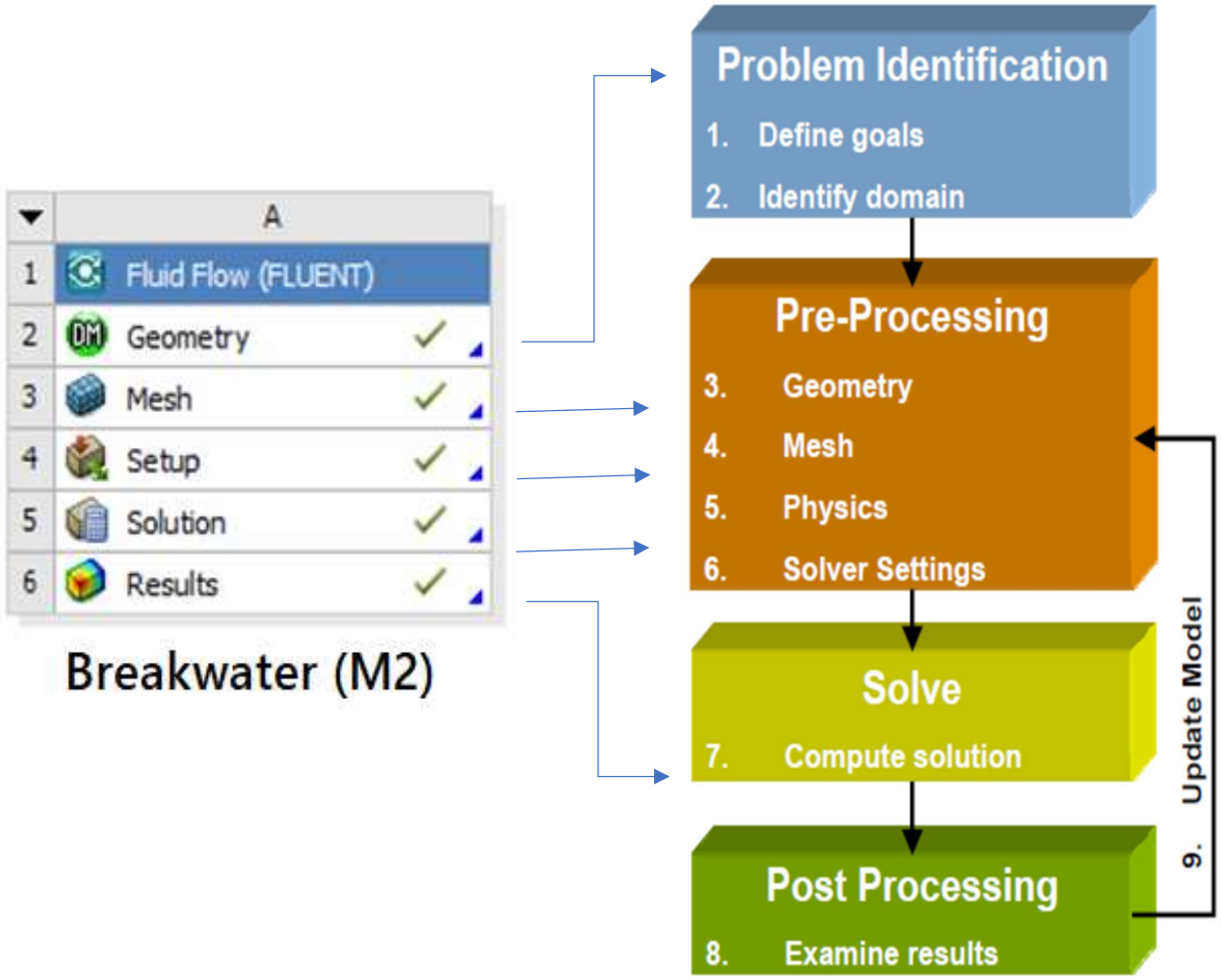

Figure (4.2) Stages for modeling by CFD (Ansys. Fluent user guide)

4.2 CFD Codes

Many codes are available for modeling CFD, such that **FLUENT**, **CFX**, **FLOW3D**, and **MIKE21 by DHI**. which is a computational fluid dynamic (CFD) tool. All these Codes are based on one theoretical principle and basis, which is the Naiver- Stock Equation. But they differ in terms of the limits of Use and the mathematical representation of the problem. In the present study **MIKE21** is used to modeling large scale model of depression Najaf Sea to capture the complexity of geometry. In addition, **FLUENT** was used to represent the capability of laboratory models to energy dispersion according to its shape, Figure (4.3) Demonstrated the CFD model.

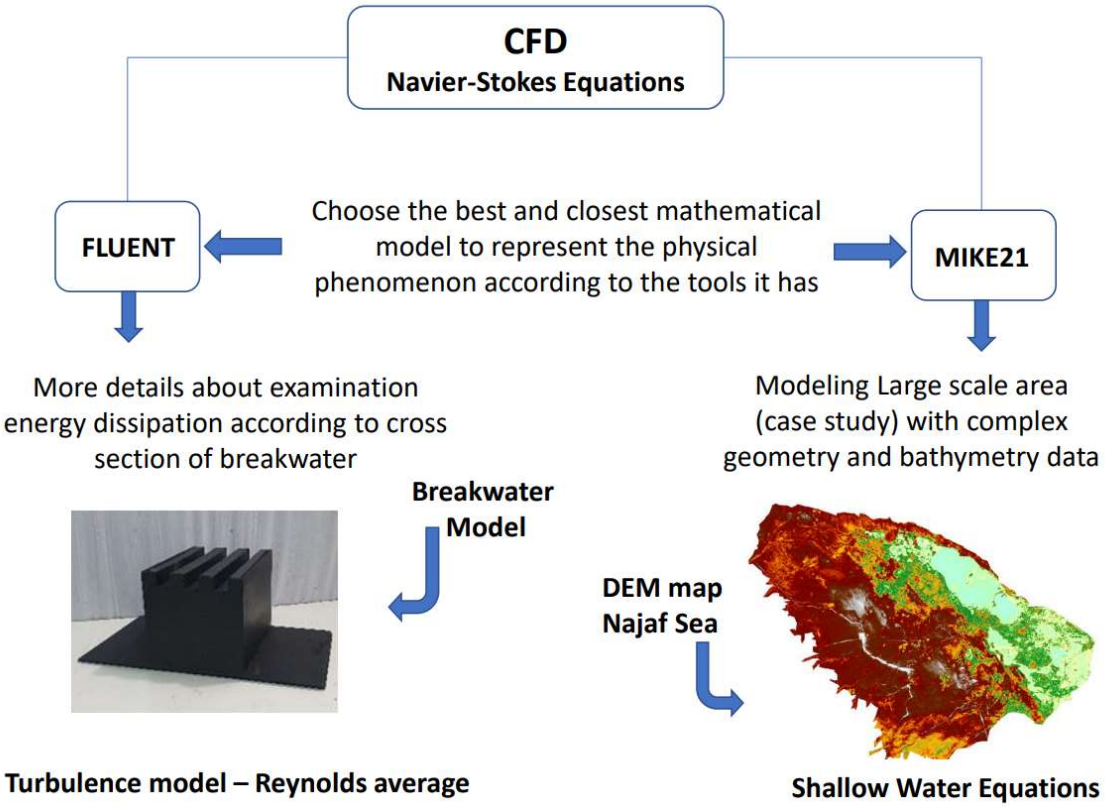

Figure (4.3) The CFD model (different codes Fluent, MIKE21)

4.3 FLUENT Solver

The present study, used the (VOF) formulation inside the FLUENT solver to construct a two-dimensional numerical model. The mathematical representation of the wave's nonlinearity and motion is established by the use of the Navier-Stokes Equation (2.20), alongside the continuity equation (2.22). It is supposed that the water under consideration is an incompressible, characterized by a constant density that remains unchanged across time, and Newtonian fluid.

So, in equation (2.20) the forces that make flow motion represented in the first part; the second part is about pressure and other forces; the third part is about how sticky the fluid is; and the fourth part is about any outside forces acting on the fluid.

4.3.1 Boundary Condition

This stage of preparing the model is very important because it determines the extent to which the physical phenomenon (waves) can be represented phasic of wave correctly. In present work, figure (4.4) shows all the boundary condition being used, the maintains zero velocity (no slip wall). Also, pressure outlet is set for the top boundary of the domain. A pressure outlet for the model top surface refer to atmospheric pressure. Absolute pressure less ambient pressure is known as static pressure or gauge pressure. The open channel option is used in the velocity inlet to model the free surface water level, which is small variation between (0.21 to 0.36m).

User Define Function (UDF) are used to model the wave condition flap type in the zone of wave generation. For the flap motion, a UDF file is created. The UDF code created in C++ language (Appendix -A). The code tries to define the motion of the flap through the following formula:

$$u_y = a\cos(\omega t) \qquad \text{..... (4.1)}$$

here a is the amplitude and ω is the angular frequency, t is defined through time step assigned in the solver, uy represents the axis of rotation in y direction which was required for the designed model. More information regarding the code is given in (Appendix A). For dynamic meshing, smoothing and remeshing is used.

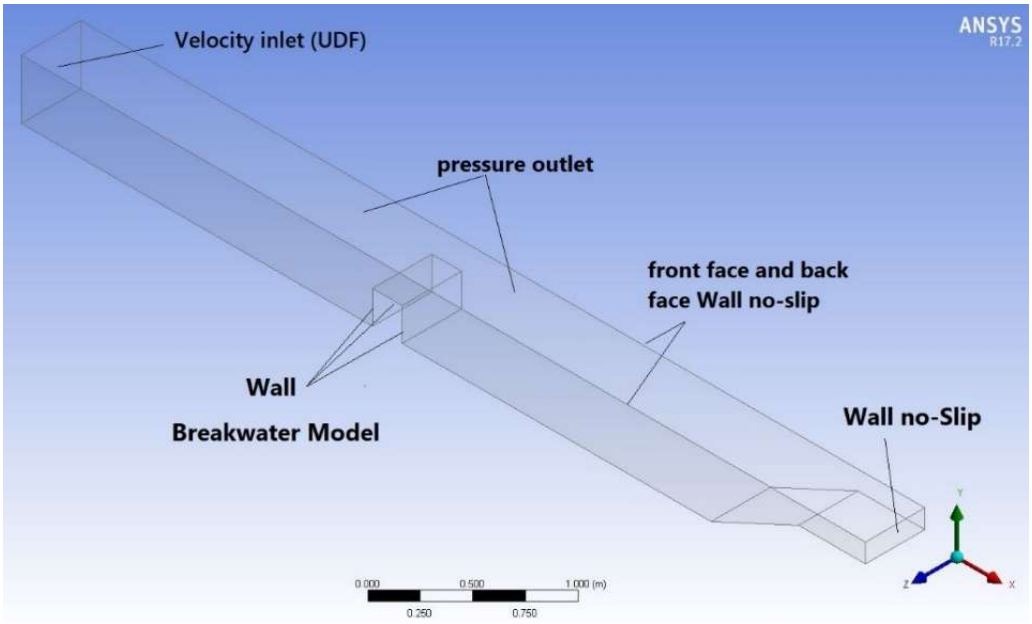

Figure (4.4) Boundary condition description

4.3.2 Setup and VOF

Volume of Fraction (VOF) it refers to model that described the interaction between air and water based on numerical discretised. VOF model are used in wide rang application in field of wave generation by described the line dividend the air and water. The transient is choosing of gravity-based model is used in this work. The volume fraction parameter is represented implicitly in the VOF model for simulation the phreatic surface of flow. Air water interaction are simulated as two phases used in the model with incompressible fluids, with constant densities 998 Kg/m^3 for the water and 1.225 kg/m^3 for the air. It is recommended to use K-omega viscous models for turbulent open channel flows. The SST k-omega viscous model is used in this

experiment to produce waves. Choose the boundary conditions in modelling wave theory is very sensitive to some parameters such as, wave steepness, and wave height to length. The appropriate wave model according to simulation condition, ranging from shallow to deep sea conditions, were outlined in DNV RP C 205 (2010), a recommended code of practice similar to FLUENT. All numerical simulations for inlet boundary are selected as velocity inlet Stokes' and a shallow/intermediate wave boundary condition.

4.3.3 Mesh Independence solution

The mesh quality has a substantial impact on the accuracy and stability of numerical calculations. The attributes of grid distribution, refinement, and skewness are interrelated factors that contribute to the overall quality of a mesh. (ANSYS .2010). Incorrect mesh selection can have an impact on simulation accuracy, computational efficiency, and solution stability. Several literature sources and studies have indicated that a model must be designed with 200 grids per wavelength as a minimum grid discretised, as stated by **Arun Kamath in 2012**. Additionally, appropriate wave generation may be achieved if the aspect ratio of an element is less than 10, as suggested by **Marques**. In the current work, element length 0.005 m is adopted to create waves with a maximum wavelength of 1.5 m. As a result, all of the tests are run with a mesh size of $25*10^{-6}$ m^2 and grid aspect ratio of mesh are selected to one, figure (4.5) represent grid discretised for rectangular breakwater model. Table (4.1) Demonstrates the five seniors to examination the mesh independent solution to minimized error and reach the convergences of solution according to the grids size and number of elements in model.

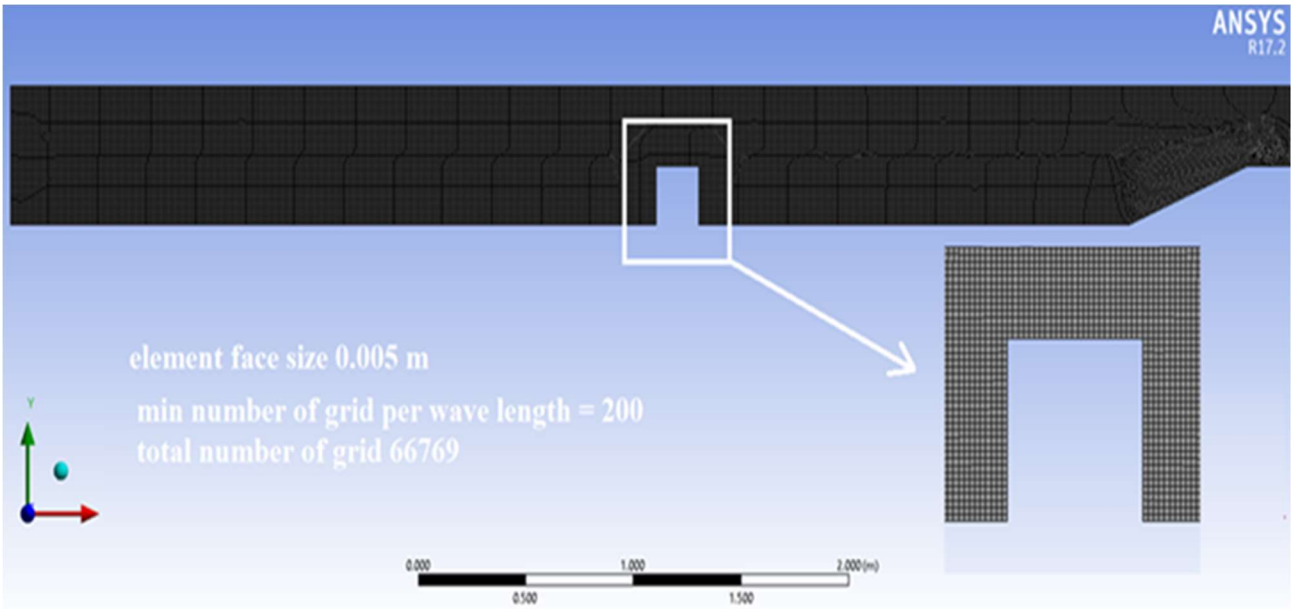

Figure (4.5) mesh description and specification

Table (4.1) mesh sensitivity analysis for minimize error

Scenario	Grid size(m)	Grid per wave length	Total element in model	Transmission coefficient Ct
1	0.004	325	89756	0.61
2	0.005	260	71980	0.61
3	0.006	216	59455	0.70
4	0.007	185	52890	0.78
5	0.008	162	48434	0.81

4.3.4 Adaption process for mesh refinement

One of the most powerful tools that FLUENT provides is to identify the areas that need to smooth the grid according to the initial solution by identifying the areas that have a high gradient slope cheeked by the specified variable such as speed, pressure or another variable. although a mesh must be refined where flow features change rapidly, Figure (4.6) shows technics in FLUENT for mesh adaption.

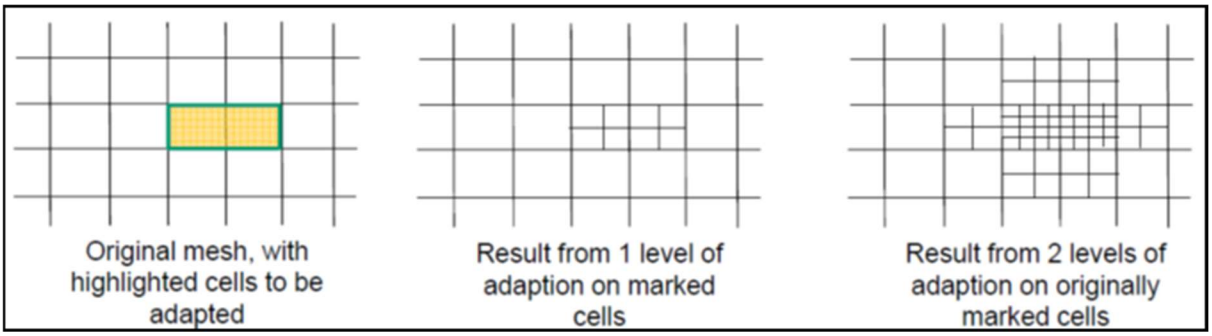

Figure (4.6) Mesh adapted specification (ANSYS 17.2, Fluent Solver)

4.3.5. Convergence of solution and stability

One of the most important criteria for accepting a numerical solution by CFD modelling is the arrival of the solution to the state of stability and convergence, which indicates that any addition or more time steps has very little or no effect on final results. Figure (4.7). Demonstrated residual verse iteration for 9 second duration. The solution reaches the limit of stability after 7000 iteration with time steps 0.01 sec.

Figures (4.8), (4.9), (4.10), and (4.11) Represent stages of free surface variations with wave period 1 sec and reach the stability after 7000 iteration with time steps 0.01 sec that reach 8.2 sec flow duration, and make the wave characteristic identical.

Stability of solution are important to minimized error, residual verse iteration represented monitored of the solution process to reach the final result and keep all the parameters at minimum .

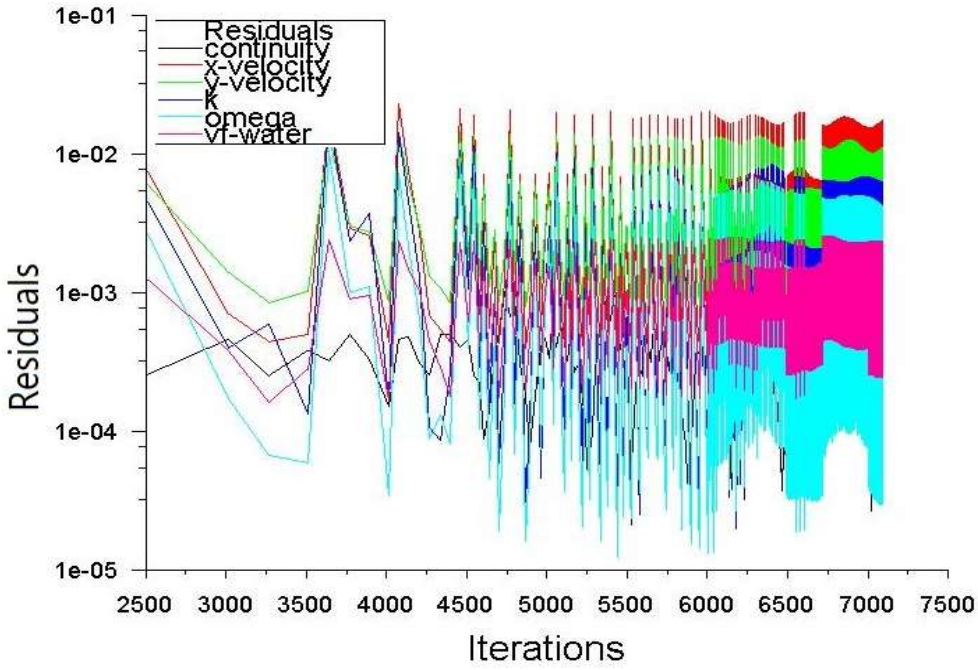

Figure (4.7) Residuals verse iterations for solution monitor

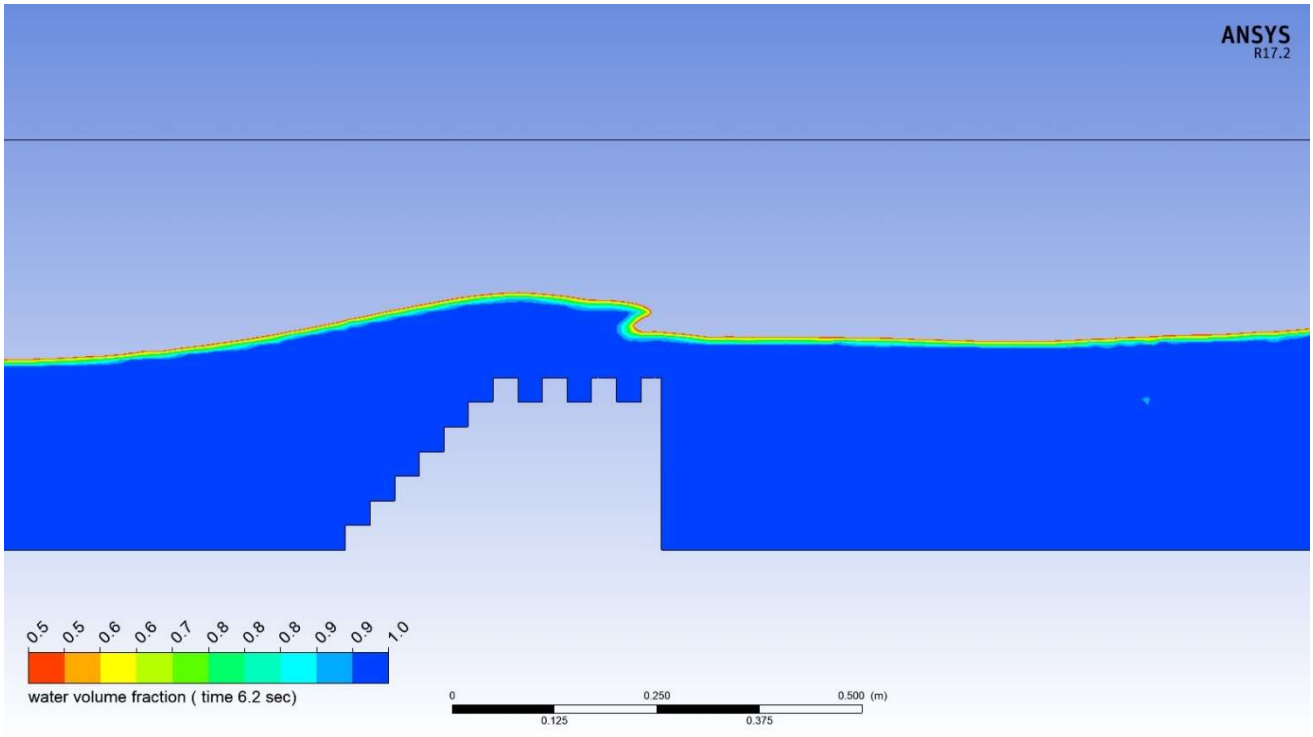

Figure (4.8) free surface profile at time 6.2 sec (solution no converge yet)

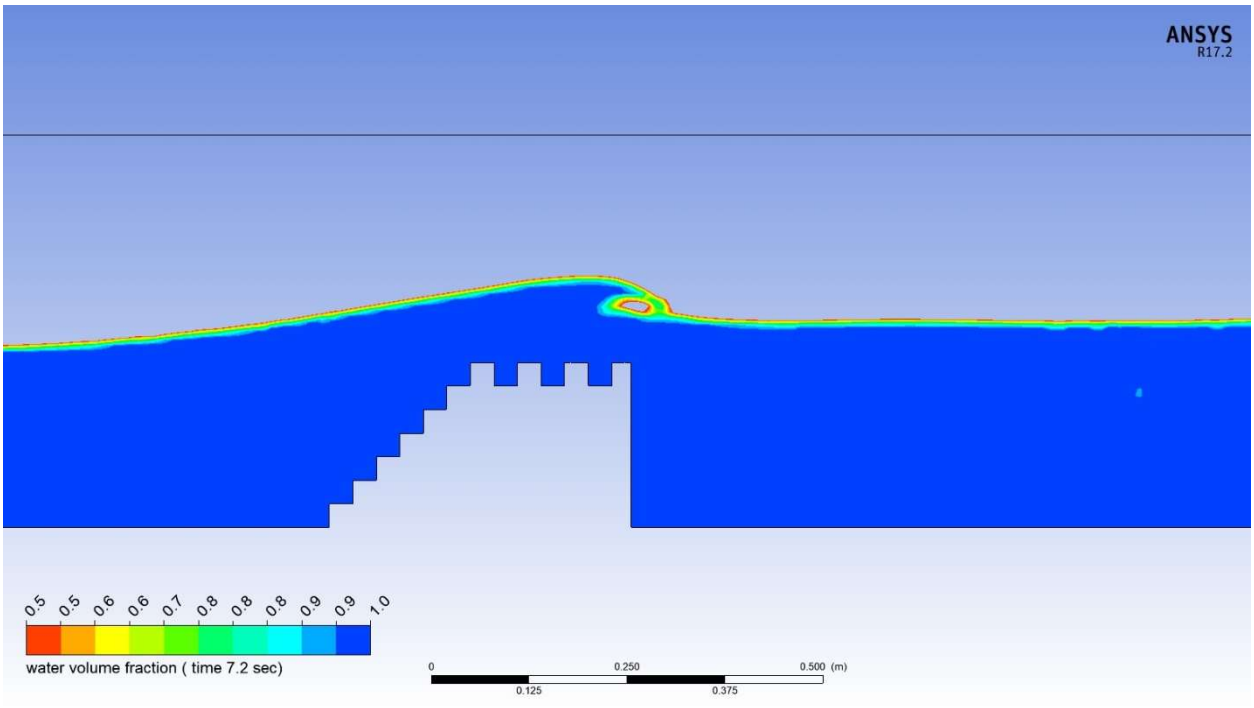

Figure (4.9) free surface profile at time 7.2 sec (solution no converge yet)

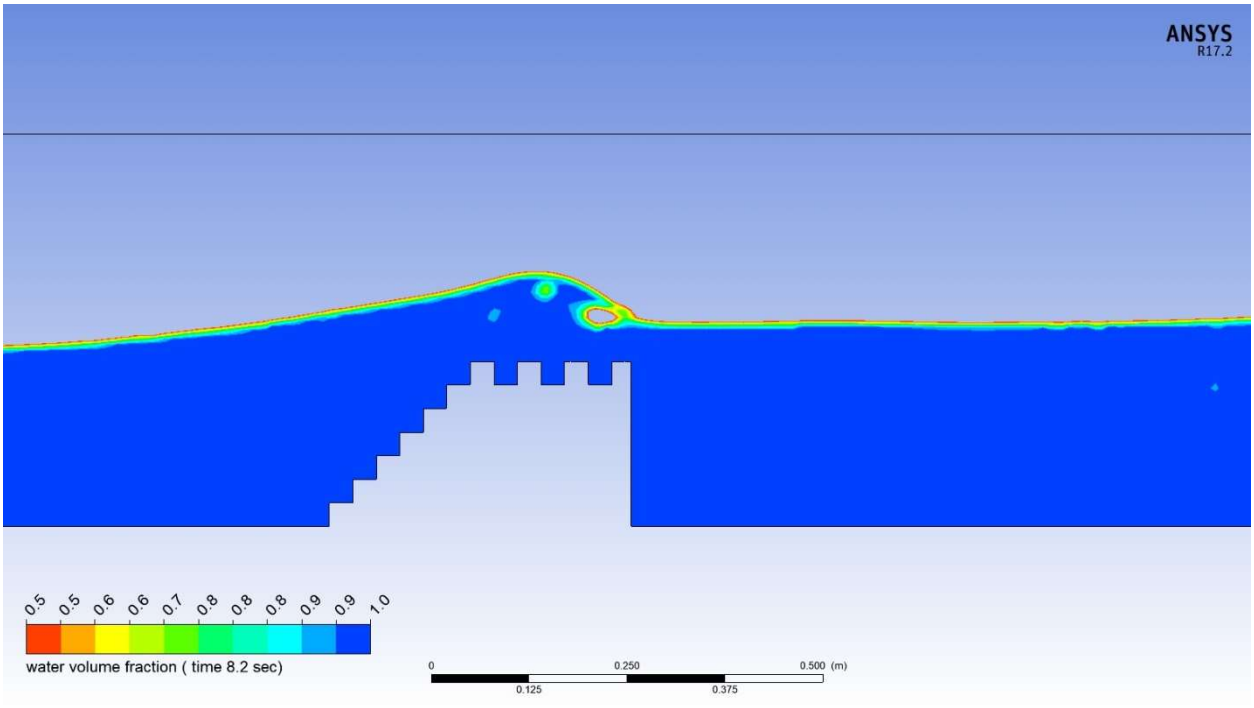

Figure (4.10) free surface profile at time 8.2 sec (solution reach converges)

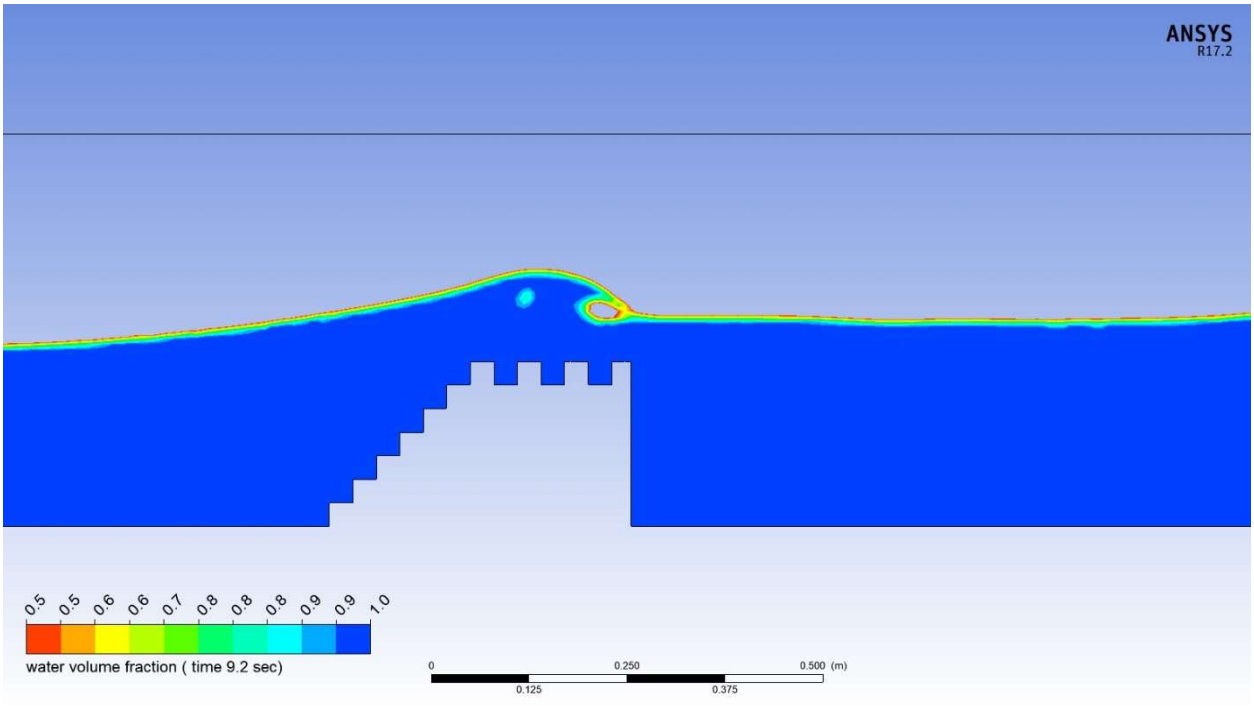

Figure (4.11) free surface profile at time 9.2 sec (solution converges)

4.4 MIKE21 Solver

MIKE 21 is a sophisticated numerical software designed for simulating coastal hydrodynamics. it is applicable to a wide range of coastal and marine environments, including oceans, bays, estuaries, and lakes. Due to the intricate nature of the programme, it necessitates a multitude of parameters. Simultaneously, it has the capability to offer a more accurate depiction of the authentic environmental circumstances.

Several numerical codes provided by the MIKE21, such as MIKE21 SW, MIKE21 Flow HD, MIKE21 ST, and MIKE 3 this is a 3D modeling program. Among all these codes mentioned the MIKE21 SW model adopts to modelling spectral wave for long period (1979-2023) in the Bahr Annajaf as a case study. This code its suitable for modelling large scale model. The wave spectrum model

"MIKE21 SW, which is used mass conservation for a bases concept, and can handle a variety of situations, including wind waves, nonlinear waves interactions, whitecaps loss, friction loss caused by bottom, wave breaking, and reflections and diffractions, shallow water deformations", **(DHI, M. 2017).**

MIKE21 model employs a central differentiation method inside limited volumes to discretize the system. Depending on bathymetric and topography conditions, unstructured and structured discretized have been used. The model has the capability to continuously adjust time step in response to changes in stability conditions. Several sequence explicit methods and a stepwise integral in time are used in this model to calculate wave transport.

4.5. Mathematical Model build-up (MIKE21SW)

The following figure (4.12) represents the stages commonly make up the model check list when using the newest generation spectral wind-wave models in MIKE21 SW to forecast the wind waves, decline, refraction, diffraction, coastal environments, and offshore conditions:

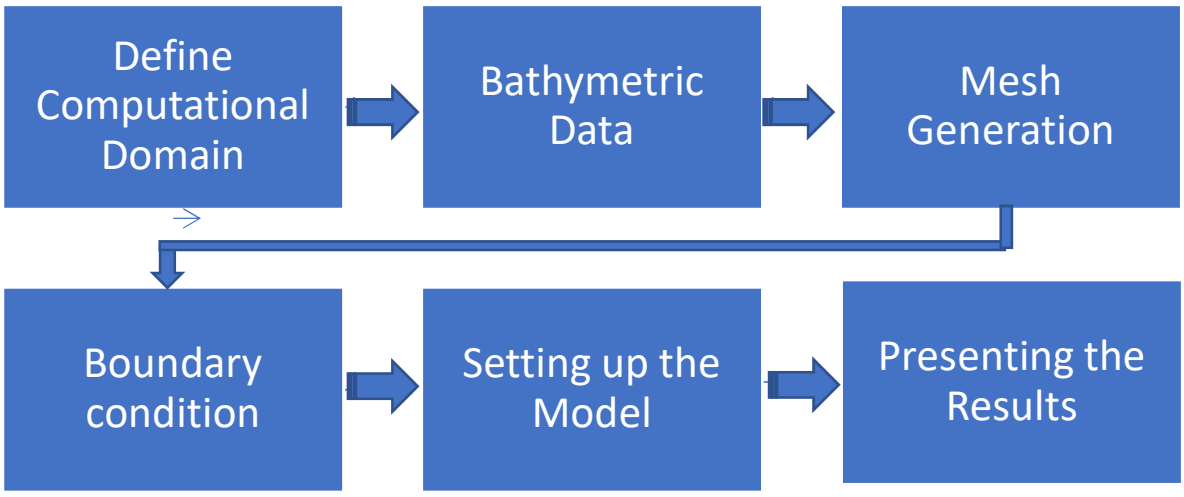

Figure (4.12) Steps of build-up MIKE21 SW model

Chapter Five

Discussion Result of CFD and Experimental

Chapter Five

Discussion of CFD and Experimental Results

5.1 Introduction

In this chapter, the experimental results of the different types of breakwater model will be presented in addition to the results of the mathematical model that is explained in detail in the previous chapter. It is necessary to compare the experimental results with the results of the **CFD** model in order to find out the extent of the possibility of using the mathematical model in modeling the optimal cross section of the breakwater, specific to the study area (for the study situation in the next chapter). The output obtained from the laboratory work was represented by calculating the value of the wave transmission coefficient Ct. The value of this coefficient was calculated for different states of breakwater and for multiple wave characteristics.

5.2 Free surface profile (CFD and Experimental)

One of the real considerations for adopting the mathematical model is to verify the accuracy of the results drawn from this model by comparing it with the laboratory results. The attached Figures (5.1), and (5.2) show the compatibility of the experimental results and the mathematical model, by tracking the free flow surface for different breakwater shape. Have to note from these Figures a very large convergence between the CFD model and the experimental result.

Figure (5.3) (5.4) show the generation of waves with time in the CFD model at time 0 second to 10 second for rectangular and step slope shape breakwater.

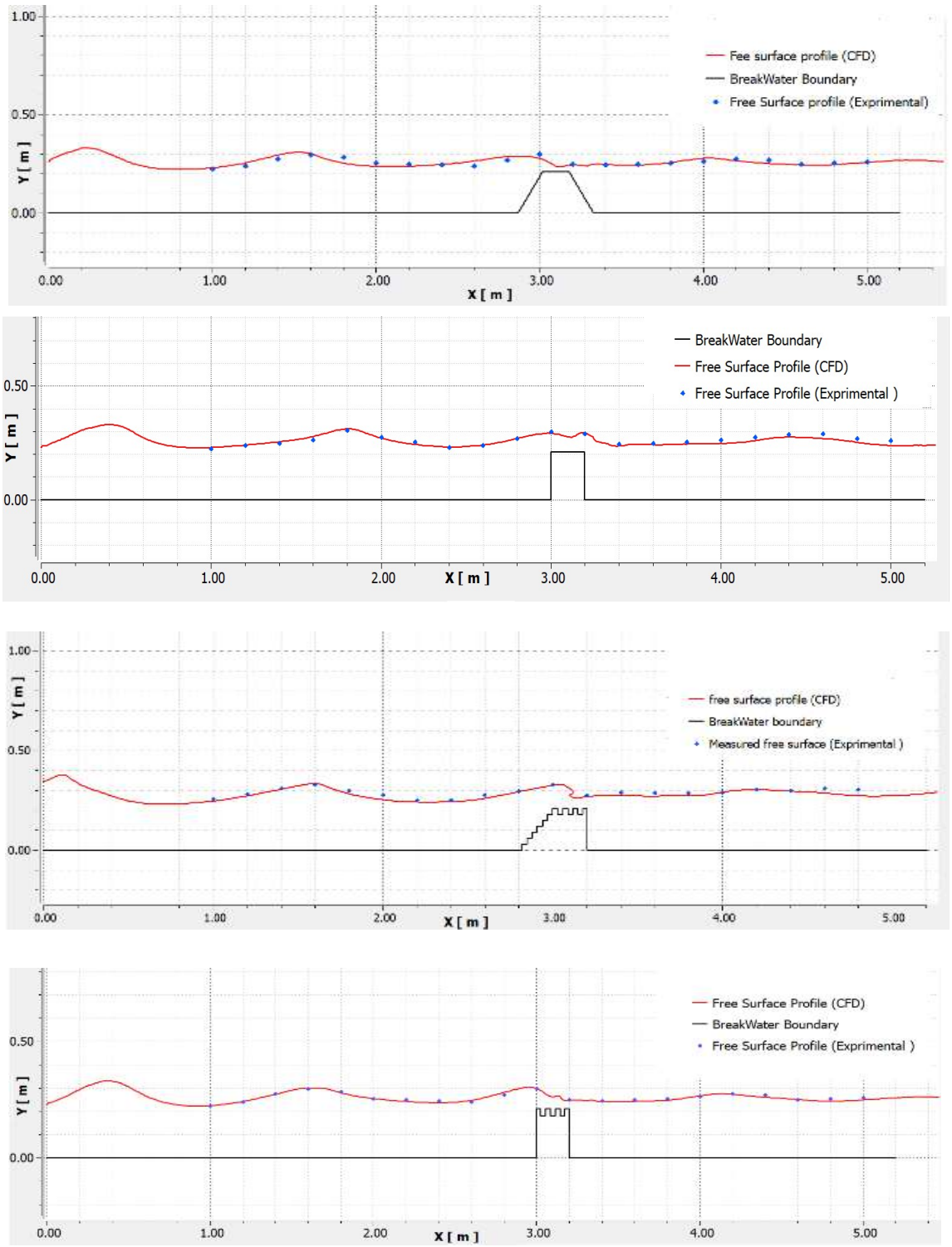

Figure (5.1) free surface profile for experimental and CFD results for different breakwater model (Run 20, Hs = 10 cm)

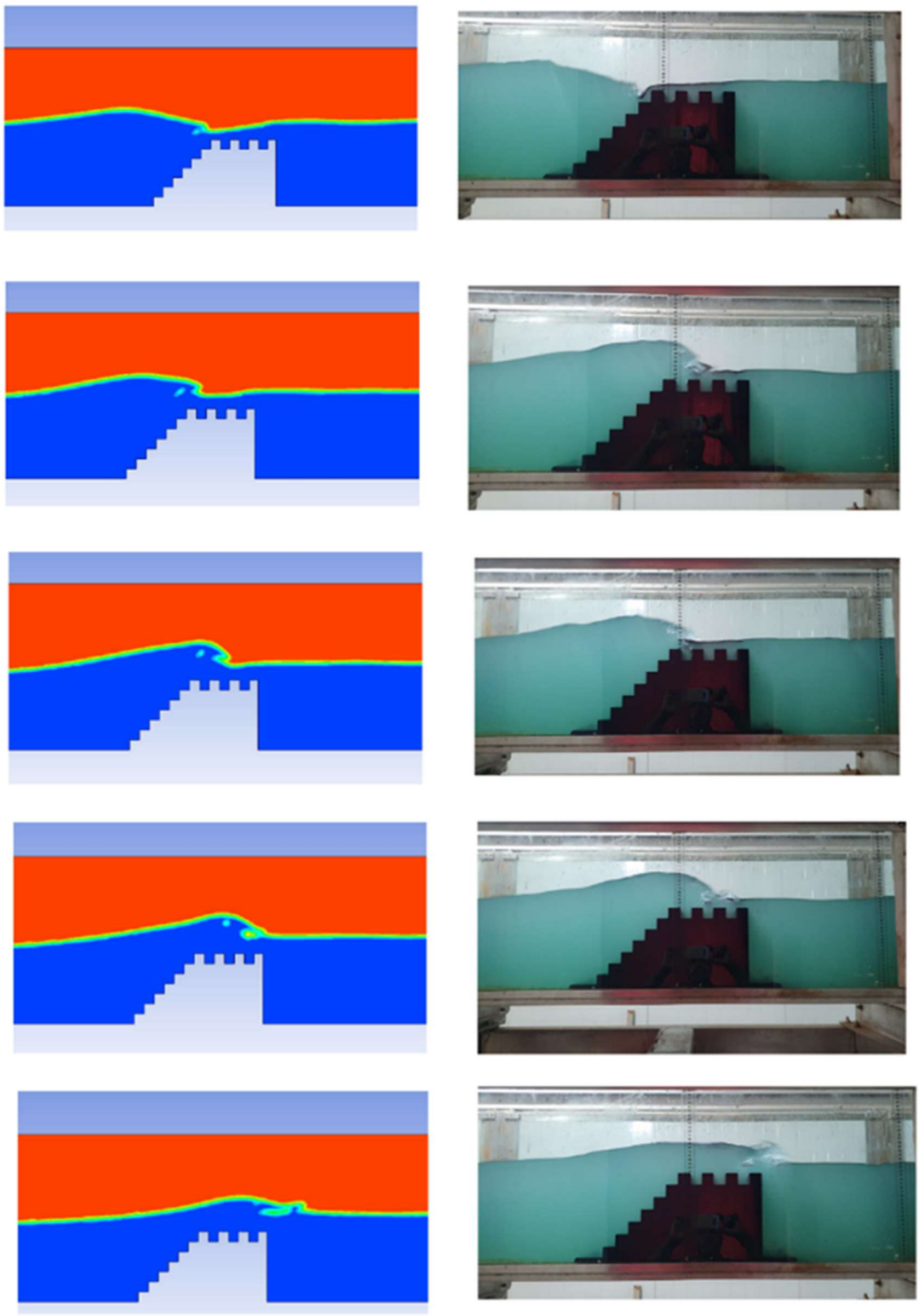

Figure (5.2) Compression for experimental and CFD model to represent the compatibility of result for flow time from 8.1 second to 8.5 second (Run 20)

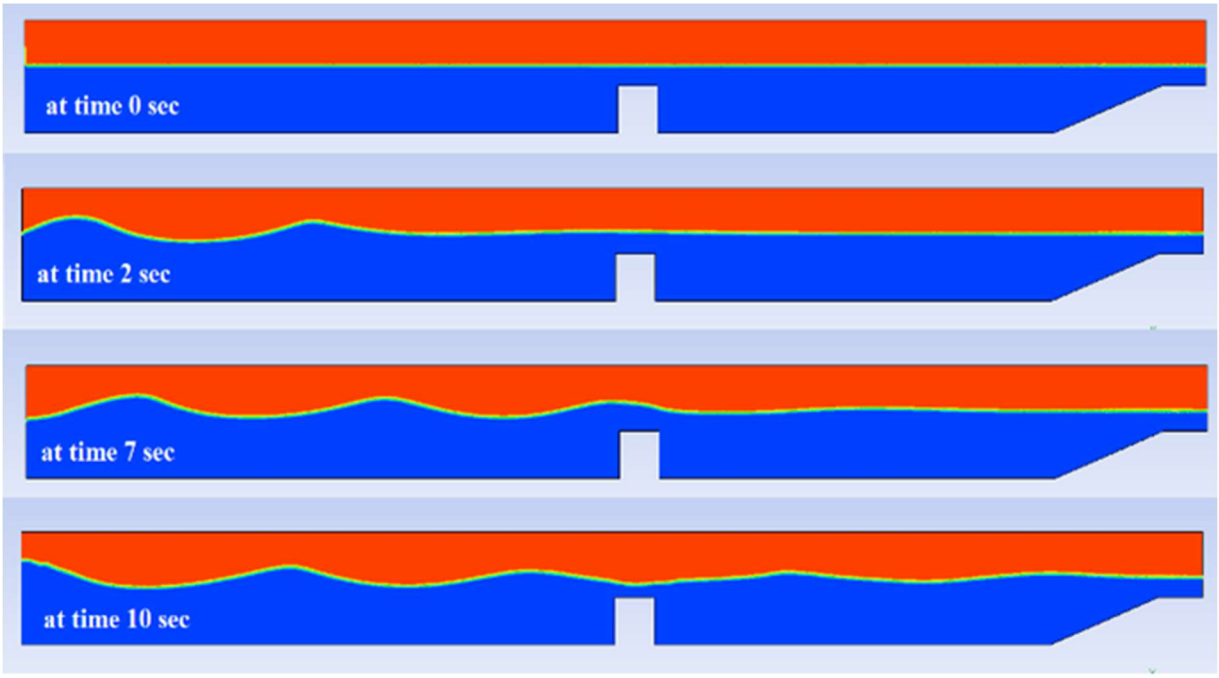

Figure (5.3) wave generation according to time (0 sec to 10 second) rectangular shape breakwater

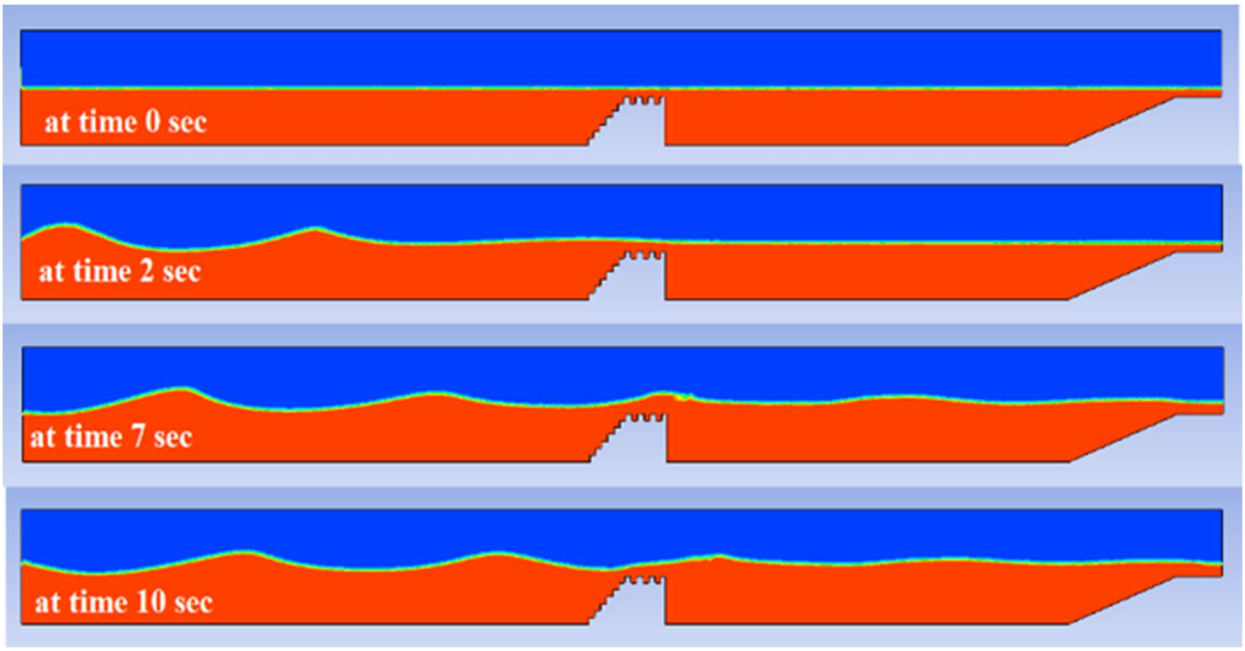

Figure (5.4) Wave generation according to time (0 sec to 10 second) slope steps shape breakwater

5.3 Transmission coefficient (Ct)

The most important coefficient that gives an impression of how efficiently the breakwater disperses energy is C_t. Figures (5.5), (5.6), (5.7) and (5.8) show that the different wave characteristic variations according to different breakwater model. Tables (5.1),(5.2),(5.3),(5.4)and (5.5) explain the variation in the value of the energy dissipation coefficient with respect the shapes of the breakwaters, as well as some variables related to the wave characteristics are changed such as wave length and wave steepness (Hi/L).

It can be seen from these Figures and Tables, the maximum energy dissipation (1- Ct) (minimum transmission coefficient) is received for sloped steps model M2, it is clear that the eddy turbulence frequency for M2 model shows the more energy dissipation at steps. The minimum energy dissipation (1-Ct) (maximum transmission coefficient is received for narrow rectangular model M5.

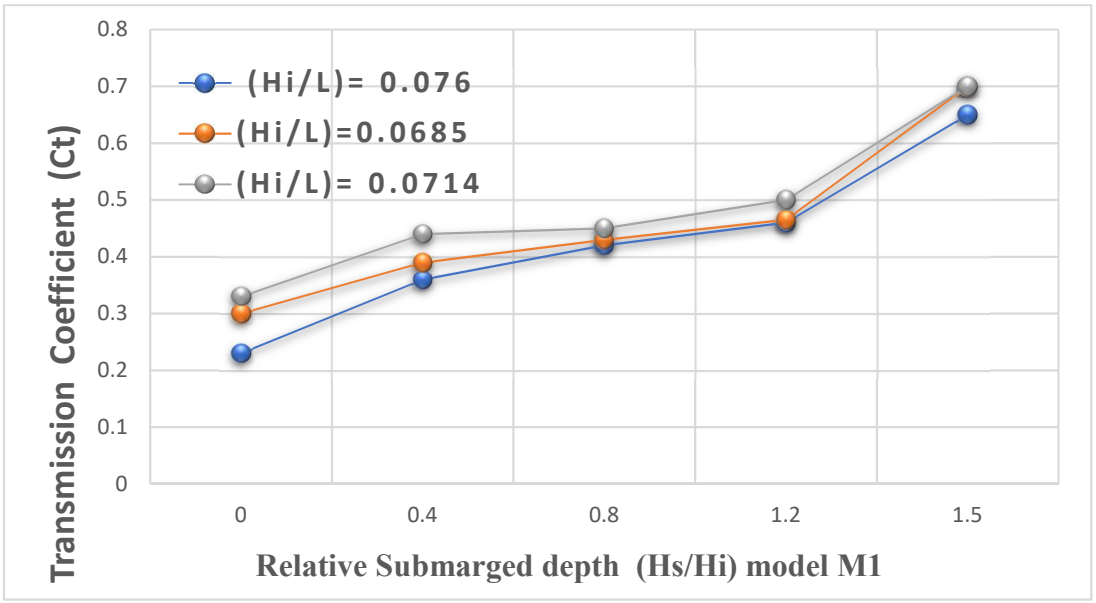

Figure (5.5) Variation of Ct according to wave steepness and relative submerged depth and Hi

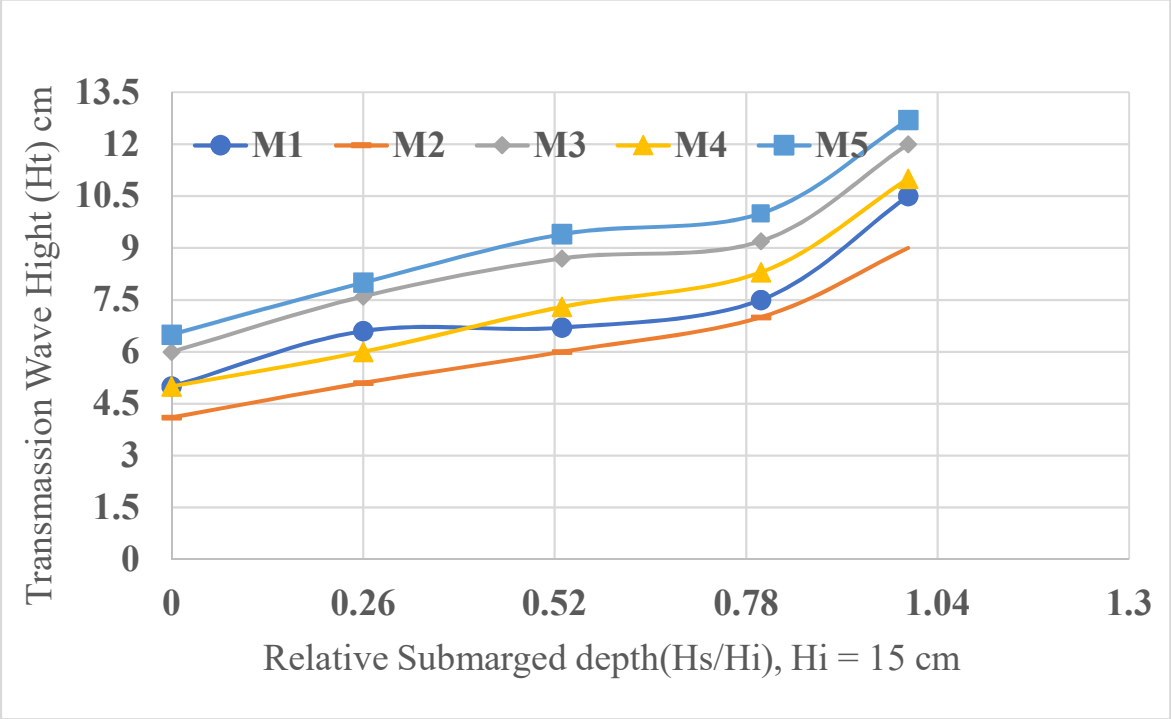

Figure (5.6) Variation of Ht according to relative submerged depth and, constant Hi = 15 cm

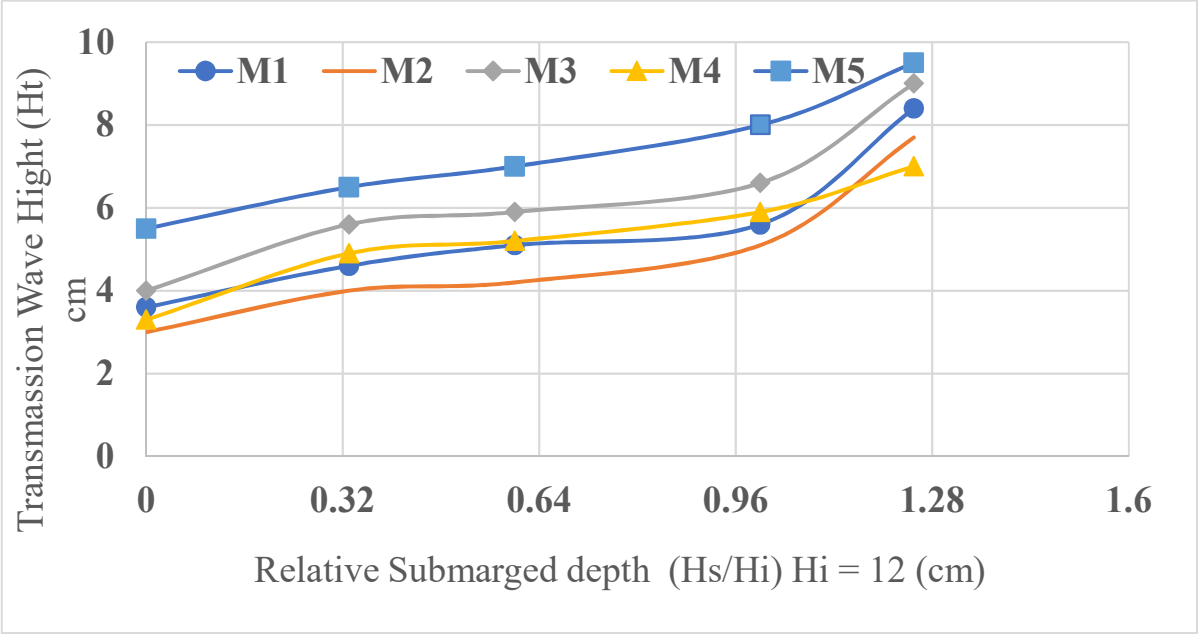

Figure (5.7). Variation H_t according to relative submerged depth and, constant H_i = 12cm

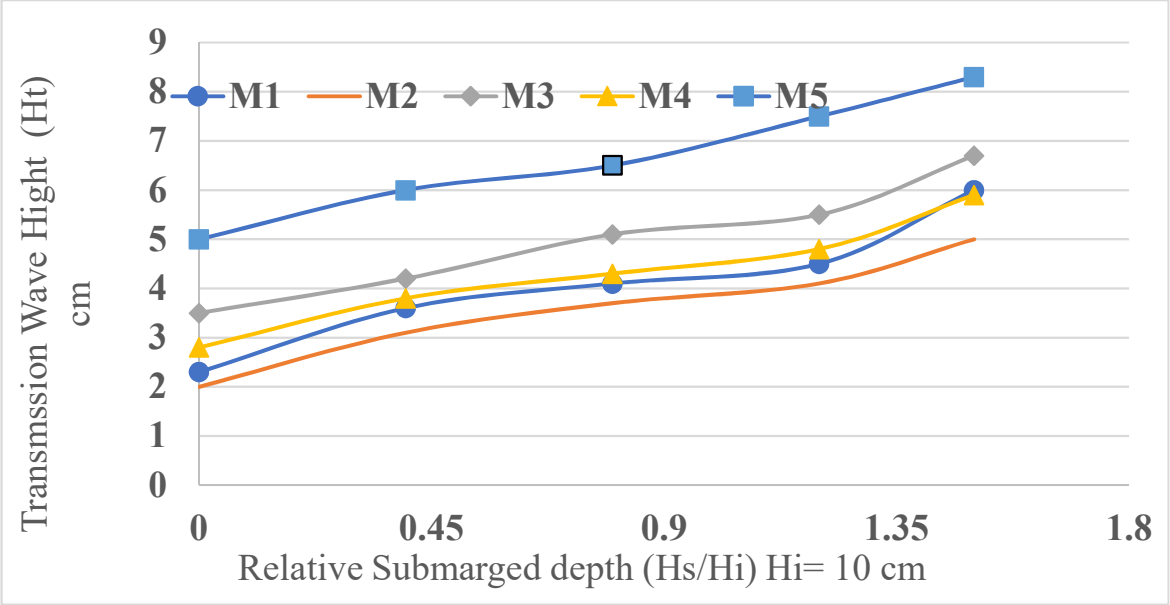

Figure (5.8) Variation of H_t according to relative submerged depth and H_i constant = 10 cm

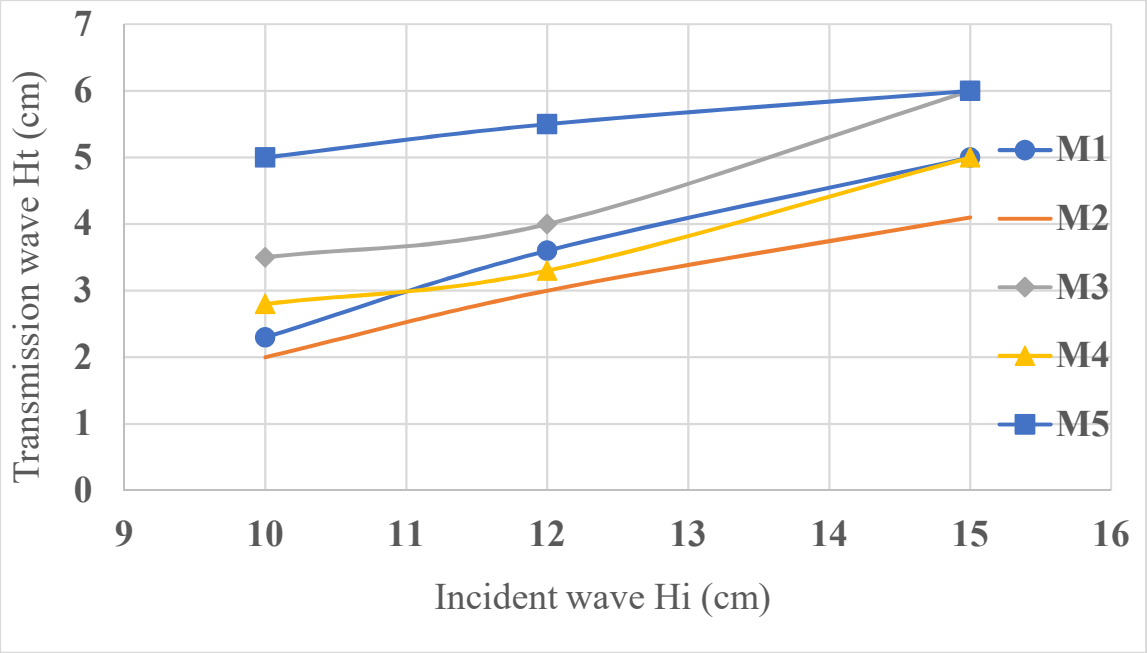

Figure (5.9) Variation of H_t according to wave incident depth H_i for different breakwater model

Table (5.1) Transmission coefficient (Ct) for different breakwater model (M1)

Model	RPM	Length 0f wave	Period T (sec)	Experimental measurement (cm)					(Ct) =(Ht/Hi)	
				Wave steepness (Hi/L)	Hs	Hi	Hs/Hi	Ht	Experimental	CFD
M1	30	1.3 m	0.75	0.0769	0	10	0	2.3	0.23	0.23
					4		0.4	3.6	0.36	0.33
					8		0.8	4.1	0.41	0.37
					12		1.2	4.5	0.45	0.41
					15		1.5	6	0.6	0.66
	35	1.75m	1	0.0685	0	12	0	3.6	0.3	0.26
					4		0.33	4.6	0.39	0.37
					8		0.6	5.1	0.43	0.39
					12		1	5.6	0.465	0.41
					15		1.25	8.4	0.7	0.66
	47	2.1 m	1.15	0.0714	0	15	0	5	0.33	0.39
					4		0.26	6.6	0.44	0.4
					8		0.53	6.7	0.45	0.39
					12		0.8	7.5	0.5	0.5
					15		1	10.5	0.7	0.73

Table (5.2) Transmission coefficient (Ct) for different breakwater model (M2)

Model	RPM	Length 0f wave	Period T (sec)	Experimental measurement(cm)					(Ct) =(Ht/Hi)	
				Wave steepness (Hi/L)	Hs	Hi	Hs/Hi	Ht	Experimental	CFD
M2	30	1.3 m	0.75	0.0769	0	10	0	2.0	0.2	0.23
					4		0.4	3.1	0.31	0.33
					8		0.8	3.7	0.37	0.35
					12		1.2	4.1	0.41	0.39
					15		1.5	5	0.5	0.47
	35	1.75m	1	0.0685	0	12	0	3.0	0.25	0.26
					4		0.33	4.0	0.33	0.36
					8		0.6	4.2	0.35	0.32
					12		1	5.1	0.425	0.40
					15		1.25	7.7	0.64	0.61
	47	2.1 m	1.15	0.0714	0	15	0	4.1	0.27	0.25
					4		0.26	5.1	0.34	0.32
					8		0.53	6.0	0.4	0.36
					12		0.8	7.0	0.46	0.411
					15		1	9	0.6	0.56

Table (5.3) Transmission coefficient (Ct) for different breakwater model (M3)

Model	RPM	Length 0f wave	Period T (sec)	Experimental measurement (cm)					(Ct) =(Ht/Hi)	
				Wave steepness (Hi/L)	Hs	Hi	Hs/Hi	Ht	Experimental	CFD
M3	30	1.3 m	0.75	0.0769	0	10	0	3.5	0.35	0.33
					4		0.4	4.2	0.42	0.39
					8		0.8	5.1	0.51	0.47
					12		1.2	5.5	0.55	0.52
					15		1.5	6.7	0.67	0.65
	35	1.75m	1	0.0685	0	12	0	4	0.33	0.29
					4		0.33	5.6	0.46	0.41
					8		0.6	5.9	0.49	0.45
					12		1	6.6	0.55	0.51
					15		1.25	9.0	0.75	0.69
	47	2.1 m	1.15	0.0714	0	15	0	6	0.4	0.4
					4		0.26	7.6	0.50	0.46
					8		0.53	8.7	0.58	0.53
					12		0.8	9.2	0.61	0.58
					15		1	12	0.8	0.72

Table (5.4) Transmission coefficient (Ct) for different breakwater model (M4)

Model	RPM	Length 0f wave	Period T (sec)	Experimental measurement(cm)					Ct =(Ht/Hi)	
				Wave steepness (Hi/L)	Hs	Hi	Hs/Hi	Ht	Experimental	CFD
M4	30	1.3 m	0.75	0.0769	0	10	0	2.8	0.28	0.24
					4		0.4	3.8	0.38	0.39
					8		0.8	4.3	0.43	0.43
					12		1.2	4.8	0.48	0.45
					15		1.5	5.9	0.59	0.53
	35	1.75m	1	0.0685	0	12	0	3.3	0.275	0.29
					4		0.33	4.9	0.41	0.45
					8		0.6	5.2	0.433	0.48
					12		1	5.9	0.5	0.51
					15		1.25	7	0.59	0.54
	47	2.1 m	1.15	0.0714	0	15	0	5	0.33	0.34
					4		0.26	6	0.4	0.44
					8		0.53	7.3	0.486	0.5
					12		0.8	8.3	0.55	0.56
					15		1	11	0.733	0.7

Table (5.5) Transmission coefficient (Ct) for different breakwater model (M5)

Model	RPM	Length 0f wave	Period T see	Experimental measurement (cm)					(C_t) =(Ht/Hi)	
				Wave steepness (Hi/L)	Hs	Hi	(Hs/Hi)	H_t	Experimental	CFD
M5	30	1.3 m	0.75	0.0769	0	10	0	5	0.35	0.33
					4		0.4	6	0.42	0.39
					8		0.8	6.5	0.51	0.47
					12		1.2	7.5	0.55	0.52
					15		1.5	8.3	0.67	0.65
	35	1.75m	1	0.0685	0	12	0	5.5	0.33	0.29
					4		0.33	6.5	0.46	0.41
					8		0.6	7	0.49	0.45
					12		1	8	0.55	0.51
					15		1.25	9.5	0.75	0.69
	47	2.1 m	1.15	0.0714	0	15	0	6.5	0.4	0.4
					4		0.26	8	0.50	0.46
					8		0.53	9.4	0.58	0.53
					12		0.8	10	0.61	0.58
					15		1	12.7	0.8	0.72

5.4 Comparison of CFD Result and Experiments

Table (5.6) presents a statistical analysis of the output obtained from the CFD (**Fluent solver**) in comparison to experimental results. The relative error equation (5.1) and, Table (5.6) shows the output data obtained for different conditions of waves (0.10 m and 0.12 m) and submerge depths (0, 4, 8, 12, and 15 cm). According to the statistical data outcome (Regression and Nash number). Figure (5.10), demonstrates the regression coefficient for observed and predicted data with regression approaches R^2 = 88 %.

$$\boldsymbol{RE = \left|\frac{Measured\ value - predicted\ value}{measured\ value}\right| * 100} \qquad \text{.....} \qquad \textbf{(5.1)}$$

The Nash Sutcliffe efficiency (NSE) is a normalized statistic that determines the relative magnitude of the residual variance (nose) compared to the measured data

variance (Nash and Sutcliffe ,1970). NSE indicates how well the plot of observed versus simulated data fit the 1:1-line, equation (5.2) represent the NSE equation

$$NES = 1 - \left| \frac{\sum_{i=1}^{n} (Y_i^{obs} - Y_i^{sim})^2}{\sum_{i=1}^{n} (Y_i^{obs} - Y_i^{mean})^2} \right| \quad \ldots\ldots\ldots\ldots\ldots \quad (5.2)$$

Where: Y_i^{obs} = is the *i*th observation for the constituent being evaluated, Y_i^{sim} = is the ith simulated value for the constituent being evaluated, Y^{mean} = is the mean observation data for the constituent being evaluated, and n is the total number of observations. For the current data analysis, the NSE number equal to o.8.

Table (5.6) Relative Error on results of Fluent and Experiments

Parameters	Wave height (m)	Submerged depth (cm)	Transmission wave Ht(m)		R.E (%)
			CFD	Exp	
Wave characteristics	0.1	0	0.04	0.044	9
		4	0.036	0.041	12
		7	0.031	0.037	16
		9	0.026	0.030	13
		15	0.018	0.018	0
	0.12	0	0.048	0.045	6
		4	0.04	0.04	0
		7	0.036	0.039	7
		9	0.031	0.037	16
		15	0.021	0.020	5

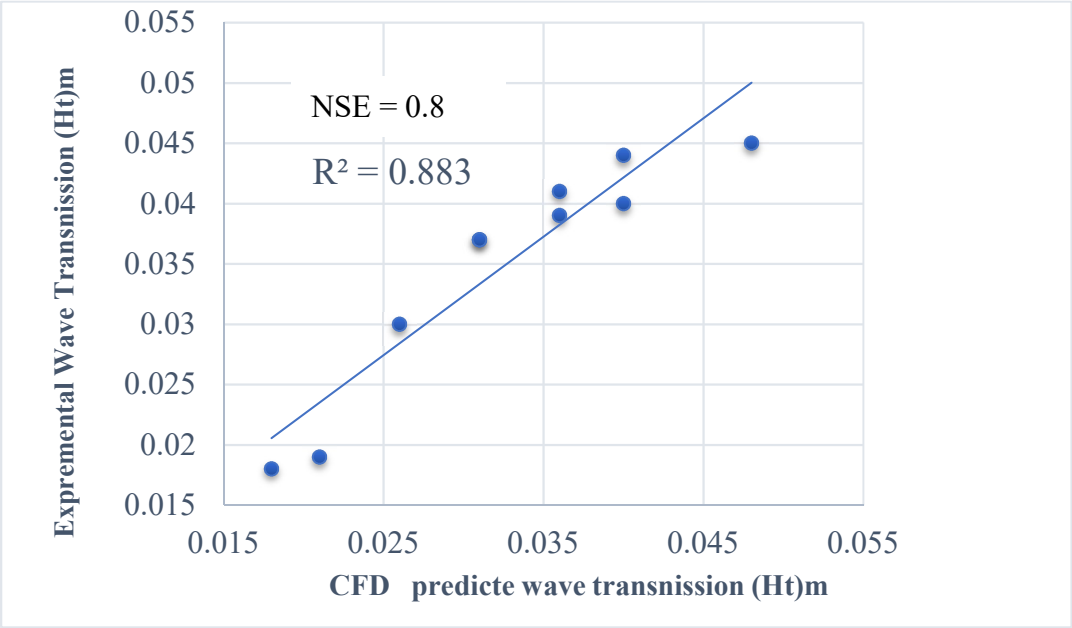

Figure (5.10) Regression for observed and predicted data

5.5 Different hydraulic waves behaviour :

One of the powerful features of CFD modelling is the graphical output of numerical variables, a small part of which represented in the following figure (5.11), (5.12), (5.13), (5.14) and (5.15). These figures represent different output for model M2 for different wave behaviour, velocity profile, eddy viscosity, turbulence frequency, pressure distribution, and stream flow victor colour by celerity of wave.

Figures (5.16), (5.17) Represent the turbulence intensity for different breakwater model, steps slope model makes the highest turbulence and dissipations more energy caused by eddy forms.

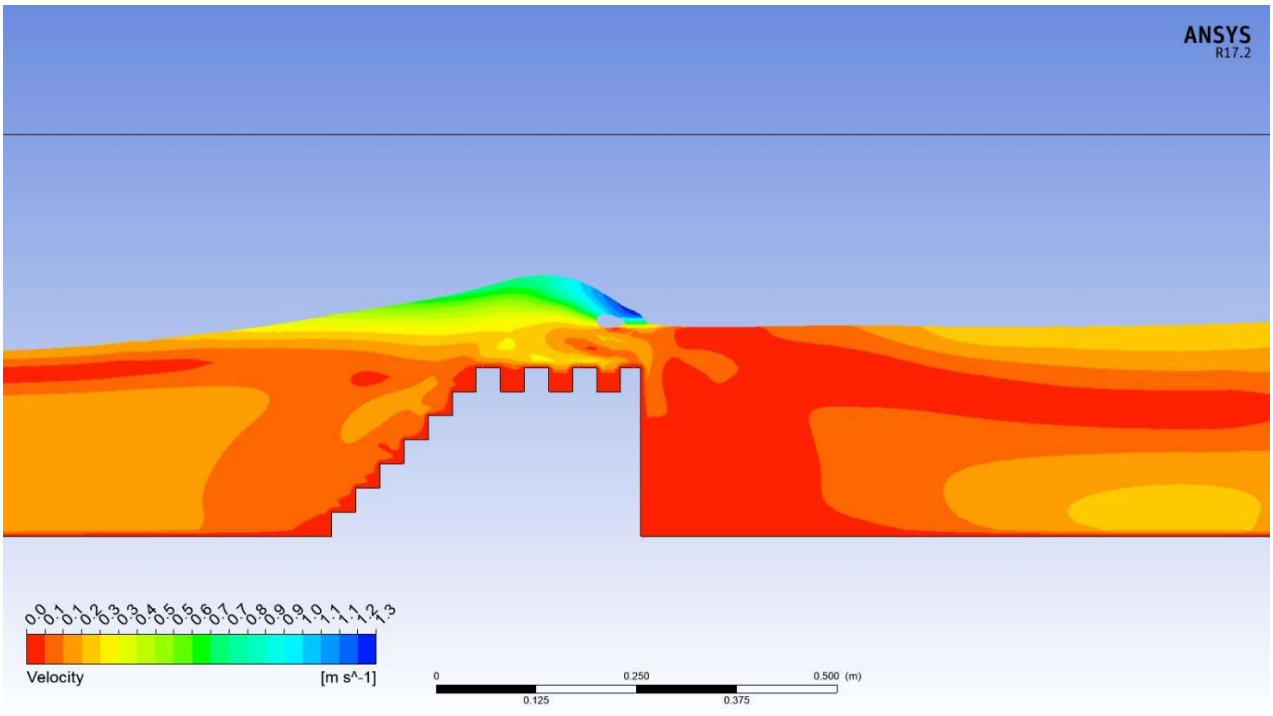

Figure (5.11) velocity distrbution for steps slope breakwater

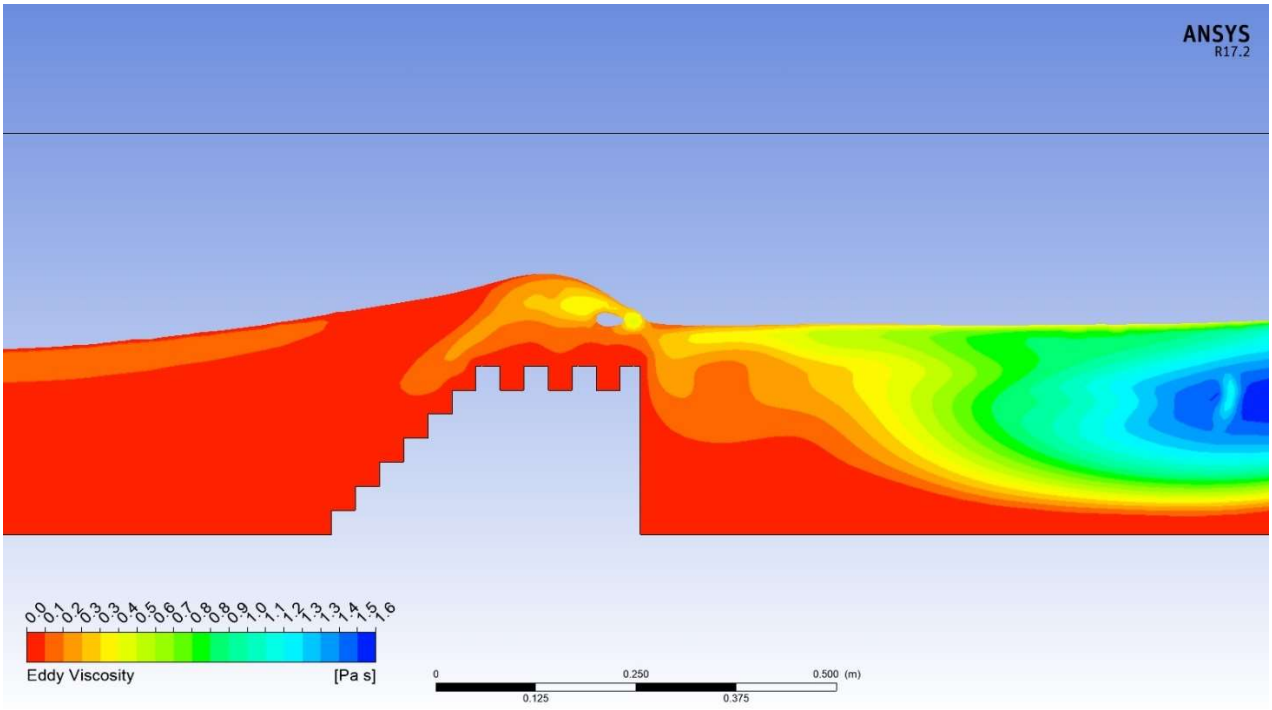

Figure (5.12) Eddy viscosity distribution for steps slope breakwater

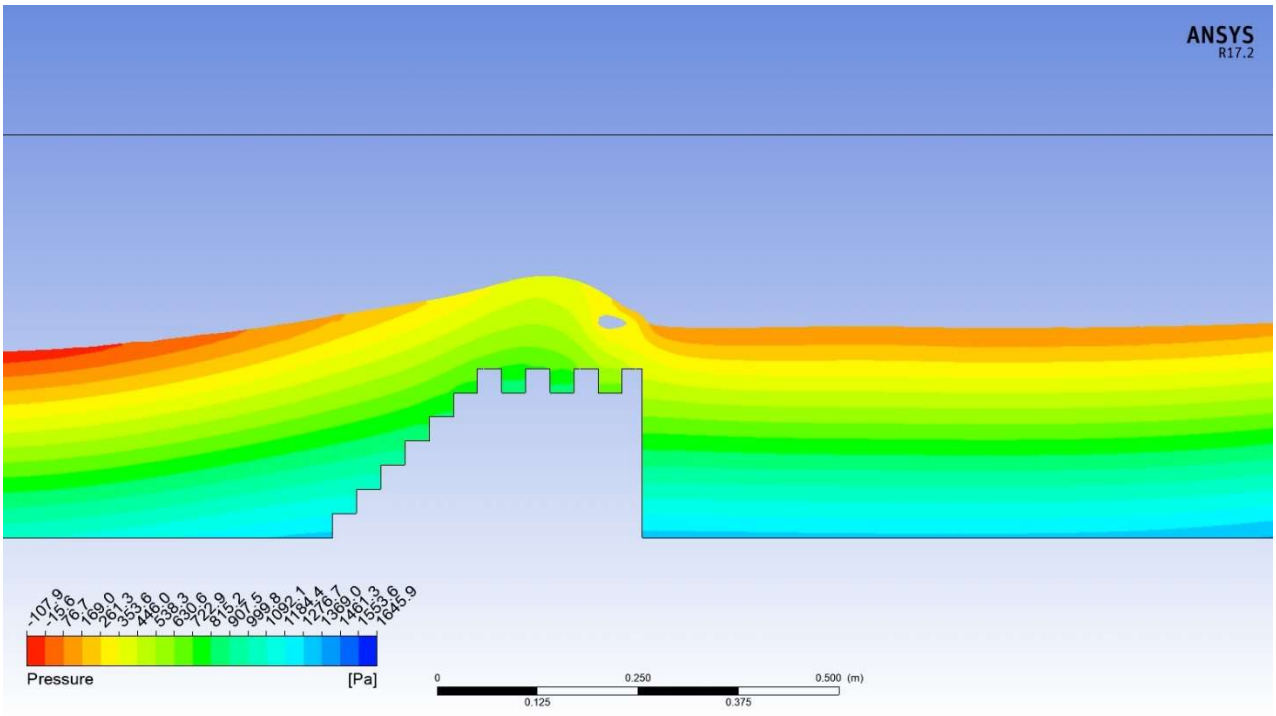

Figure (5.13) pressure distribution for steps slope breakwater

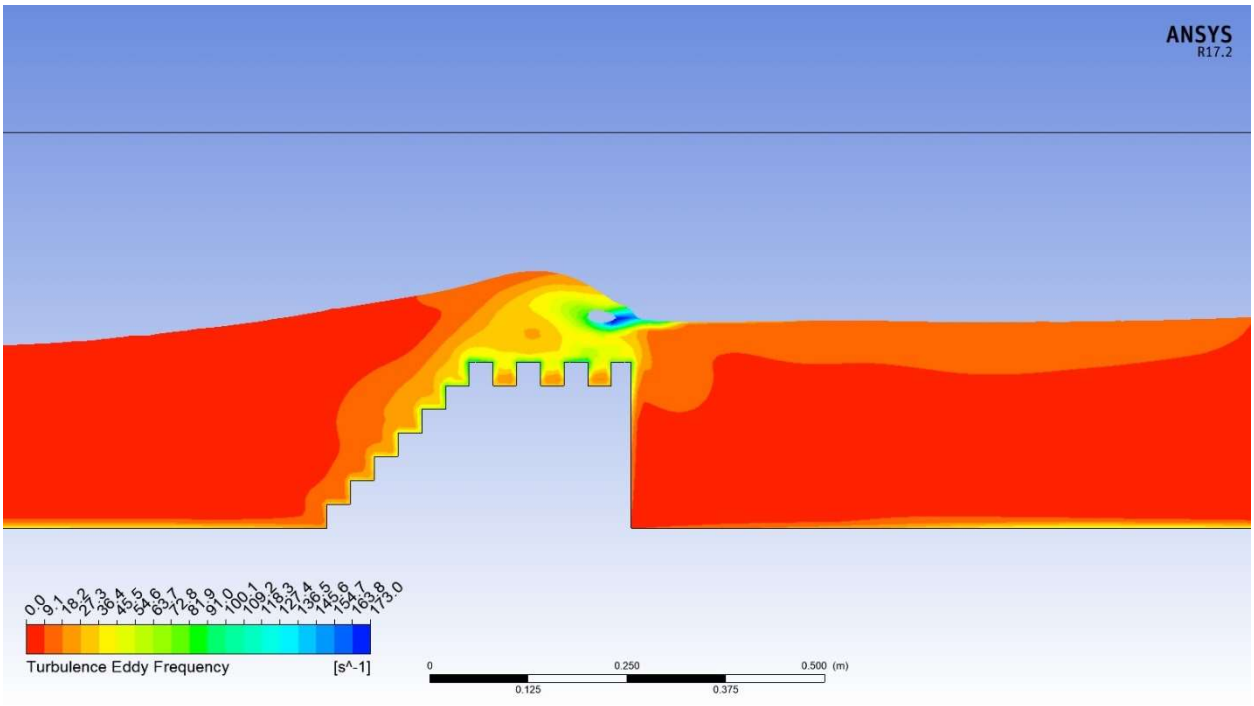

Figure (5.14) Turbulence eddy frequency for steps slope breakwater

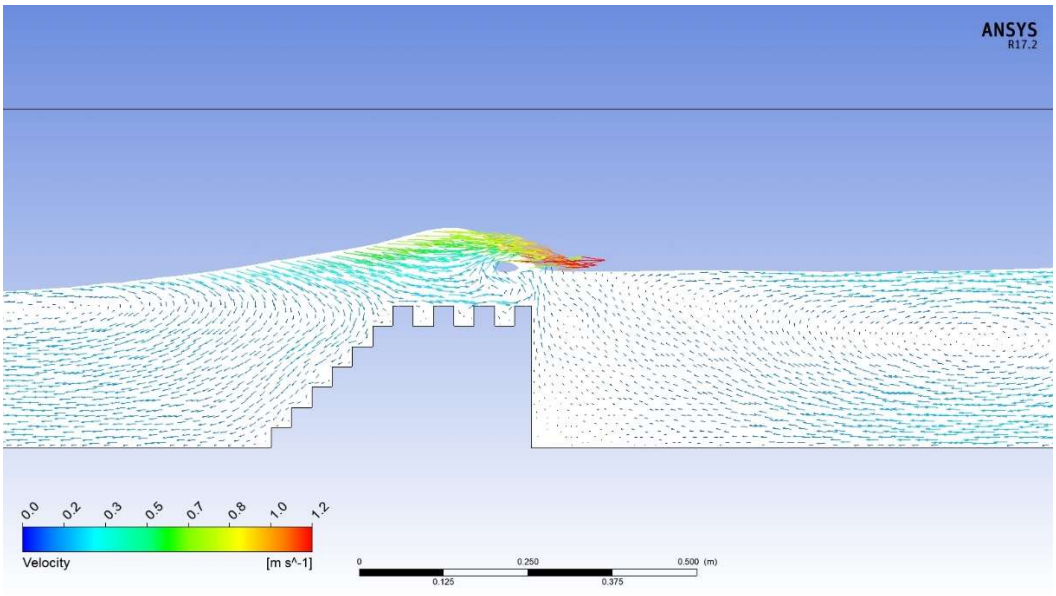

Figure (5.15) flow vectors colour by velocity for steps slope breakwater

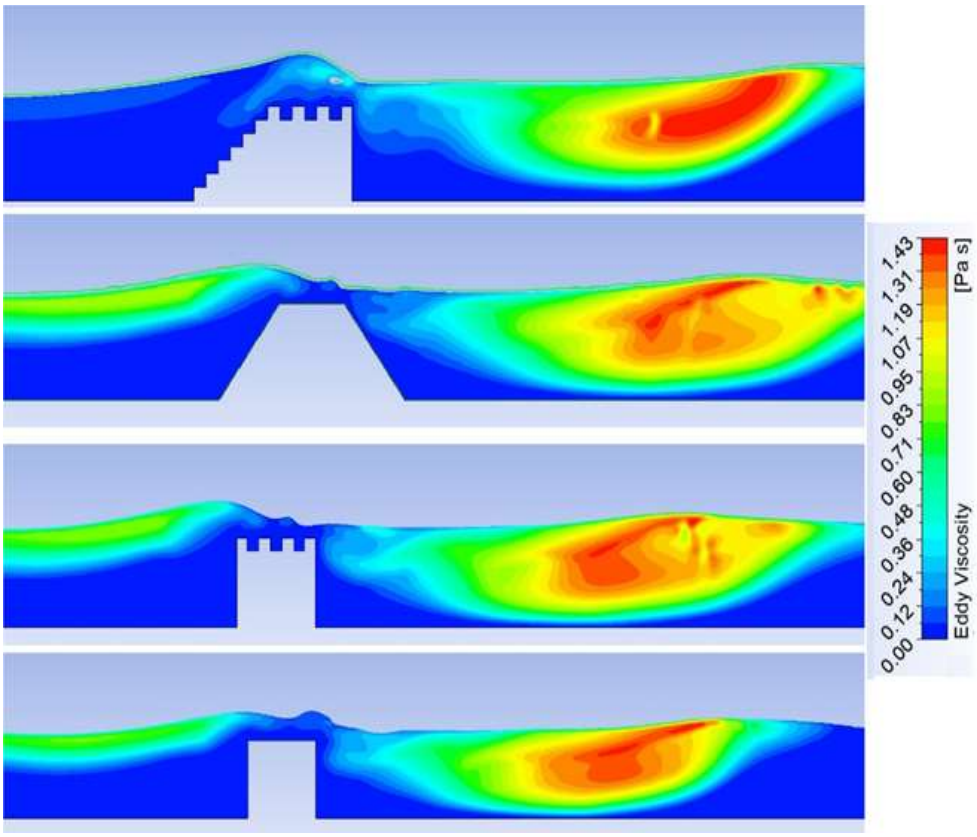

Figure (5.16) Eddy viscosity for different breakwater model

It is noticeable through the results of the mathematical model and laboratory work, that there is a very good match between the results of laboratory and the mathematical model (ANSYS. Fluent 17).

It is observed that, by comparing the results of the free surface and the wave tracing from the wave generating zone until reaching the breakwater zone , Figure (5.1) shows a clear match between then .The results showed that it is possible to rely on the mathematical model to represent various models (shape, size, wave conditions) in order to reduce the time and the number of laboratory experiments test. One of the things that was also clear is that the representation of the wave absorption region is very necessary to minimize the effect of the reflecting wave on the value of the transmission coefficient Ct.

If compare the results of models studied (M_1, M_2, M_3, M_4, and M_5), the highest energy dissipations values were obtained from the model (M2). The model work to disturb the wave and break it gradually starting from its arrival at the face side (roughness surface) of breakwater until crossing it beyond the breakwater.

The highest value for energy dissipations (1 - Ct) % are received for zero submerged depth in model of sloped steps model (M_2) is 80 %.

By reviewing the results of the CFD model, the wave dissipations process goes through three stages, starting from the front of the breakwater with a distance not exceeding one wavelength, where the breaker begins to affect the characteristic of the wave, then when the wave reaches the breakwater body, the breaker acts as a barrier to the passage of the wave. The irregularity of the breaker surface (Roughness of surface), here it plays as an auxiliary factor for the dispersion of energy on the lateral slope and the upper breaker surface.

On the other hand, Table (5.2) shows that the presence of steps at the front of the breaker have a limited effect on transmissions coefficient which is obvious to a certain extent to the heights of the submerged depth (Hs), for height of submerged depth exceeding the wave height or more.

The results also showed that the values of the wave dispersion coefficient depending on the breakwater cross section (such as ruble mound, rectangular, sloped steps, narrow, and inclination), starting from the least effective, the narrow shape, and the most effective breaker with a wide cross section, which is considered the most efficient in terms of performance.

Through the results obtained from table (5.1) and (5.2), for model MI, M2 respectively, the effect of the rough surface of the breakwater is determined by certain wave heights, and its effect is obvious at wave heights that exceed the height of the submerged depth (10 cm ,12 cm) or more. And this is really an important conclusion that leads to the fact that the surface roughness of the breaker has a limited effect on the dispersion performance depending on the wave height and the submersible depth of the breaker.

Chapter Six

Case Study

Chapter Six

Case Study

6.1 Introduction

In this chapter, the mathematical model will be employed to model the entire case study (Annajaf-sea depression), which needs to employ the breakwater an optimal location, and practically studied taking into account all the influencing factors, wind speed, wind direction, water level, topography, bathymetry, and other factors.

Annajaf sea depression located in south-middle of Iraq was exposed to many storms during many years depending on the weather condition and geographical nature of this area. In 2019 and 2020, specifically in the October, the region was exposed to high intensity rain storm and very strong winds, which led to the flooding of the road adjacent to the sea and large costal erosion of some neighboring areas. In fact, this area does not have weather gauge stations, but there are two measurement stations considered nearby the site and it is possible to rely on them to estimate the speed values recorded in the area according to the correspondence of the nature extending between the study area and the measurement station. In addition

In order to modeling these storms and their impact on neighboring areas, the MIKE21 by DHI was used to model the worst-case scenario that could occur in the study area and propose possible optimal location of mitigation structure to avoid the damage caused by wind induced wave.

6.2 Description of the Study Area

One of Iraq's historic low water bodies is the Bahr Al-Najaf depression. It was regarded as a natural lake and was situated in the southwest of the Al-Najaf city

Centre. The region has a total surface area of 251 km^2, and its position may be determined by the coordinates 44° 11' 34" to 44 ° 22' 37", and 31° 47' 11" to 32 ° 04' 08," respectively. It has a lake within that has a about 90 km^2 size. Due to influx, precipitation, and seasonal weather changes, that area fluctuated between increases and decreases. The area is classified as a desert where water levels rise throughout the winter owing to increasing rainfall. **(Omran, et al., 2014).**

The water shades area's slope progressively steepens as it moves from the west and south-west to the north and northeast. Three major valleys, Kharr, Shoaib Al-Rahimawi, and Maleh, have a wide area and riles multiple source (Runoff and Ground water) to the Bahr Al-Najaf lake. These valleys also help to replenish the groundwater in the area. **(Farhan, and Abed, 2021)**. Figure (6.1) shows position of Bahr Al-Najaf depression.

In fact, the study area is located within a high stipe gradient area, figure (6.2) shows the high gradient in elevation. The Digital Elevation (DEM) of the adjacent areas demonstrated the vary high difference in elevation between the lake and surrounded areas. This high difference in elevation it makes the lakes as a collector of rainwater and runoff of water shaded area that leads to makes the water level in the lake variable continuously.

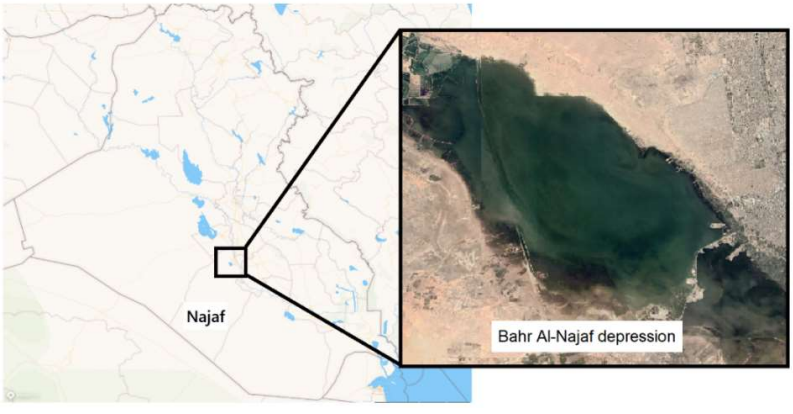

Figure (6.1) Bahr Annajaf depression according to Iraqi Map

This area was exposed to flood waves resulting from the flocculation rise of the water level in the lake, in addition to the waves generated by high winds recorded at Gauge stations adjacent to the area, the following figure (6.3) shows the road strategic line in Bahar Al-Najaf, which is always exposed to the erosion as a result of the waves generated by the wind and water level rises.

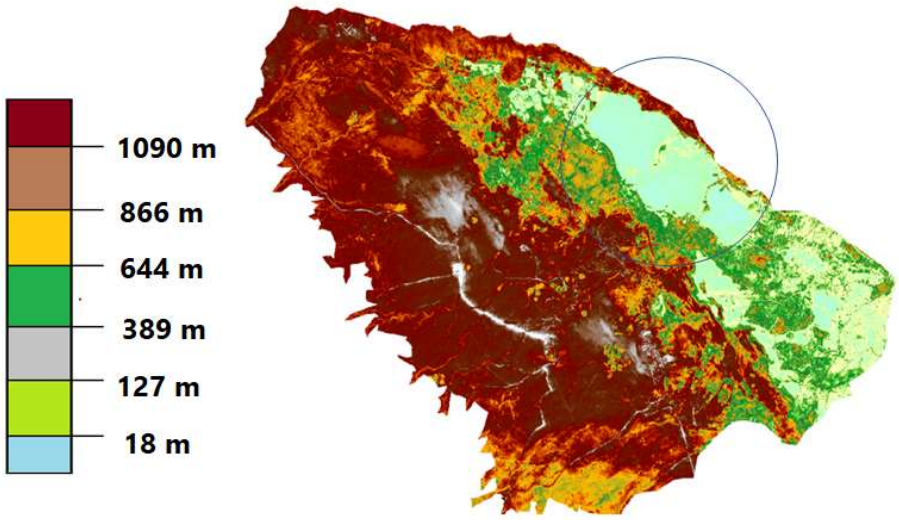

Figure (6.2) Digital Elevation Model for surrounded area of Bahr Annajaf (https://earthexplorer.usgs.gov)

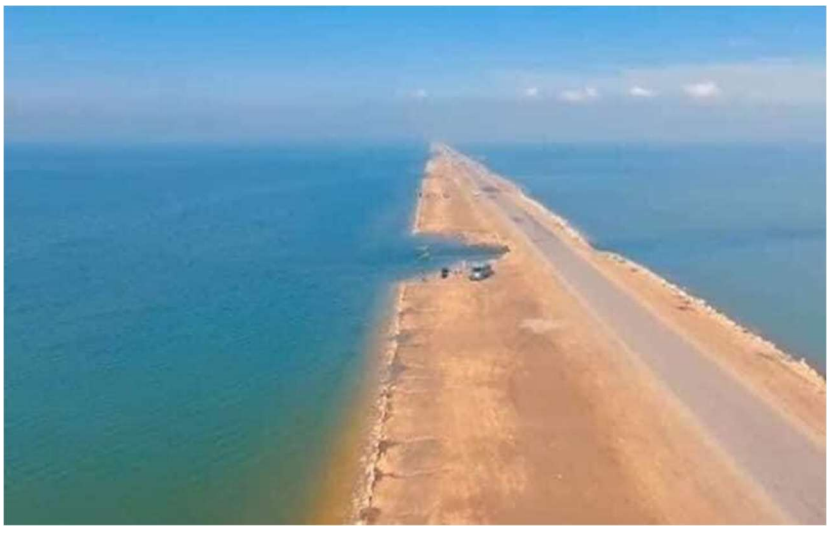

Figure (6.3) Damage in the strategic line in Bahr Annajaf

6.3 Weather Data

The climate of Iraq fundamentally is continental, subtropical semi-arid type and a Mediterranean climate in the mountainous regions at the north and north-eastern side. The occurrence of precipitation is seasonally and concentrates in the winter from December to February, with the exception in the north and northeast region of Iraq in which the season of rainfall extends from November to April. The annual rainfall ranges fall between 1200 mm in the northeast to less than 100 mm which represents over 60 percent of the country area in the south, while the overall average value of precipitation is 216 mm, **(Ali , 2020)**.

Accurate wind field data collected by meteorological models and analysis are required for excellent wave hindcasting and forecasting. Because the wind field is the primary driving factor in spectral wave models. **Xiana, et al (2019)**.

Shebja gauge station, it's automatic weather stations belonging to the Iraqi Ministry of Agriculture that have been installed and operated near the southern Bahr Annajaf (Lat 31.68: log 44.3). The historical data records at **(Shbicha**, and **Annajaf)** gauge stations near the site for a short period (2013 to 2023) don't contain consistent data, such as wind direction, and cannot be relied on to determine the wind characteristic prevailing in the area. So integrated data was adopted from MERRA-2 Sat, **NASA** (Modern-Era Retrospective analysis for Research and Applications) for a long time period (1980-2023) that were calibrated with correlation (R^2) equal to 0.71 for the same time period recorded for the **Shbicha** station, figure (6.4) shows the correlation between measured data and predicted by MERRA-2Sat

The weather statistics according to MERRA-2 Sat in table (6.1) show that, a North-West (NW) 315^O wind direction predominates with a frequency of 25 %. The windiest direction over a longer period is NW, with a Max wind average multiyear

15 (m/s). With winds gusting to 12 m/s, the N and W directions have the second-strongest winds. as seen in figure (6.4). For the simulation experiments, the least safe wind speed and direction combinations are chosen. Table (6.1) Shows wind parameters in the study area for a period (1979-2023).

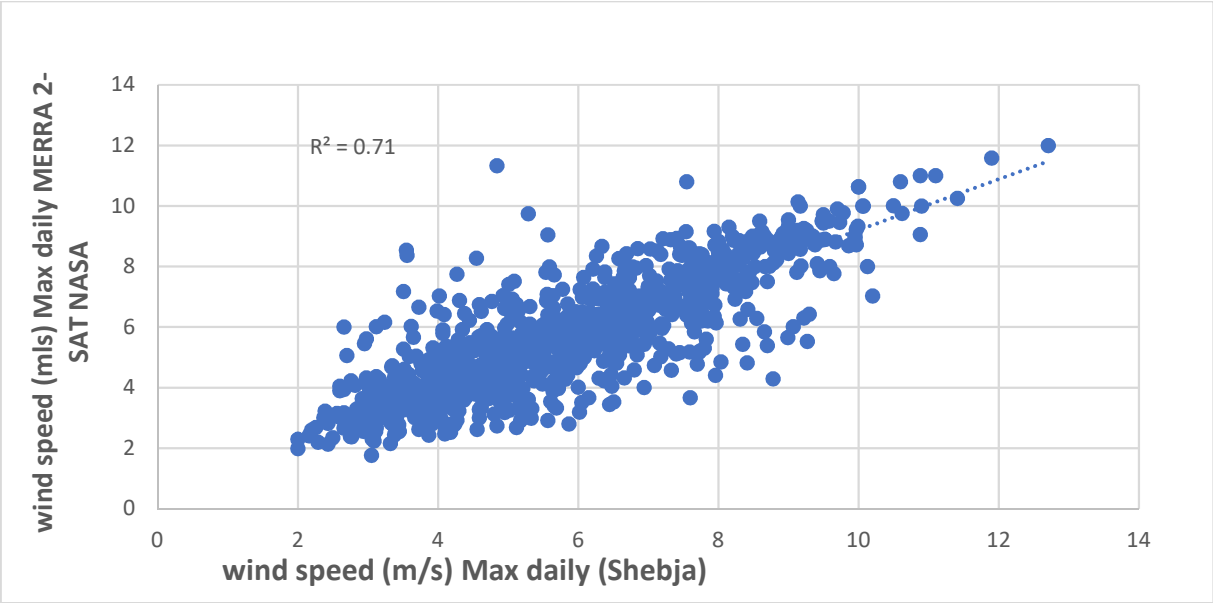

Figure (6.4) Correlation between the Shebja Gauge Station (2013-2021) and data prediction by MERRA-2 Sat NASA

Table (6.1) Wind Characteristics for the study area for a period (1979-2023)

Location	Wind direction (degree)	Max wind average multiyear (m/s)
North	360	9
North – northwest (NNW)	337.5	12
Northwest (NW)	315	15
West-northwest(WNW)	290	7
West (W)	270	9
South(S)	180	7

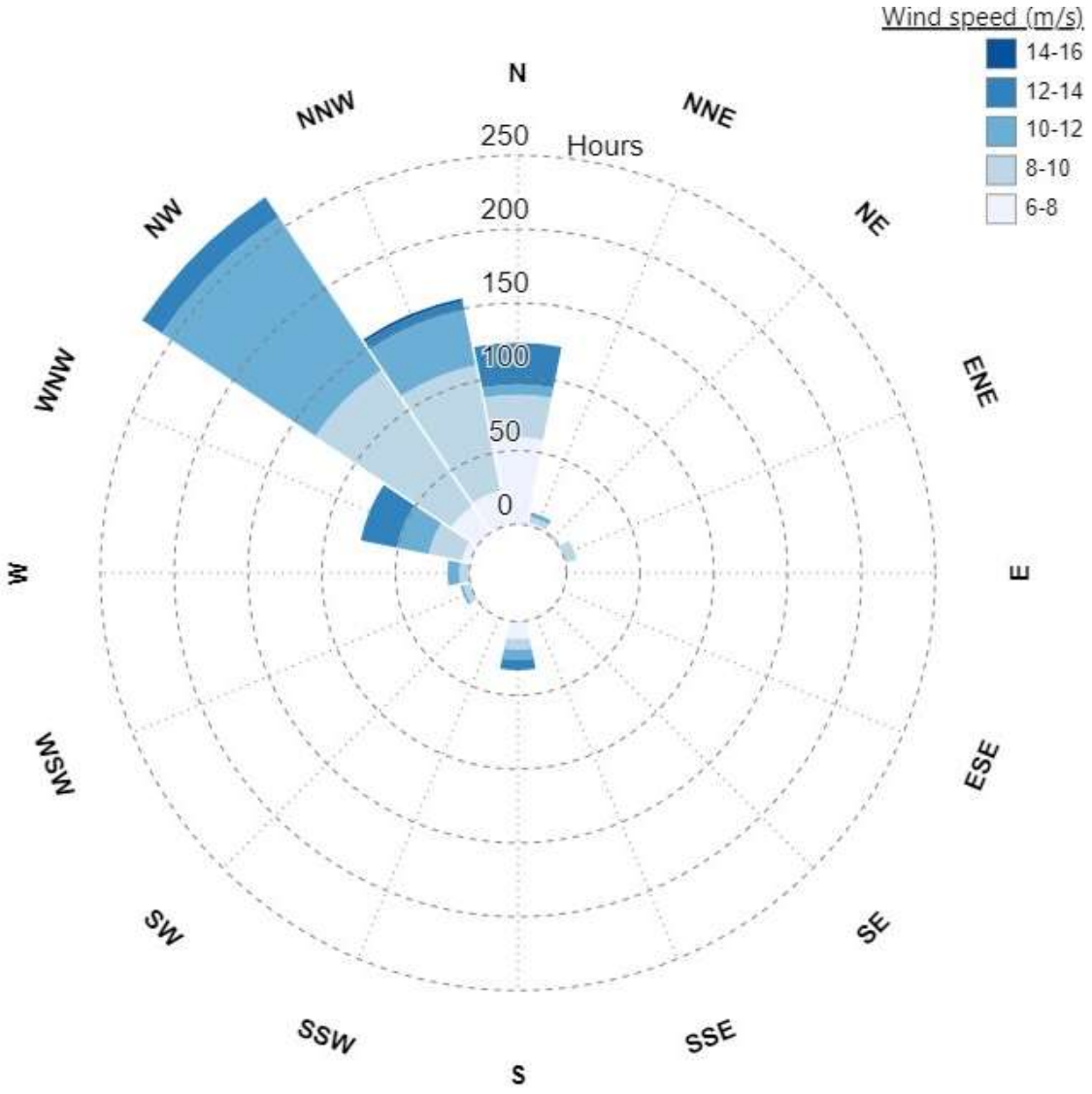

Figure (6.4) Rose chart and frequency of wind recorded of Bahr Annajaf.

6.3.1 Wind Speed and Probability of Occurrence

The probability of occurrence of a certain wind speed is the likelihood that the wind will reach that speed in a given period of time. This probability is often expressed as a percentage or a fraction. The recurrence interval, commonly referred to as the return time, is defined as:

$$T = \frac{1}{P} \qquad \ldots\ldots\ (6.1)$$

This is the typical interval between wind events with magnitudes equal to or higher than X. The correct formula offers the probability P that an event will occur with a value of equal to or higher than. **Chanson, H. (2004).**

$$P = \frac{m+0.41}{N+0.53} \quad \ldots\ldots\ldots \quad (6.2)$$

After calculating P for each event in the series, the variation of the velocity wind magnitude is shown on a semi-log graph against the matching P. The velocity wind magnitude of specified height for any P may be determined using proper extrapolation of this figure within applicable constraints. **Chanson, H. (2004).**

$$K = -0.7797 * \left[0.5772 + \ln(ln\frac{T}{T-1})\right] \quad \ldots\ldots\ldots\ldots\ldots\ldots (6.3)$$

According to Chow (1951), the general equation of hydrologic frequency analysis may be used to describe the bulk of frequency distribution functions relevant to hydrologic investigations. X_T=u+K*s; where u is the mean, s is the standard deviation, and K is the frequency factor that depends on the return period, T, and the assumed frequency distribution, and X_T is the value of the variate X in a random hydrologic series with a return time T.

$$ST = 2\sqrt{\left[\{1 + 1.1396K + 1.1K^2\} * \frac{s^2}{N}\right]} \quad \ldots\ldots\ldots \quad (6.4)$$

Table (6.3) displays the wind speeds for various return period that were translated to 10 meters above sea level. **Chanson, H. (2004).**

Table (6.3) Wind speed at the Bahar AL-Najaf for different Return Periods (unit: m/s) for maximum monthly for a period (1979-2023).

T (once in)	K	MaxWind speed (m/s)
25 year	2.043	21.17
50 year	2.592	22.80
75 year	2.911	23.74
100 year	3.136	24.41
Mean speed = 15.12 (m/s). Standard deviation = 2.96. Coefficient of variation = 0.195. Coefficient of skewness = 0.3082. Alfa parameter= 2.3086. Beta parameter = 16.4575, Kurtosis coefficient = 3.0462 (parameters for return period 50 years)		

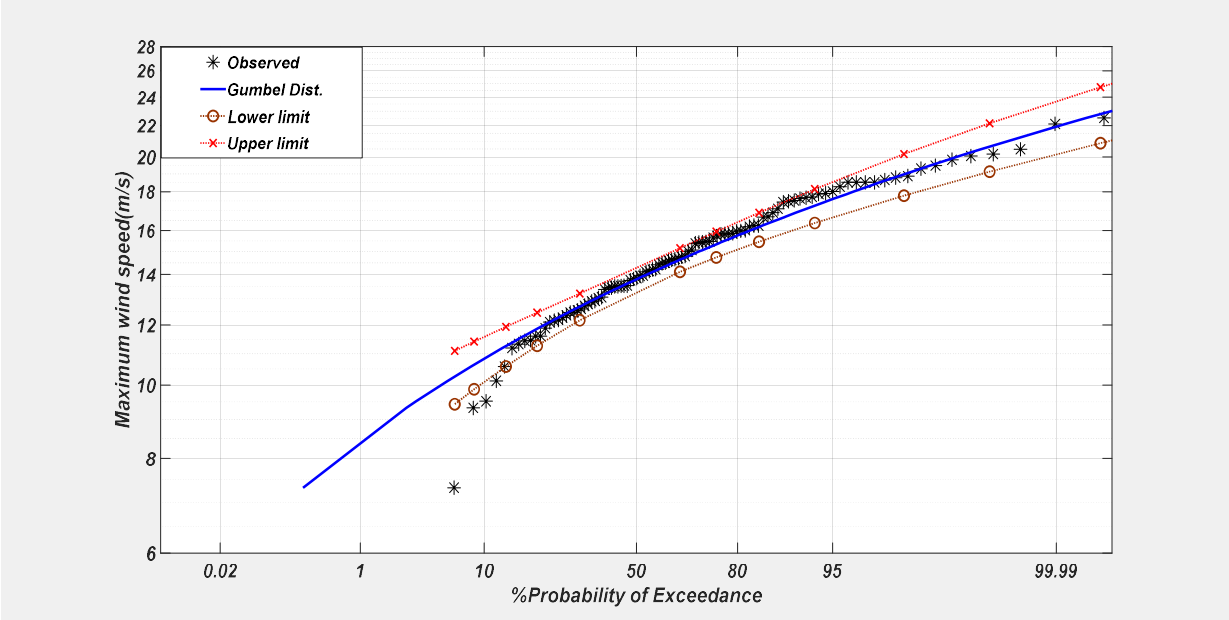

Figure (6.5) probability of exceedance for 50 years return period

6.3.2 Monitoring Water Bodies (USGS) and (NASA):

Landsat 8 and 9 are two satellites that are part of the Landsat program, which is a joint effort between the U.S. Geological Survey (USGS) and NASA. These satellites are equipped with sensors that can capture images of the Earth's surface in various wavelengths, including visible and infrared light. This allows them to monitor changes in land cover, vegetation, and water bodies over time.

Both satellites orbit the Earth and capture images of the entire planet, providing a valuable resource for monitoring changes in water cover over land. These images can be used for various applications, including tracking changes in water bodies, monitoring water resources, and assessing the impact of natural disasters such as floods. (https://landsat.gsfc.nasa.gov).

The Landsat 8-9 collection contains imagery from the two most recently launched Landsat satellites (Landsat 8 and Landsat 9, provided by NASA/USGS). Both carry the Operational Land Imager (OLI) and the Thermal Infrared Sensor (TIRS), with 9 optical and 2 thermal bands. These two sensors provide seasonal coverage of the global landmass.

The data collected by Landsat 8 and 9 can be used to create radar images of water cover over land, providing valuable information for environmental monitoring, resource management, and scientific research.

Overall, Landsat 8's high-resolution imagery and bands of water bodies are valuable tools for monitoring and managing river systems, lakes, and reservoirs, contributing to the sustainable management of water resources and ecosystems.

Normalized Difference Water Index (NDWI):

The NDWI is used to monitor changes related to water content in water bodies. As water bodies strongly absorb light in visible to infrared electromagnetic spectrum, NDWI uses green and near infrared bands to highlight water bodies. It is sensitive to

built-up land and can result in over-estimation of water bodies. The index was proposed by McFeeters, 1996. The normalized difference water index is most appropriate for water body mapping. Values of water bodies are larger than 0.5. Vegetation has smaller values. Figure (6.6) NDWI for Najaf lake at (10-9-2022).

Monitoring the height of the highest water level in the lake is very important to identify areas that may be at risk of being flooded by waves and also identify areas that need to be control points to determine the location of the breakwater. The Bands visuals by NASA/USGS were used for the study area to monitor the highest recorded level of the lake for a period (2002 to 2023).

The lowest level of the lake was recorded during 2003 and the highest rise was recorded during the years 2020, as shown in the attached figures (6.7)

Table (6.4) historical received of water bodies surface area in Bahar Al-Najaf during (2002-2023), sources. Sentinel-2 satellite, provided by NASA/USGS

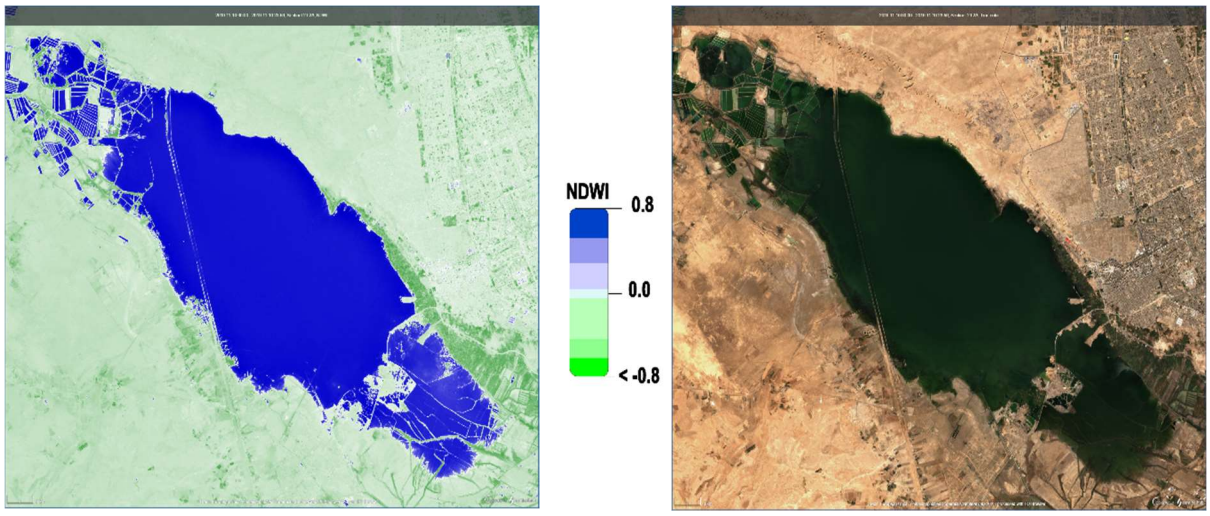

Figure (6.6) NDWI for Najaf lake; **https://custom-scripts.sentinel-hub.com**

Table (6.4) historical received of water bodies surface area in Bahar Al-Najaf during (2002-2023), sources. Sentinel-2 satellite, provided by NASA/USGS

Year	2002	2003	2004	2005	2006	2007	2008	2009	2010	2011	2012
Water body (Km^2)	9.7	4.7	7.45	30.78	33.67	40.34	47.78	46.77	55.76	40.67	44.25
m.s.l (m)	12.1	12.5	12.67	13.1	13.45	14.00	15.12	15.00	15.7	14.1	14.88
year	2013	2014	2015	2016	2017	2018	2019	2020	2021	2022	2023
Water body (Km^2)	52.535	84.455	85.64	87.45	88.27	108.25	111.86	130	129.99	120.41	110.32
m.s.l (m)	15.36	16.00	16.23	17.13	17.34	18.5	19.00	20.00	20.00	19.48	18.7

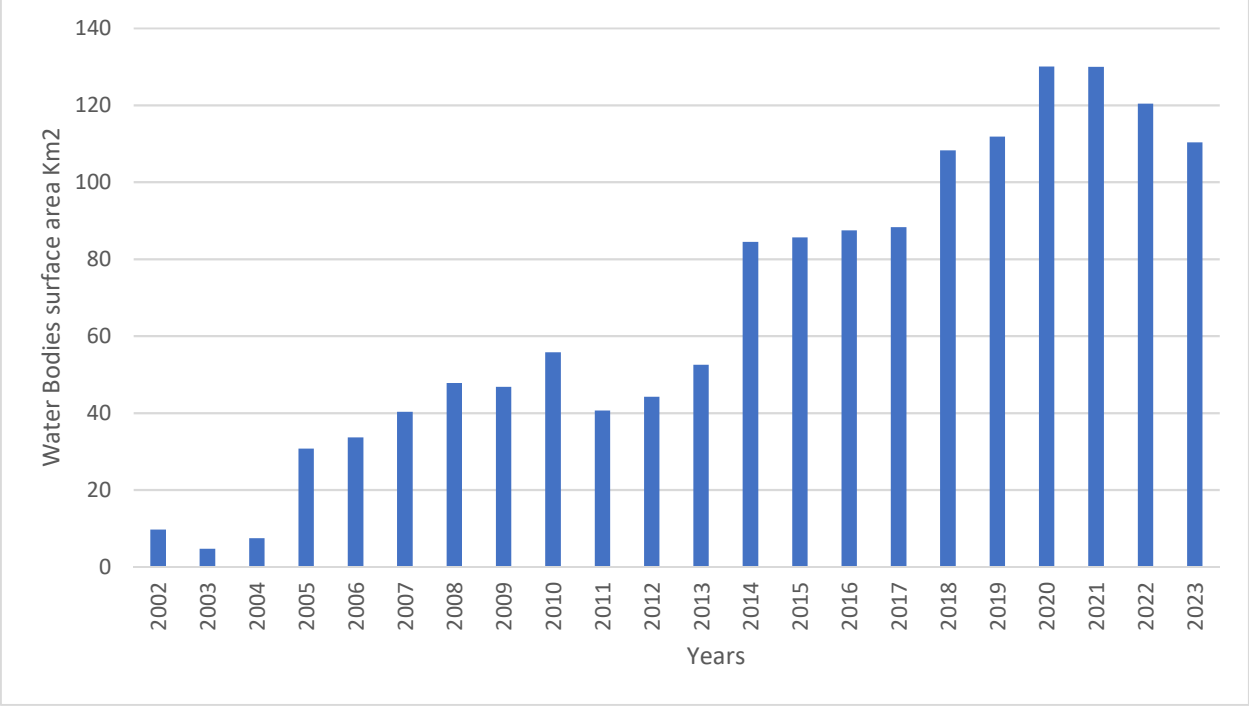

Figure (6.7) water bodies area for long period recorded (2002-2023), sources. Sentinel-2 satellite, provided by **NASA/USGS**

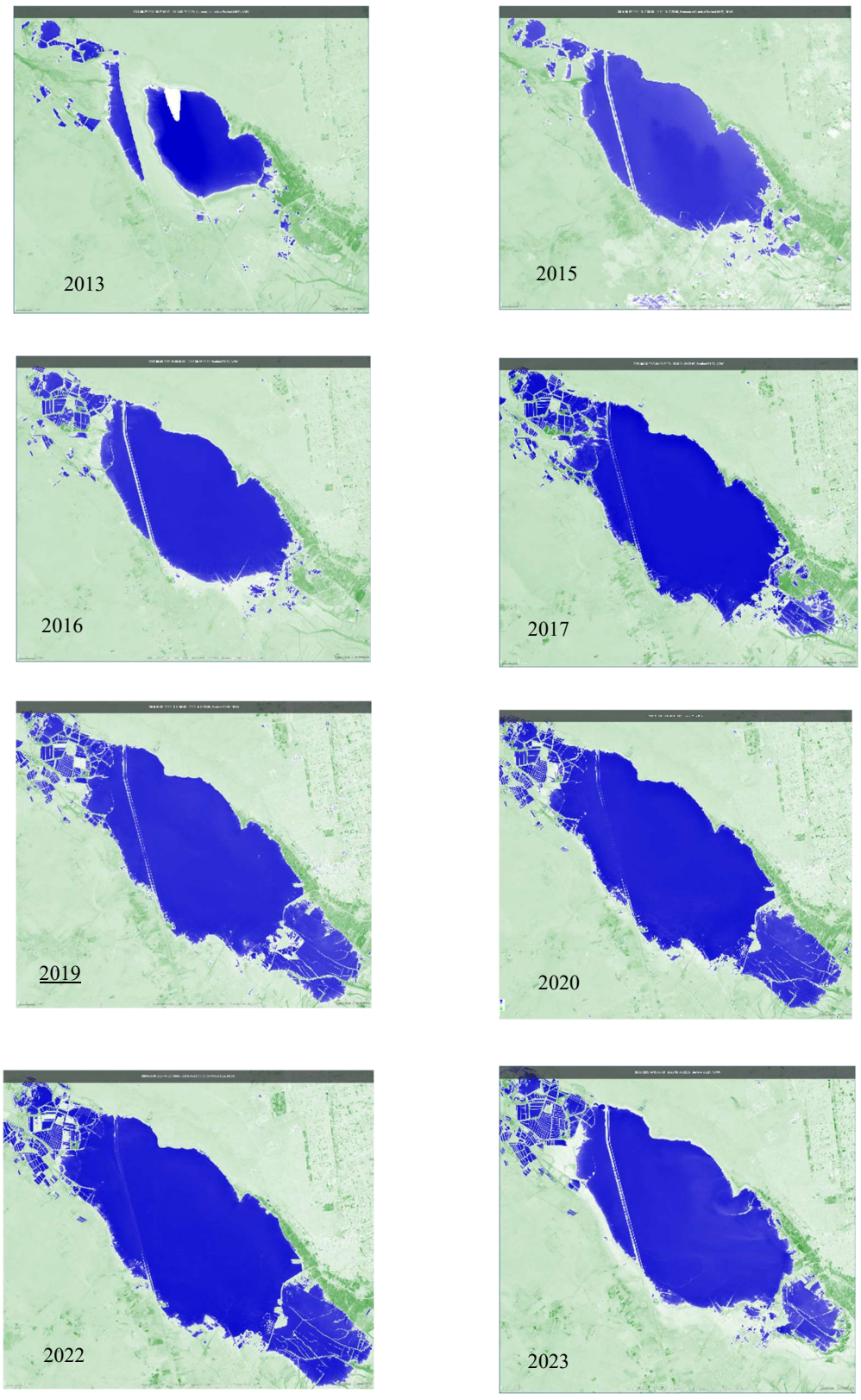

Figure (6.8) water bodies propagated during period (2013-2023). NASA/USGS

6.4 Watershed and Runoff estimation

Many studies have dealt with the hydrological aspect of the study area, which have reached the results that the source of water in the lake is the result of feeding through groundwater and Runoff. The most important study prepared by **Ali (2020)**. This study used a mathematical model SWAT and the model was fed data for more than 30 years and worked on predicting the values of Runoff for very long periods, the following figures (6.9), (6.10), (6.11) and (6.12) represent some of results of this study.

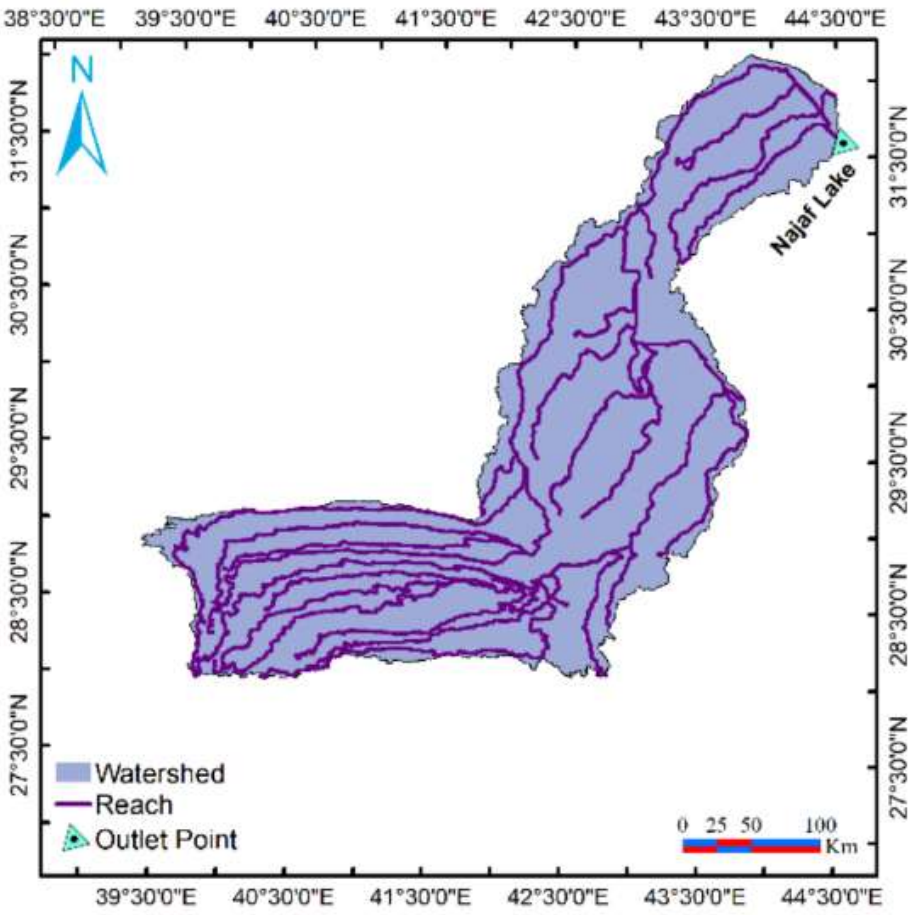

Figure (6.9) Watershed delineation of Najaf Lake, **(Ali, 2020)**

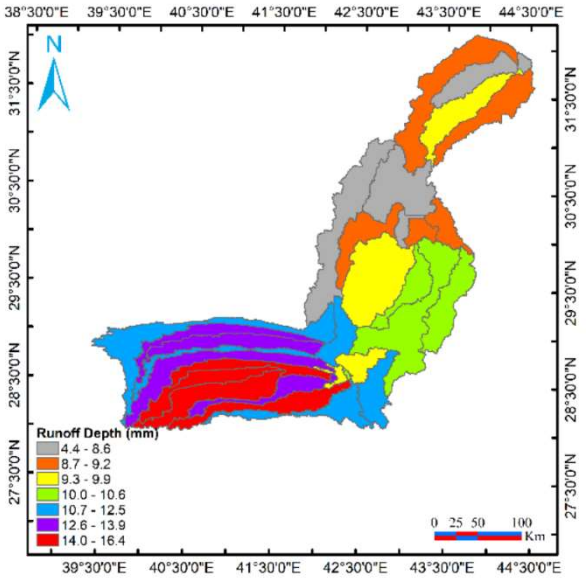

Figure (6.10) Runoff depth predicted by SWAT model, **Source (Ali , 2020)**

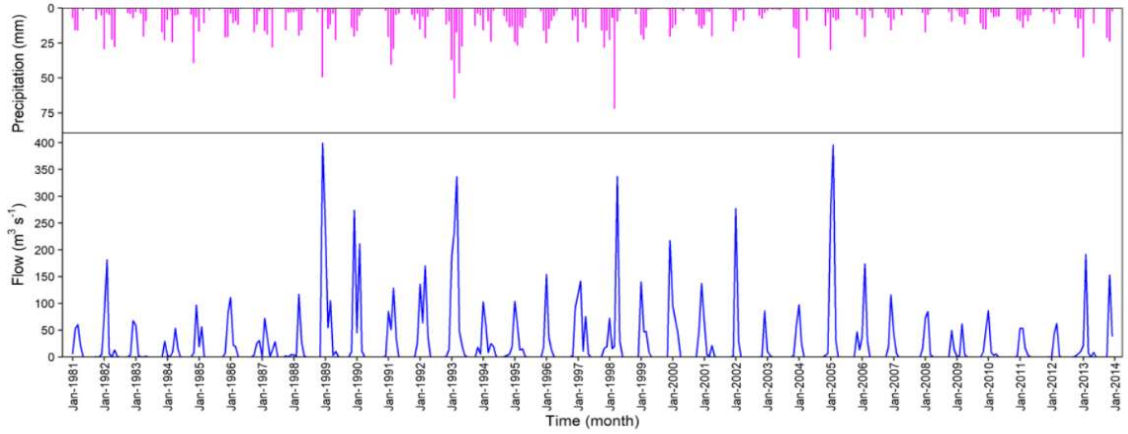

Figure (6.11) Simulated monthly stream flow of Najaf lake watershed. Source **(Ali.2020)**

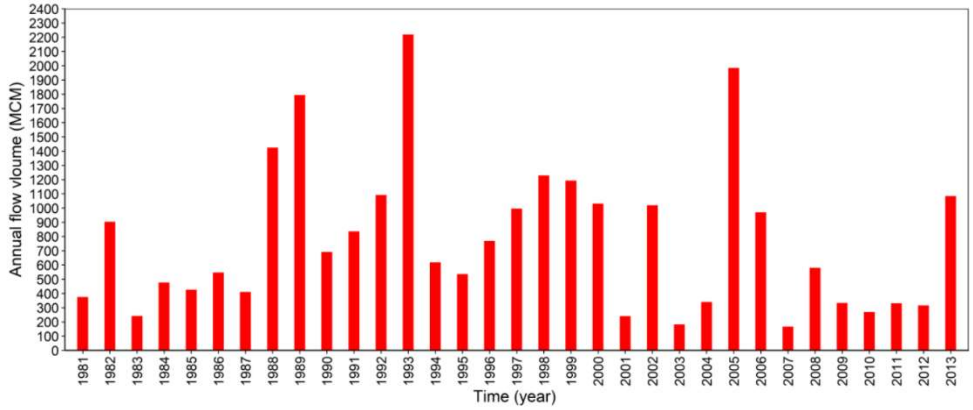

Figure (6.12) Simulated annual runoff as an inflow to Najaf lake. Source **(Ali, 2020)**

6.5 Mathematical Model Build-Up (MIKE21)

Figure (6.13) represented six steps will commonly make up the Model Checklist when using the generation spectral wind-wave models in MIKE21 SW to forecast the onset, decline, and transformation of wind-generated waves and swell in offshore and coastal environments. Each stage will consistence many details according to the conditions of physical phenomena need to be model and boundary condition.

The first step in preparing the model is to selected (bounded outline) the study area by making a shape file by uploading a high-resolution aerial image and bounded the outer boundaries of the area, then a geo-referencing of the map is made using the GIS program or any geographic information program.

The next step. Make abstract of the downloaded bathymetry data according to the boundaries of the region in the previous step. And then build up a map that has the three coordinates XY and Z.

The third step is very important, making meshing of the area, and remark the most important zone (breakwater location) in the study by determining it with a polygon for the purpose of increasing the density of division in this zone in order to obtain results with high accuracy. It must be ensured that the solution is no longer dependent on the values of the meshing size (mesh independent solution).

After that, the last steps depend on the values of the boundary condition by determining the direction and speed of the wind and the equations that describe the spectral of the projected wind and the type of model used.

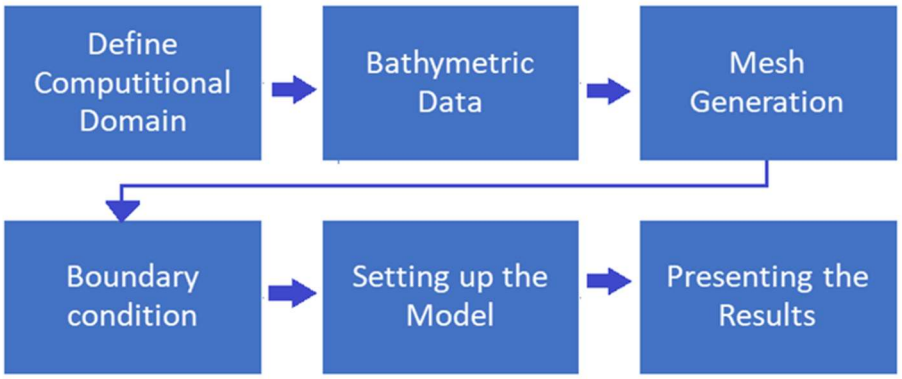

Figure (6.13) Steps of build-up **MIKE21 SW** model.

6.5.1 Computational Domain and Bathymetric Data

A global team of professionals in ocean mapping makes up the General Bathymetric Chart of the Oceans and Wet Land (GEBCO). The most accurate publicly accessible water level of the world's seas is provided by this group. Bathymetric data at each site, where available, was provided in the form of hydrographic charts (Iraq, Najaf) or in digital X, Y, Z format and additional gridded data from GEBCO. Using MIKE 21 Go-Referencing, the hydrographic charts were digitalized, and the digital data entered was transformed to MIKE21 forms. The computational grids for target area were then made utilizing these data sets and the Mesh editor in MIKE21-mesh generation. Figure (6.14) shows scatter data downloaded and abstract to specified area (case study).

After downloaded scatter data X, Y, and Z of selected area, the bathymetry map was build-up and interpolation of these data are represented the final shape of area with three-dimensional, figure (6.15) shows bathymetry map after interpolations

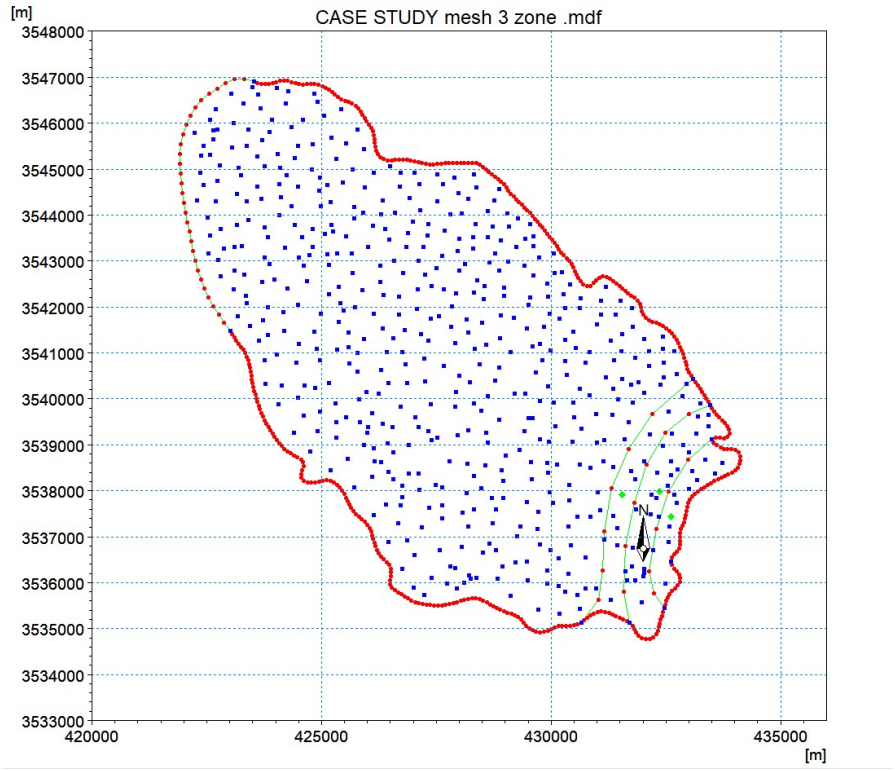

Figure (6.14) Scatter data abstracted to selected area

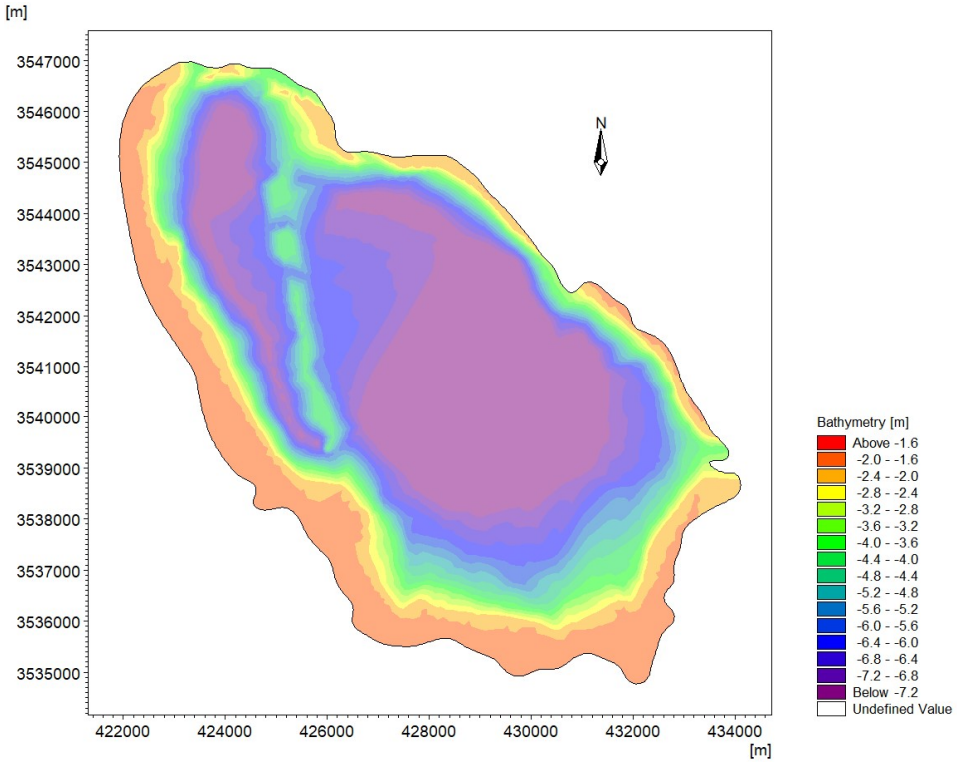

Figure (6.15) Bathymetry data after interpolation overall area

6.5.2 Validation of Bathymetric Data

Validity, a very important expression when dealing with mathematical models that directly depend on this data. Ten random points were identified near the confluence of the lake with the road and the height of the water at these points was measured conventionally using a measuring ruler with the coordinates of these points determined using GPS. Figure (6.16) shows the random points selected for compression between measured water level and GEBCO data downloaded.

The following Table (6.5) shows the differences between the actual values measured with the loaded bathymetric data (GEBCO).

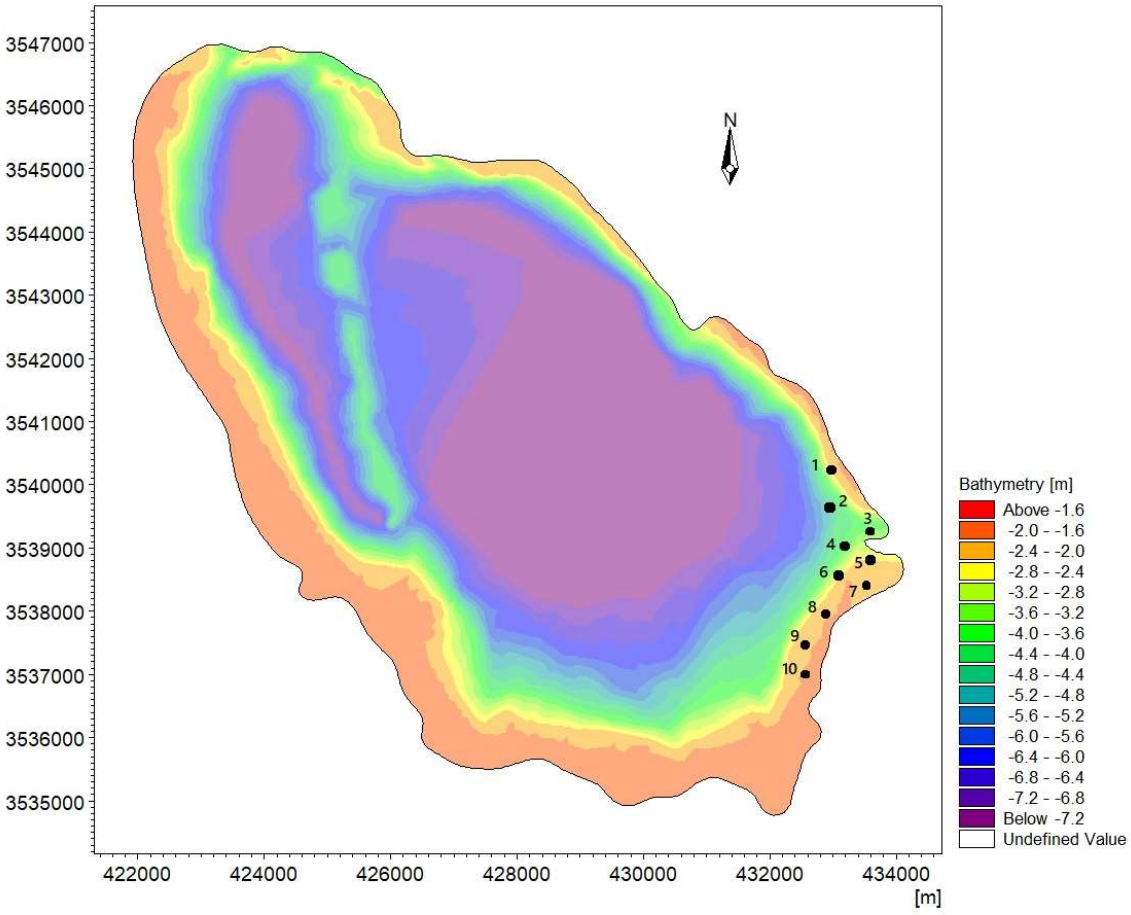

Figure (6.16) points selected to validation GEBCO data

Table (6.5) shows the differences between the actual values measured with the loaded bathymetric data GEBCO

POINT	Coordinate		Bathymetric	
	X	Y	Imported (GEBCO)	Measurement
1	432886.788	3540520.976	-2.311	-2.109
2	433016.876	3539821.752	-4.11	-3.72
3	433569.751	3539366.443	-3.62	-3.31
4	433195.747	3539252.616	-4.12	-3.90
5	433683.578	3538829.829	-2.51	-2.31
6	433114.524	3538748.524	-2.86	-2.60
7	433666.034	3538526.159	-2.178	-2.101
8	432900.838	3537956.332	-2.002	-1.92
9	432705.469	3537370.225	-1.992	-1.82
10	432622.234	3536881.123	-1.991	-1. 81

It is clear from the observation of the table above that the difference between the GEBCO values and the field measured values is very small and may not exceed 10 %.

6.5.3 Discretized the domain and mesh

Numerical solutions in most engineering codes (ANSYS , MIKE , FLOW3D, WAVEWATCH ,) require checking the validity of the element size in the division to avoid instability of the results .A lot of scientific articles and researches in this regard , most of them recommend using the optimal size of the mesh so that the divisions are not too smooth making the solution very complex and needs large processors to accommodate, and the size of the network is not large so that the physical phenomenon cannot be represented very correctly,(mesh independent solutions) .

In the current study, more than one model was tested and the best result was obtained for dividing the mesh using the method of specific zone of the smoothing

areas (zone of proposal breakwater layout). Figures (6.17), (6.18) shows the default mesh discretized and unstructured mesh discretized with zone adoption near the breakwater layout respectively, mesh size was selected with mesh independent solution for many sizes tested (200,175,120, 90, 75, 55, 46, 35, and 27 m). the optimum mesh discretized had been selected for the present work with mesh element size 35 m length.

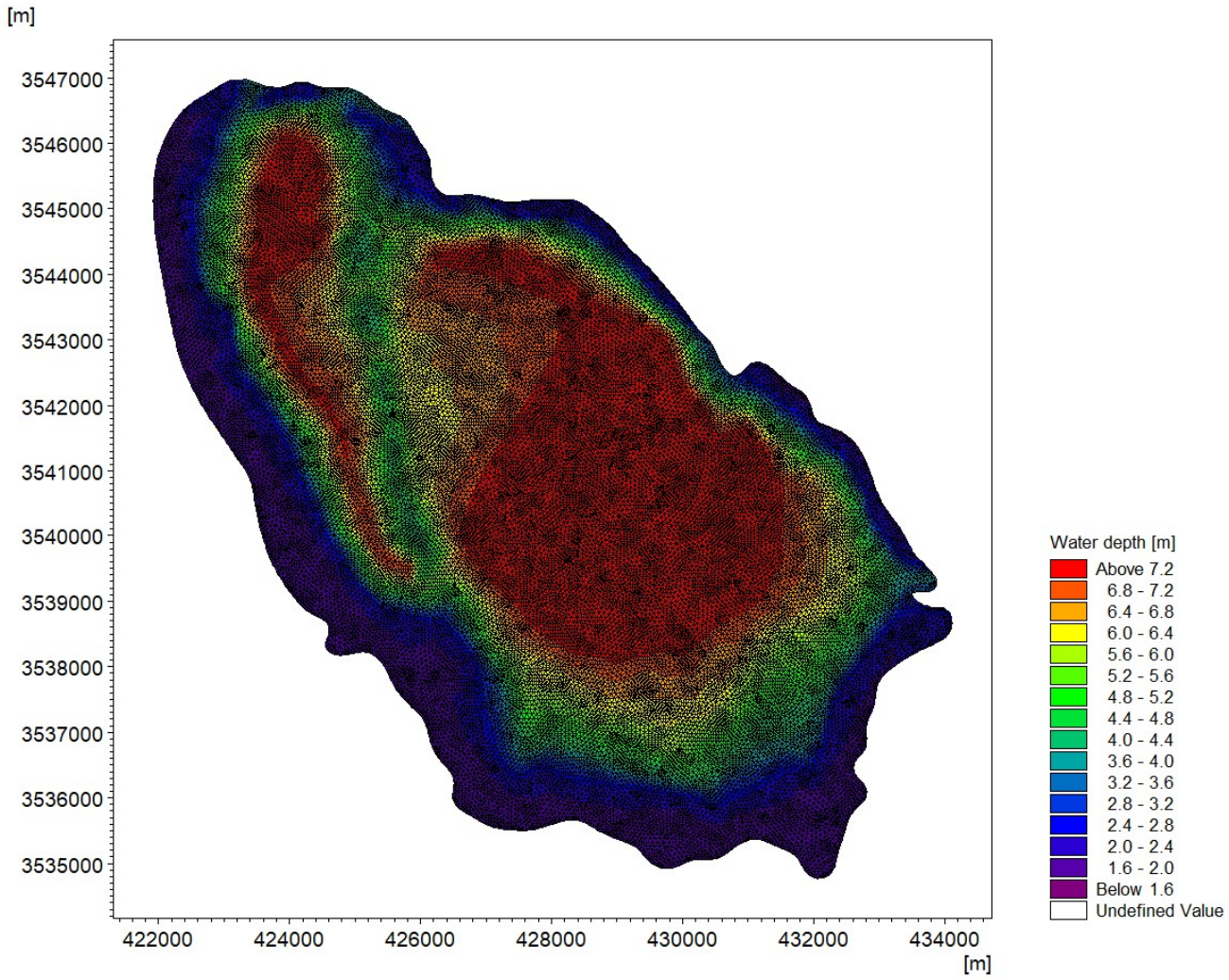

Figure (6.17) default mesh discretized without any zone adaption

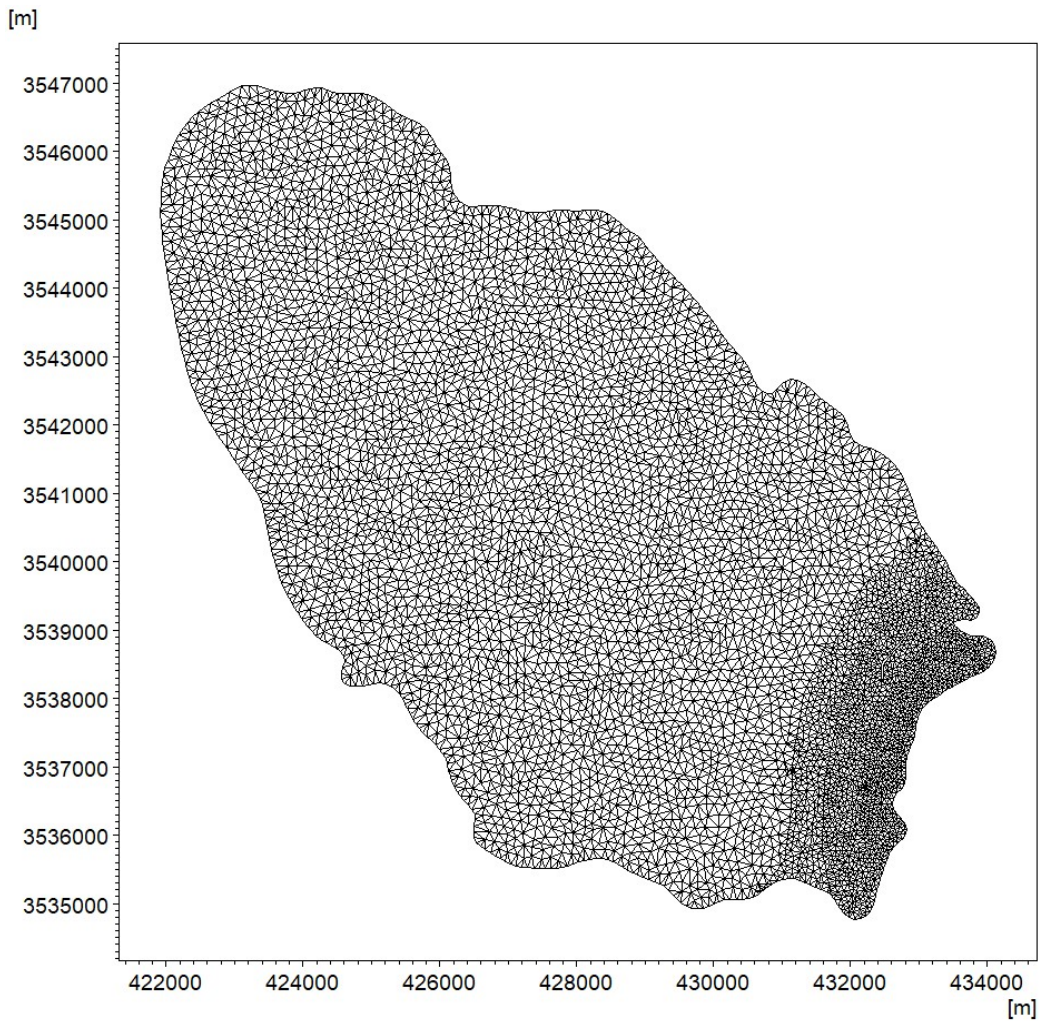

Figure (6.18) unstructured mesh discretized with zone adaption

6.5.4 Validation of Mathematical Model (MIKE21)

In clearly, the validation of a mathematical model (**MIKE21SW**) involves comparing its predictions with actual observations measurements to ensure its accuracy and reliability for real-world applications.

The **Guanting**, **Hedi**, and **Putian** formulas are three of the most often used empirical formulae for wave high and period measurements. Consistent with the research conducted by **Li et al. (2006)**, the use of the Putian formula may be employed for the estimation of the mean height and duration of water waves. the Putian formula was proposed by (Duan 1996) to calculate wave run-up height

according to six years of observation at the seawall of Putian, China. In 2002, and made agood results in many studies as mention above. Equation (6.5) represent the wind induce wave growth formula is as follows:

$$\frac{gh_m}{w^2} = 0.13\, tanh\left[0.7\,(\frac{gHm}{W^2})^{0.7}\right]\, tanh\left\{\frac{0.0018\left({}^{gD}/_{W^2}\right)^{0.45}}{0.13\tanh\left[0.7\left({}^{gHm}/_{W^2}\right)^{0.7}\right]}\right\} \qquad \ldots\ldots\ldots (6.5)$$

where: D represent fetch (meters), H_m : sea depth in average (meters), h_m : average wave height (m), T_m is the average wave period (s), and w is the computed wind speed (m/s).

In order to validate the accuracy of the MIKE21 SW model, wave heights are computed for the designated research region in accordance with both the model itself and the empirical formula outlined in equation (6.5). The empirical formula findings, in relation to the SW model, are shown in Table (6.6) and Figure (6.19).

Table (6.6) Result of average wave height (empirical formula and numerical model)

Points	Water depth H_m (m)	Wind direction	Wind speed W (m/s)	Fetch length (m)	h_m Empirical	h_m Numerical	hm Empirical-hm Numerical
O1	5.10	NNW (360 º)	9	11345	0.89	1.01	0.12
O2	5.60	NW (315 º)	15	12678	1.25	1.31	0.06
O3	4.75	NNW (290º)	12	11690	1.21	1.29	0.08
O4	4.11	NNW (270º)	7	7689	0.76	0.73	0.03
O5	4.67	NNW (260 º)	5	6567	0.52	0.5	0.02

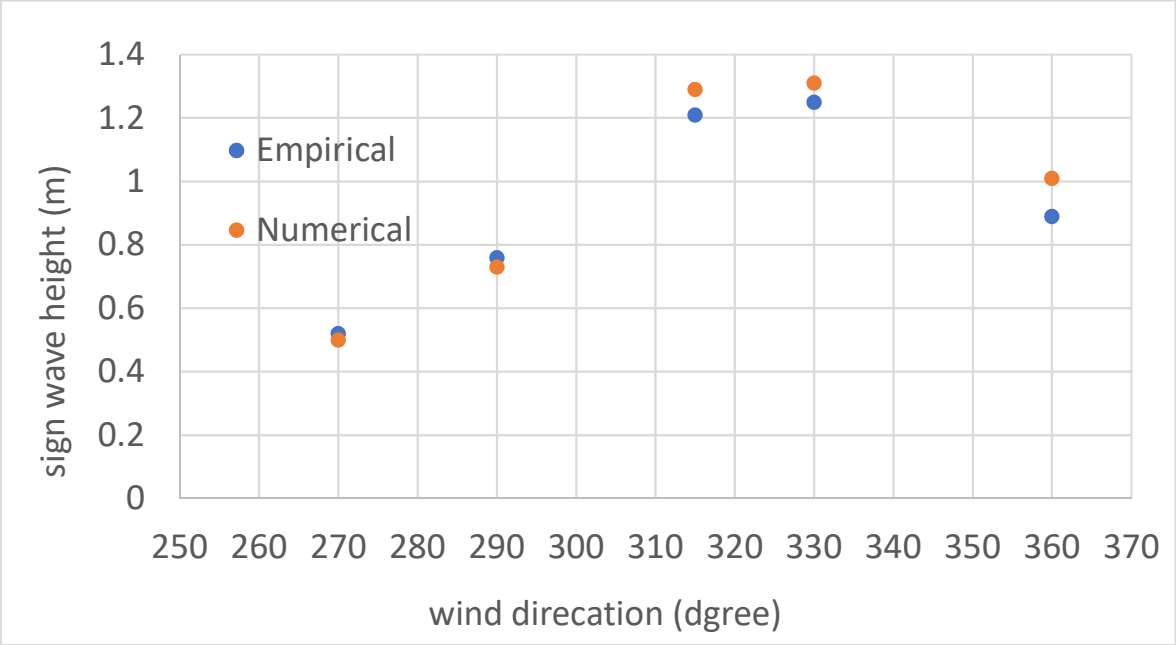

Figure (6.19) Compression between empirical and numerical results.

6.6 Layout of Breakwater Specification

The main purpose of preparing this section was how to employ energy dispersal facilities and breakwater orientations to protect the zone selected in the figure (6.20) road of Maamal. It can be seen that in figure (6.21), the shore line alone the road of Maamal are subject to the risk of wave induced flood for any point with land elevations less than 0.7 m from zero water level of lake (20 m.s.a.)

Figure (6.22) shows three distinct layouts (scheme 1, 2, and 3) with varied breakwater length and directions were considered. The impact of the breakwater on the wave field under various circumstances was then studied in order to give the construction unit with accurate simulation results. Figure (6.23) depicts the breakwater's points monitors (P1 -P10) for all scheme type to demonstrated the reduction in wave high in each point.

Figure (6.20) satellite image demonstrated the proposed breakwater location

Figure (6.21) Some of point elevation along the line of land-water (red points inside zone of protection) (blue points outside zone of protection)

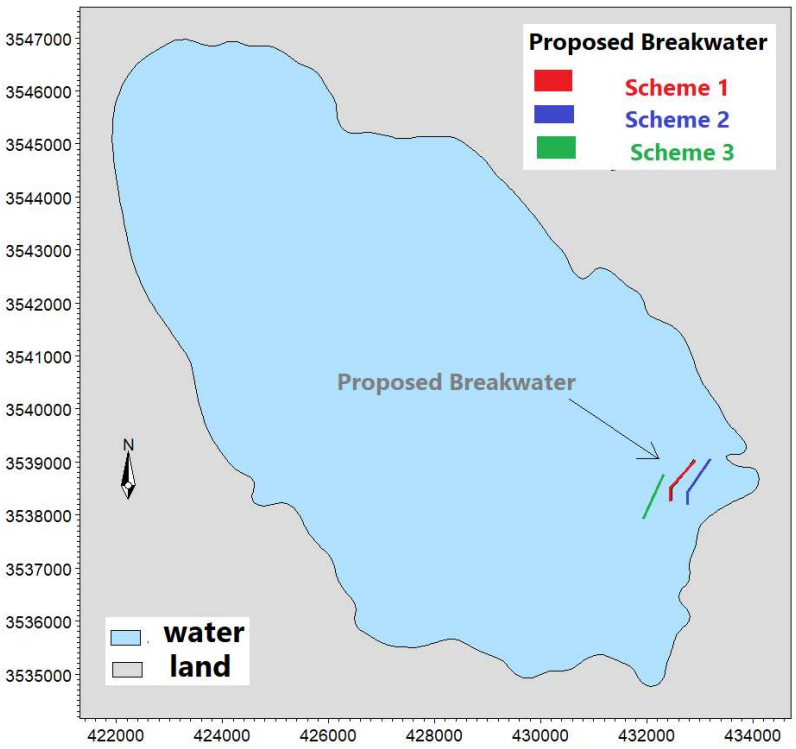

Figure (6.22) layout of proposed breakwater

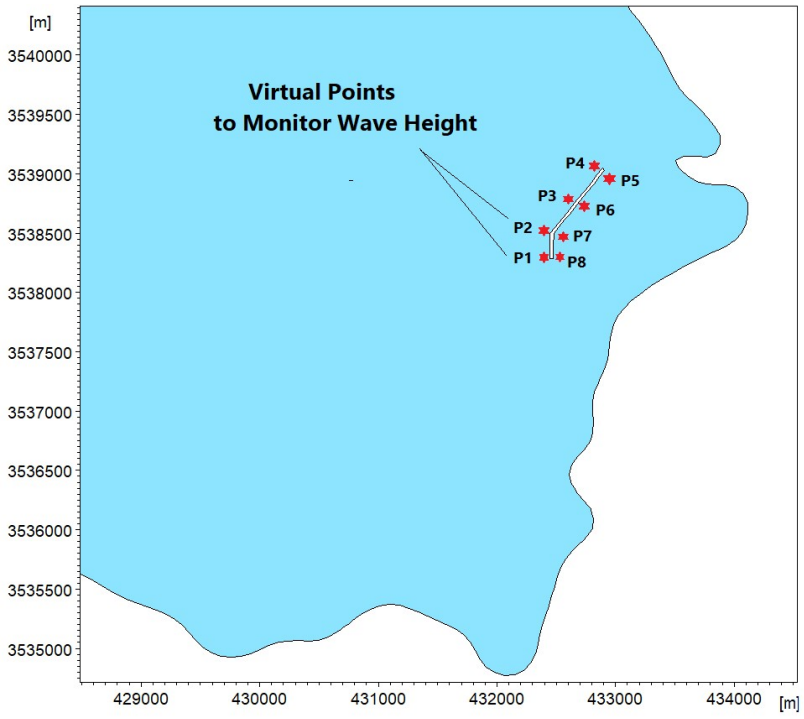

Figure (6.23) virtual points to monitor wave high in proposed breakwater.

Table (6.7) below described the three-scheme layout for breakwater specification used to represented the optimal location of breakwater layout in the different orientation.

Table (6.7) layout of breakwater

Scheme proposed	Details of proposed Breakwater
Scheme 1	The breakwater is 800 meters long in total; the broken line sections on the south and east sides are each 170 meters long. Crest level = mean sea level MSL, wave direction orthogonal on breakwater (315°)
Scheme 2	The breakwater is 862 meters long overall; the sections with broken lines on the west and east sides are each 177 meters long. Crest level = mean sea level MSL, wave direction (295°)
Scheme 3	The breakwater is 879 meters long and is oriented in a straight line at a 36-degree angle from the azimuth. Crest level = mean sea level MSL

In this part, a set of graphical outputs will be presented for modeling the study area, which represents the worst case of wind induced wave necessity as mentioned earlier. Figures (6.24), (6.25), (6.26) and (6.27), represented water depth, sign wave height, and wave period respectively.

Figure (6.28), (6.29), and (6.30) shows the Significant wave height in the direction NNW (315°) for three different Scheme, it is clear from these figures that the scheme 1 scenario of the breaker layout gives the highest efficiency to reduce the wave height in the concerned area and covers the highest area on the coast and the adjacent area of wave activity.

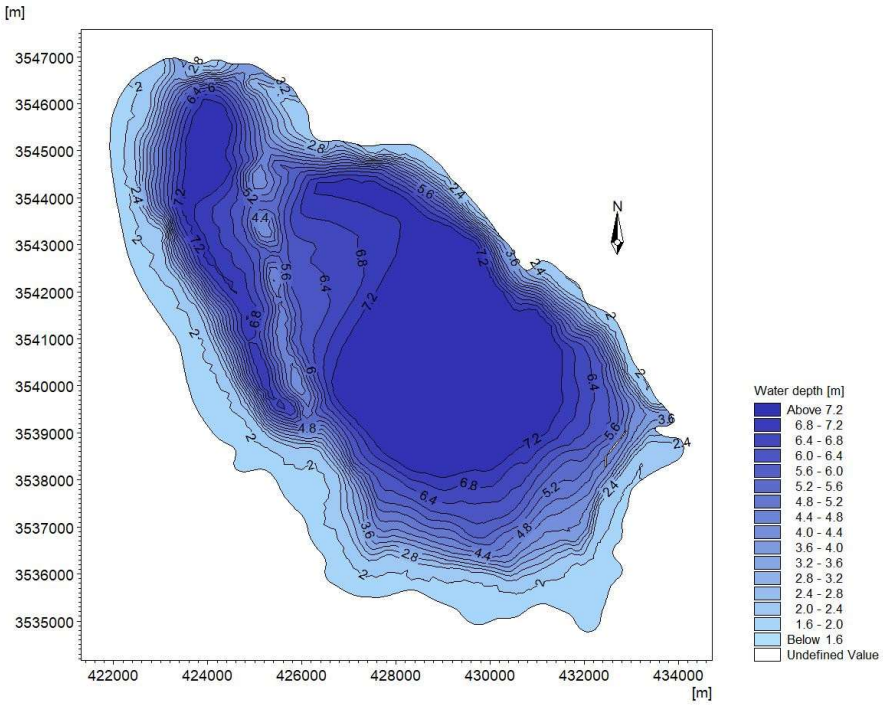

Figure (6.24) water depth and boundry of lake

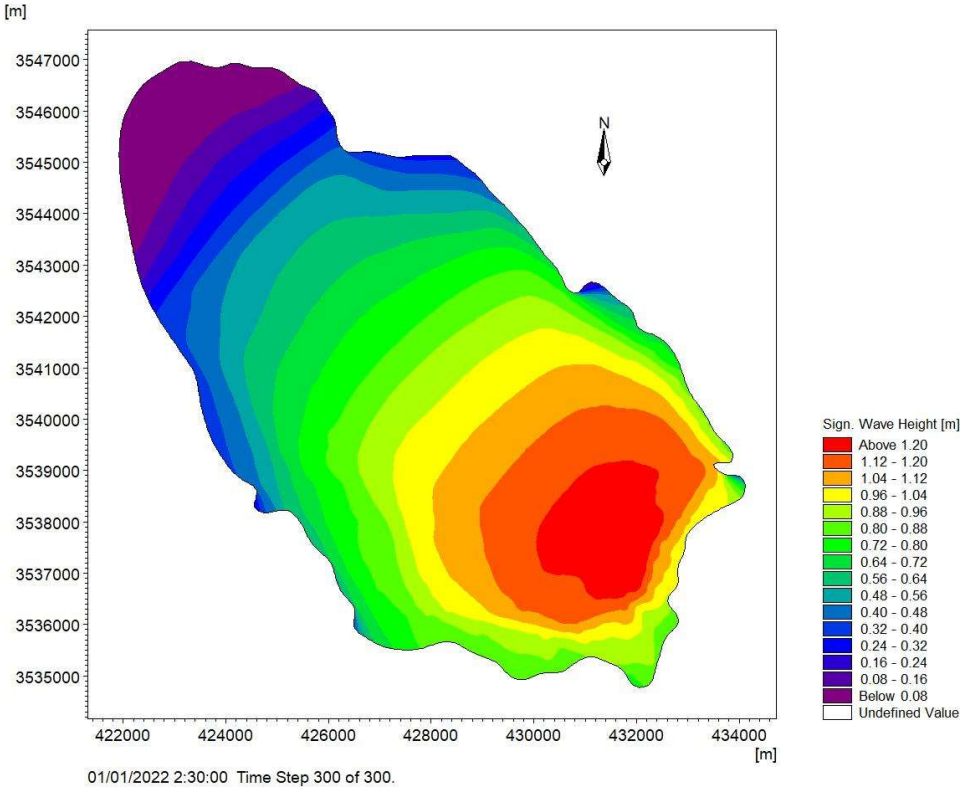

Figure (6.25) sign wave hight (wind direction 315^{o})

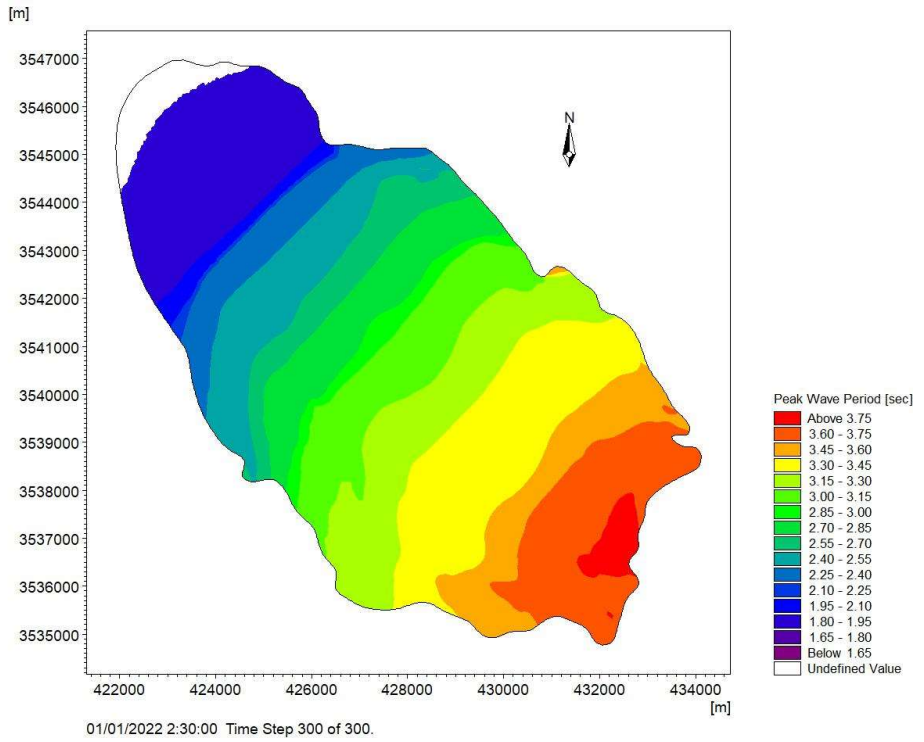

Figure (6. 26) wave period (wind direction 315º)

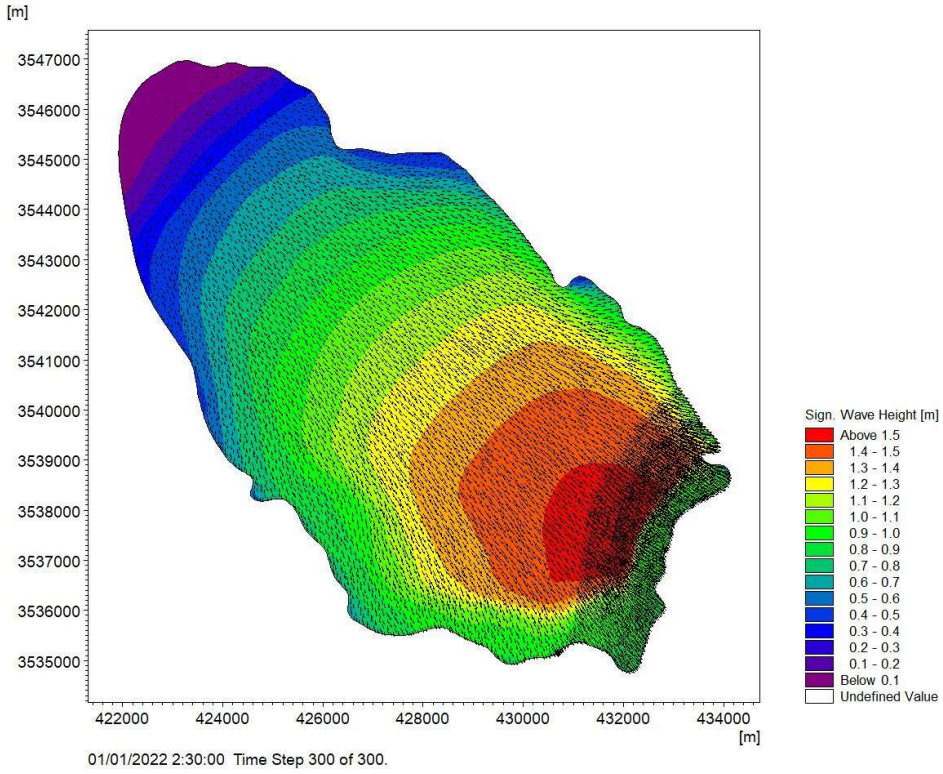

Figure (6.27) velocity vector distribution (wind direction 315º)

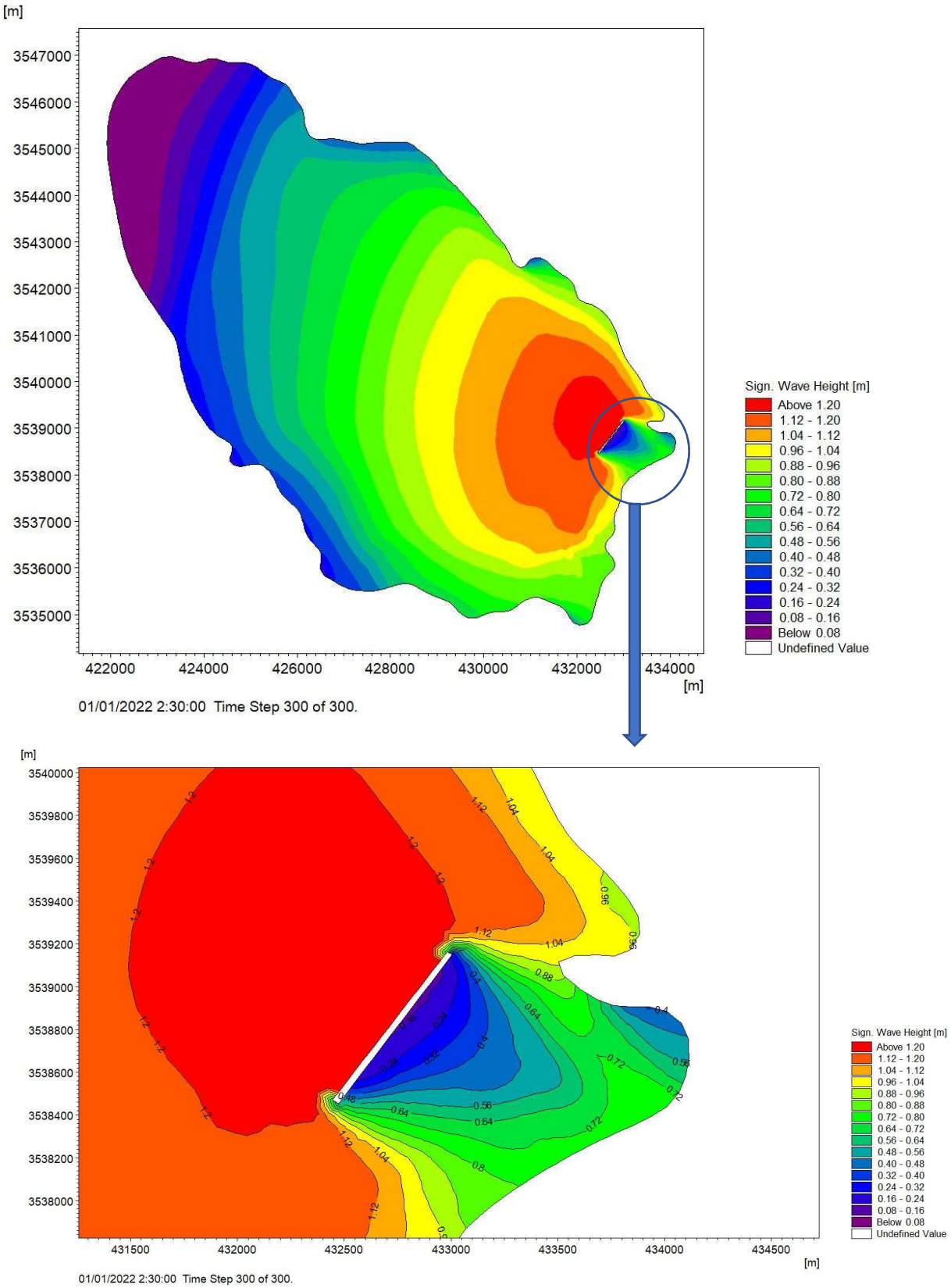

Figure (6.28) sign wave height distrbution (scheme 3 line breakwater)

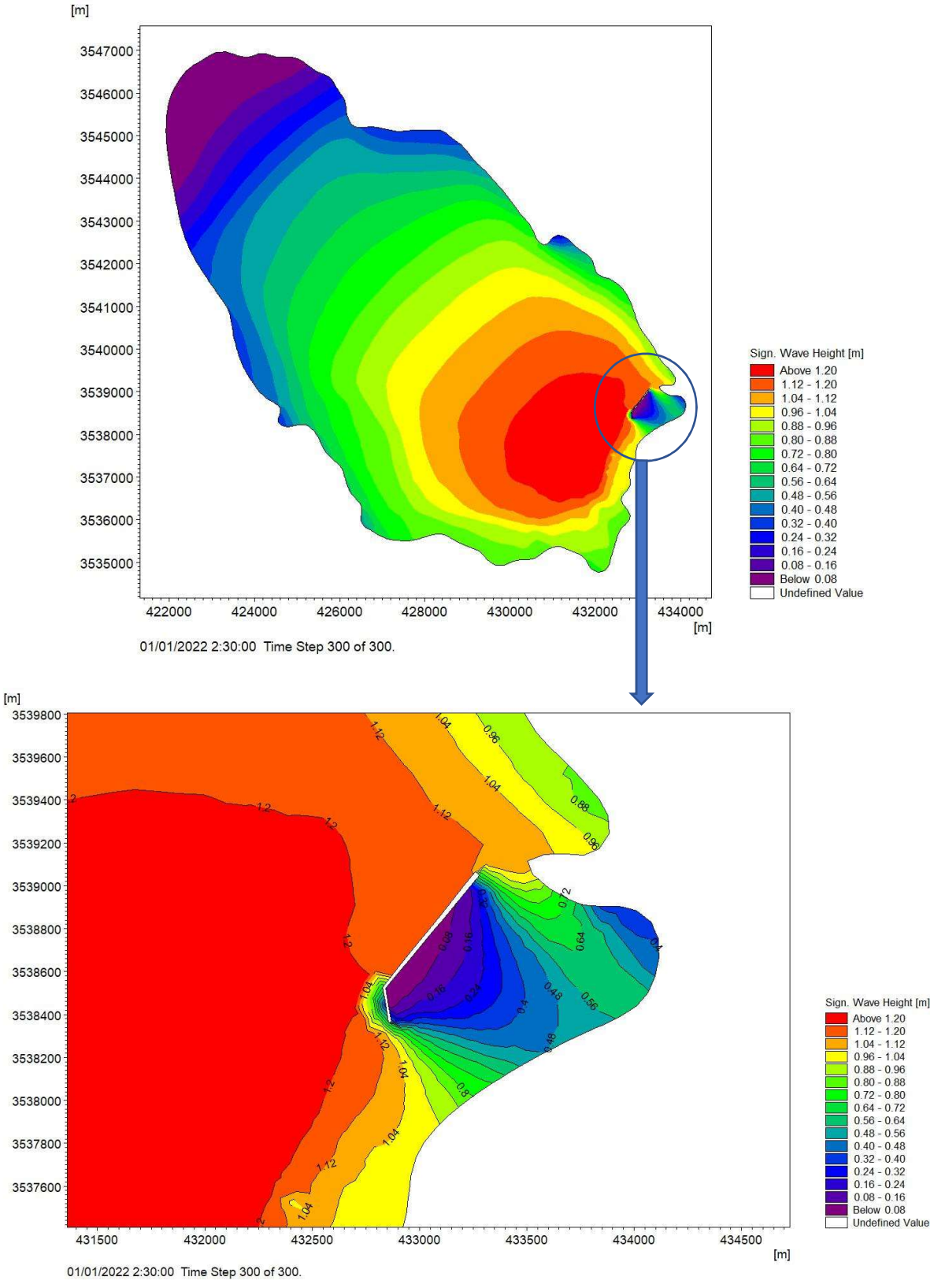

Figure (6.29) sign wave height distribution (scheme 2 breakwater)

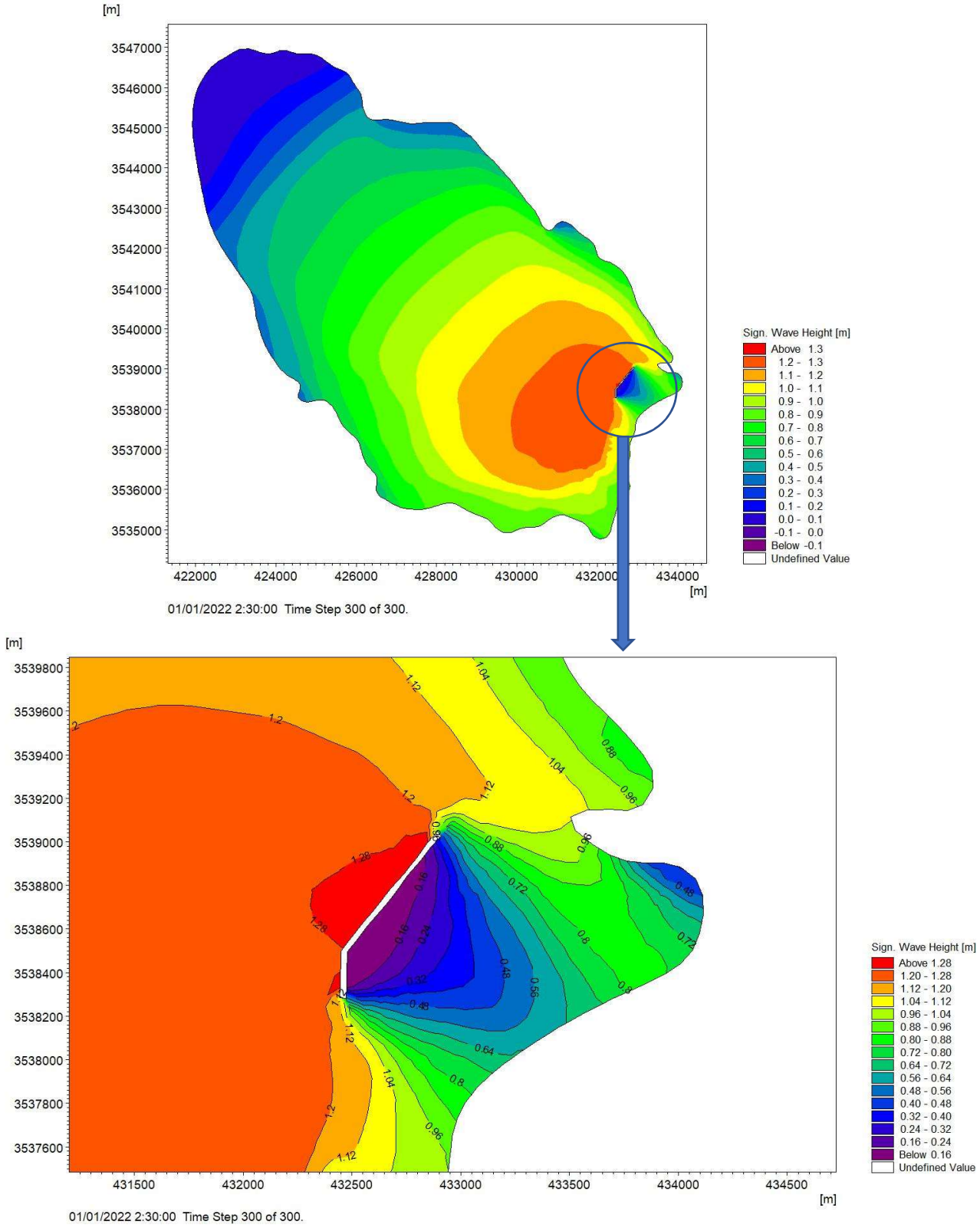

Figure (6.30) sign wave height distribution (scheme 1 breakwater)

The following tables (6.8),(6.9) and (6.10) represent result of implantation of three scheme of breakwater for different wind induced wave direction (315°,290°, and 270°).

Table (6.8) details of three schemes breakwater layout and results of MIKE21 SW model and points features (wind direction 315°).

Breakwater Scheme	Point monitor (1 to 8)	x-coordinates m	y-coordinates m	Sign Wave high (m)	Covering area with wave sign height less than 0.7 m (km^2)	Length of shoreline protect (Km)
Scheme 1	**Points (1-8)**	432431.798	3538289.742	0.77	1.19	1.89
		432449.762	3538501.743	0.76		
		432658.172	3538778.423	1.22		
		432884.546	3539051.509	1.23		
		432913.292	3539026.356	0.72		
		432557.345	3538778.423	0.12		
		432482.103	3538494.557	0.09		
		432482.103	3538296.929	0.54		
Scheme 2	**Points (1-8)**	432844.678	3538361.876	0.79	0.889	1.65
		432822.900	3538522.123	0.77		
		433034.678	3538811.900	1.21		
		433257.123	3539062.122	1.15		
		433279.124	3539044.234	0.65		
		433077.236	3538800.129	0.11		
		433850.234	3538525.789	0.08		
		432869.654	3538361.876	0.50		
Scheme 3	**Points (1-8)**	432444.157	3538478.203	0.833	1.11	1.77
		432617.372	3538705.032	1.22		
		432800.898	3538940.110	1.23		
		432969.989	3539164.8.77	0.78		
		433000.009	3539137.213	0.253		
		432851.053	3538934.092	0.148		
		432661.473	3538685.832	0.168		
		432489.949	3538464.655	0.54		

Table (6.9) details of three schemes breakwater layout and results of MIKE21 SW model and points features (wind direction 290°).

Breakwater Scheme	Point monitor (1 to 8)	x-coordinates m	y-coordinates m	Sign Wave high (m)	Covering area with wave sign height less than 0.7 m (km^2)	Length of shoreline protect (Km)
Scheme 1	**Point (1-8)**	432431.798	3538289.742	0.72	1.08	2.11
		432449.762	3538501.743	0.71		
		432658.172	3538778.423	1.20		
		432884.546	3539051.509	1.18		
		432913.292	3539026.356	0.79		
		432557.345	3538778.423	0.14		
		432482.103	3538494.557	0.08		
		432482.103	3538296.929	0.56		
Scheme 2	**Point (1-8)**	432844.678	3538361.876	0.78	0.92	1.68
		432822.900	3538522.123	0.74		
		433034.678	3538811.900	1.91		
		433257.123	3539062.122	1.12		
		433279.124	3539044.234	0.66		
		433077.236	3538800.129	0.13		
		433850.234	3538525.789	0.09		
		432869.654	3538361.876	0.53		
Scheme 3	**Point (1-8)**	432444.157	3538478.203	0.81	1.08	1.70
		432617.372	3538705.032	1.20		
		432800.898	3538940.110	1.23		
		432969.989	3539164.8.77	0.78		
		433000.009	3539137.213	0.24		
		432851.053	3538934.092	0.12		
		432661.473	3538685.832	0.15		
		432489.949	3538464.655	0.56		

Table (6.10) details of three schemes breakwater layout and results of MIKE21 SW model and points features (wind direction 270°).

Breakwater Scheme	Point monitor (1 to 8)	x-coordinates m	y-coordinates m	Sign Wave high (m)	Covering area with wave sign height less than 0.7 m (km^2)	Length of shoreline protect (Km)
Scheme 1	**Point (1-8)**	432431.798	3538289.742	0.75	1.10	1.92
		432449.762	3538501.743	0.77		
		432658.172	3538778.423	1.21		
		432884.546	3539051.509	1.21		
		432913.292	3539026.356	0.73		
		432557.345	3538778.423	0.12		
		432482.103	3538494.557	0.085		
		432482.103	3538296.929	0.55		
Scheme 2	**Point (1-8)**	432844.678	3538361.876	0.76	0.917	1.69
		432822.900	3538522.123	0.71		
		433034.678	3538811.900	1.23		
		433257.123	3539062.122	1.13		
		433279.124	3539044.234	0.68		
		433077.236	3538800.129	0.11		
		433850.234	3538525.789	0.08		
		432869.654	3538361.876	0.52		
Scheme 3	**Point (1-8)**	432444.157	3538478.203	0.81	1.2	1.73
		432617.372	3538705.032	1.21		
		432800.898	3538940.110	1.24		
		432969.989	3539164.8.77	0.77		
		433000.009	3539137.213	0.24		
		432851.053	3538934.092	0.12		
		432661.473	3538685.832	0.15		
		432489.949	3538464.655	0.56		

Figures (6.31), (6.32), and (6.33) demonstrated the sign wave height distribution for scheme 1 breakwater according to different wind direction, it can be seen from these figures the wave distribution are very sensitive to the wind spectral direction. according to above details of wave distribution the optimal location of breakwater was selected according to the most dominated wind direction and frequency (315°).

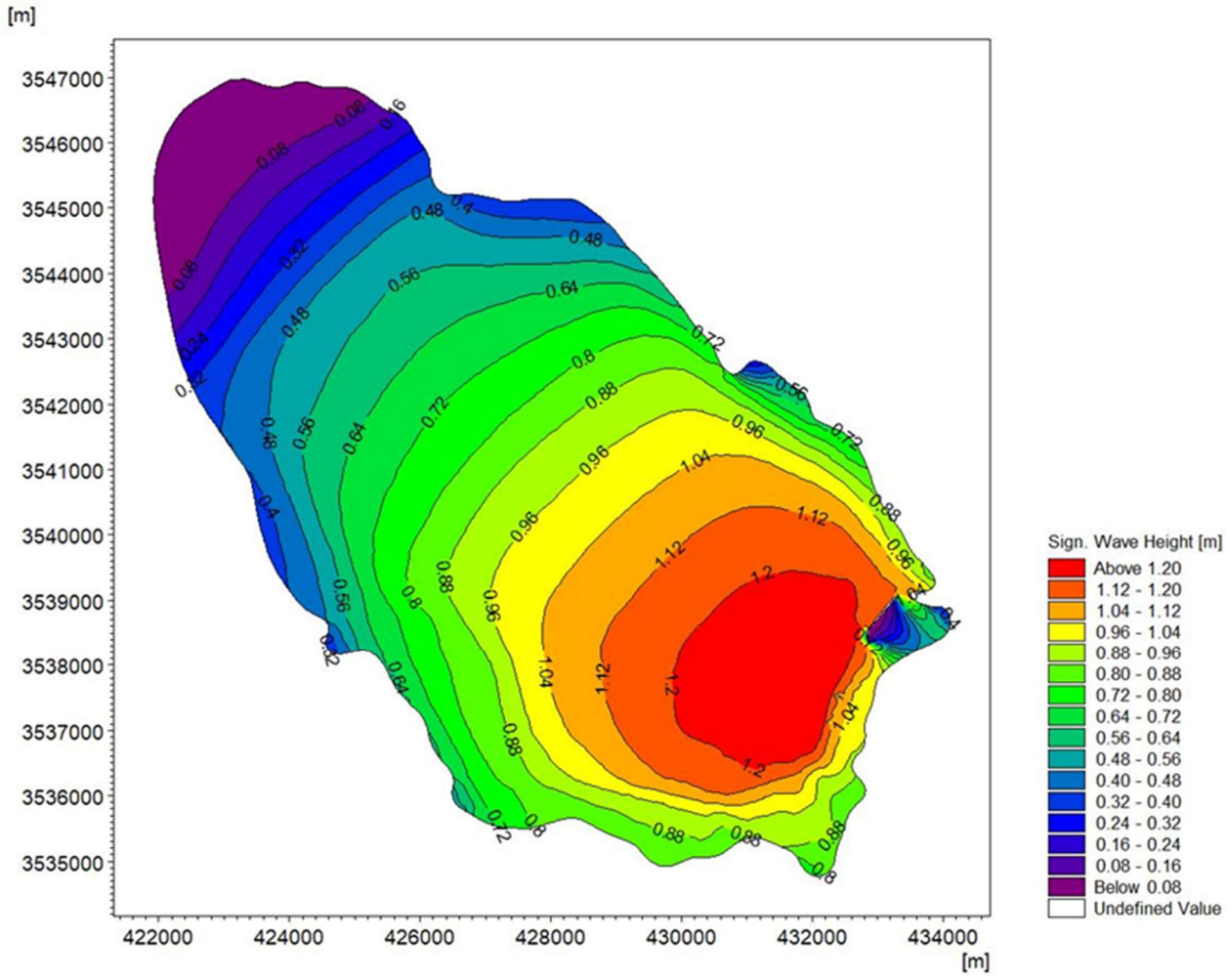

Figure (6.31) sign wave height distribution for scheme 1 (315°)

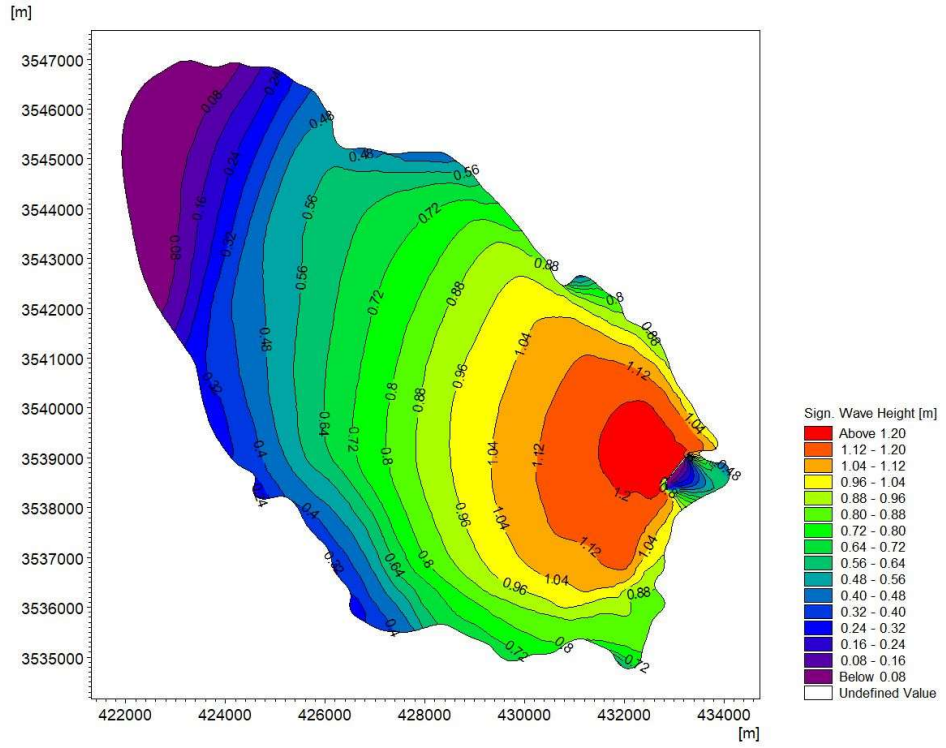

Figure (6.32) Sign wave height distribution for scheme 1 (290º)

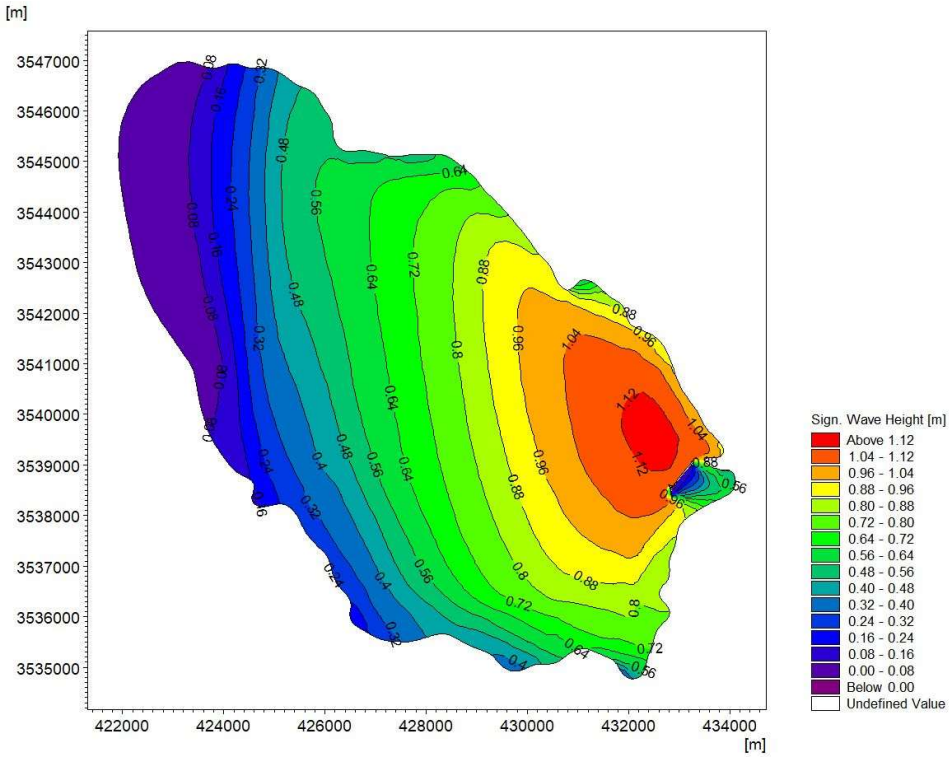

Figure (6.33) Sign wave height distribution for scheme 1 (270º)

6.7 Design Breakwater (Cross -Section)

The selection of the breakwater cross-section is a complementary part to the selection of the breakwater location specified in the previous section. In the chapter four of this study, many shapes cross section of Breakwater has been tested experimentally and mathematically, and the best form among these shapes was determined according to the highest energy dispersion coefficient and the lowest wave transmission (Ct) through the breakwater. The steps slope model (M2) that make the highest dispersion coefficient.

In this part of the research. Based on the full-scale spectral wave model SW result outcome (wave height, wave length, wave period, bathymetry data, for depression of Najaf see, an addition to the optimal location of breakwater layout (scheme 1).

Four models derived from the best shape (M2) chosen in the chapter four of this study with the adoption of the wave characteristics resulting from the mathematical model of SW.

Table (6.11) shows the four models that were tested for the purpose of determining the best cross-section that meets the requirements of the breakwater in terms of its performance in dispersing wave energy.

All the four model (MD1, MD2, MD3, and MD4) had been simulated by Fluent solver to demonstrated the efficient each model according to values of transmission coefficient (Ct), rate of energy dissipation, and large eddy disturbances.

Table (6.12) shows the results of transmission coefficient and rate of wave dissipations for different model. It can be seen that the largest energy dissipations are received for model MD1, and MD2.

A set of graphical image outputs such as turbulence energy frequency and wave breaking profile shows the difference between the four models tested.

It is noticeable that the first and second models (MD1, MD2) gave the highest value of the wave dispersion coefficient. It is possible that the reason for that the upper part of the structure of the breakwater play as a stiling Basin and the inclined part breaks the wave before it reaches the top of the breakwater.

Figures (6.34), (6.35), (6.36), and (6.37) demonstrated the cross-section shape and dimensions of breakwater for different model had been used. Wave generation according to time steps presented in figure (6.38).

Figure (6.39) shows the wave breaking stages cross the breakwater for different breakwater model.

Table (6.11) Characteristics of model derived from M1

Model	**Symbol**	**Description**	**Number of steps**	**Steps size (m)**	**Wave Characteristics**
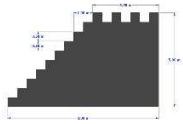	MD1	Figure (6.34)	13	0.05 *0.05	Result of spectral wave model (SW)
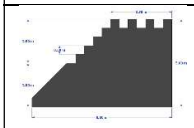	MD2	Figure (6.35)	8		
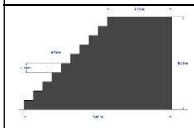	MD3	Figure (6.36)	10		
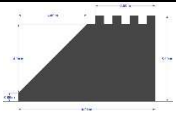	MD4	Figure (6.37)	4		

Table (6.12) Results of transmission coefficient for different breakwater model

Model	Symbol	Incident wave height(m)	Wave length (m)	Wave period (sec)	Submerged depth (m)	Wave transmission height (m)	transmission coefficient (Ct)	Wave dissipations rate (%)
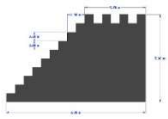	MD1	1.4	17	3.76	0	0.27	0.192	80
					0.5	0.33	0.23	77
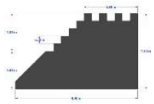	MD2	1.4	17	3.91	0	0.28	0.20	80
					0.5	0.33	0.23	77
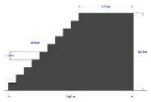	MD3	1.4	17	3.82	0	0.34	0.24	76
					0.5	0.38	0.27	73
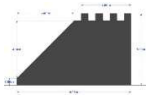	MD4	1.4	17	3.65	0	0.30	0.21	79
					0.5	0.35	0.25	75

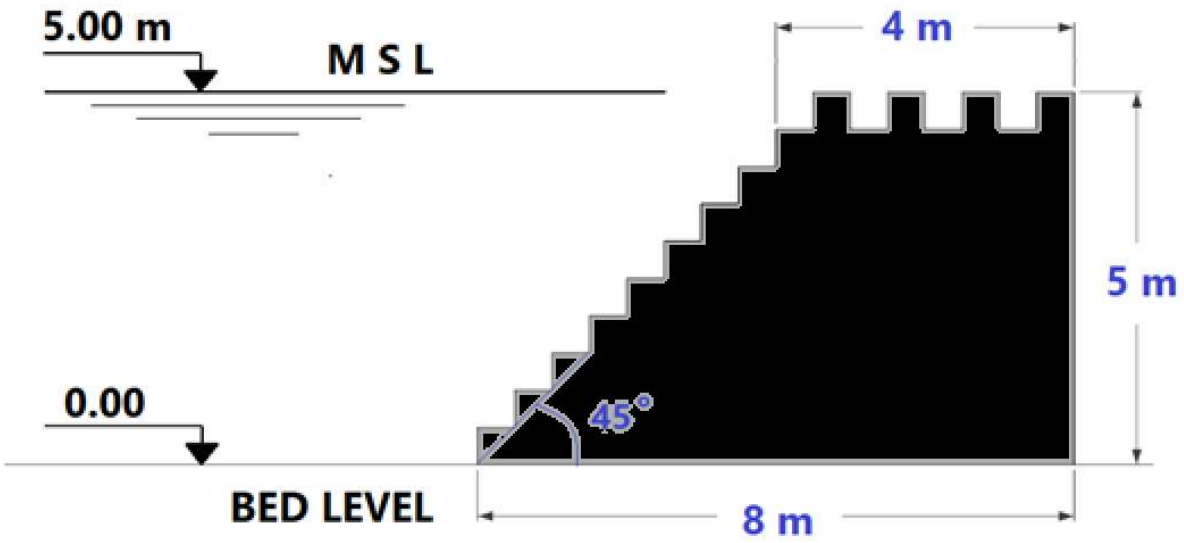

Figure (6.34) Shape of proposal design breakwater model (MD1) according to specified position of scheme 1

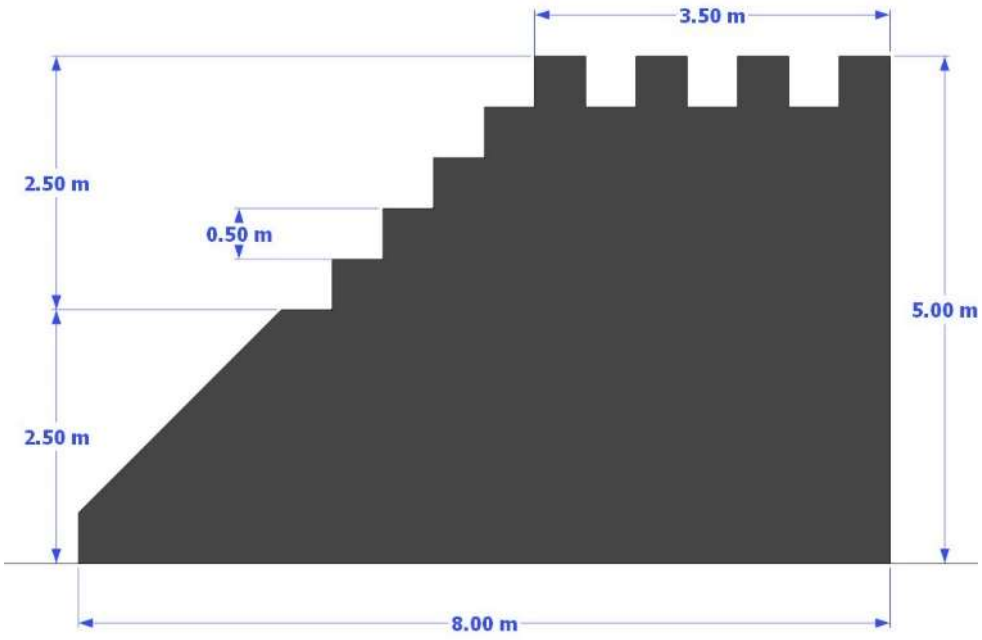

Figure (6.35) Shape of proposal design breakwater model **(MD2)**

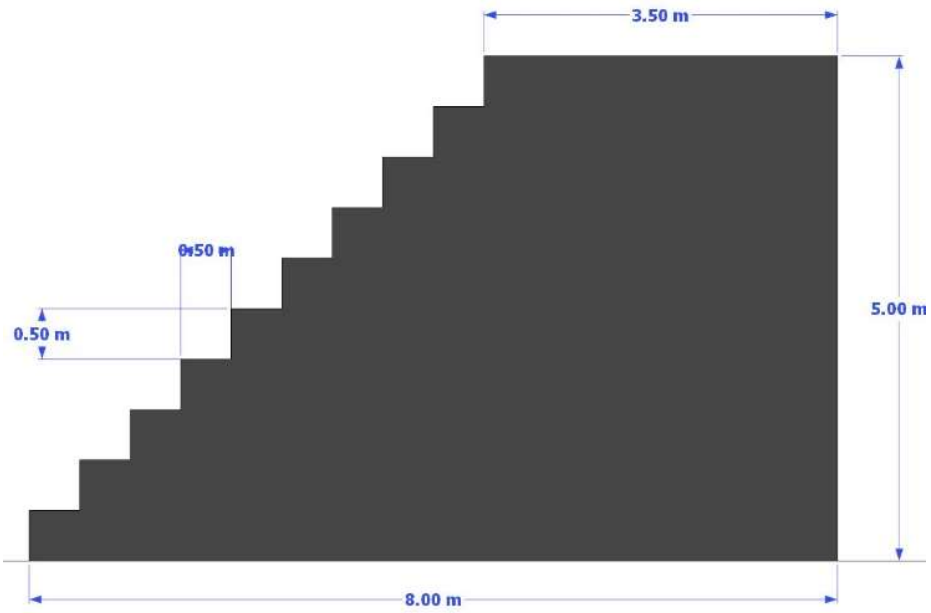

Figure (6.36) Shape of proposal design breakwater model **(MD3)**

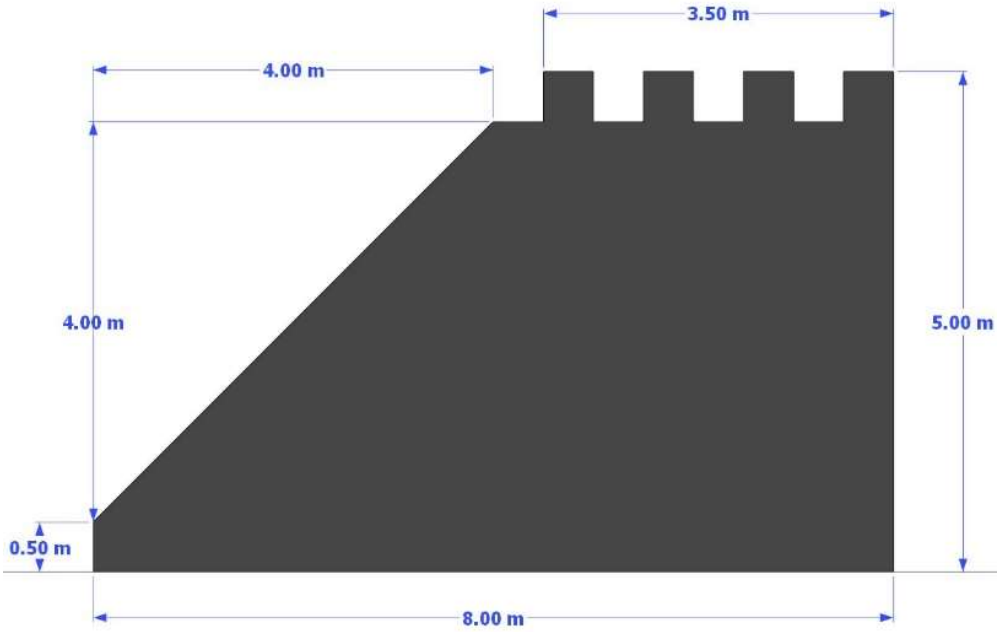

Figure (6.37) Shape of proposal design breakwater model **(MD3)**

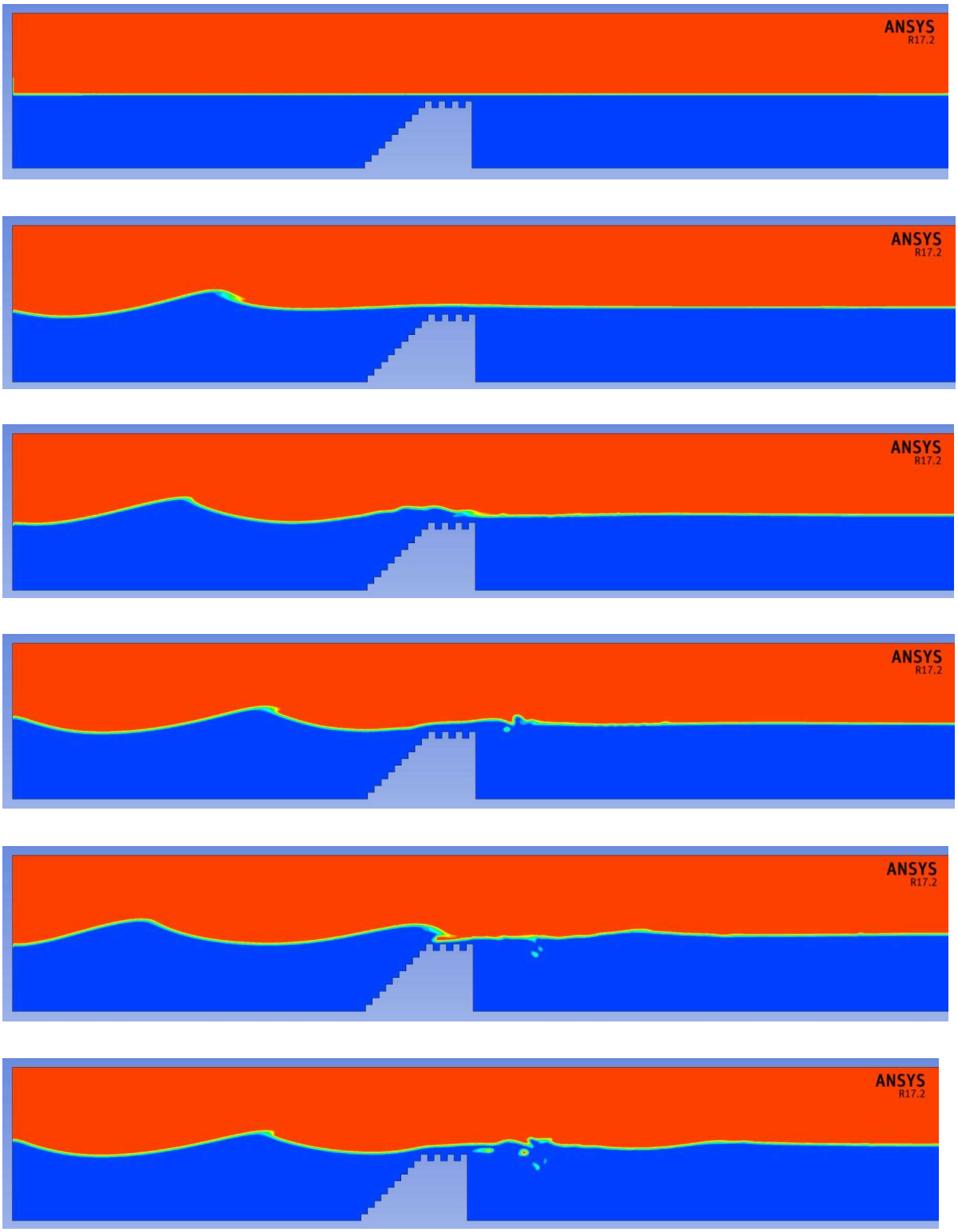

Figure (6.38) Wave generation according to time steps (0 sec to 13 sec)

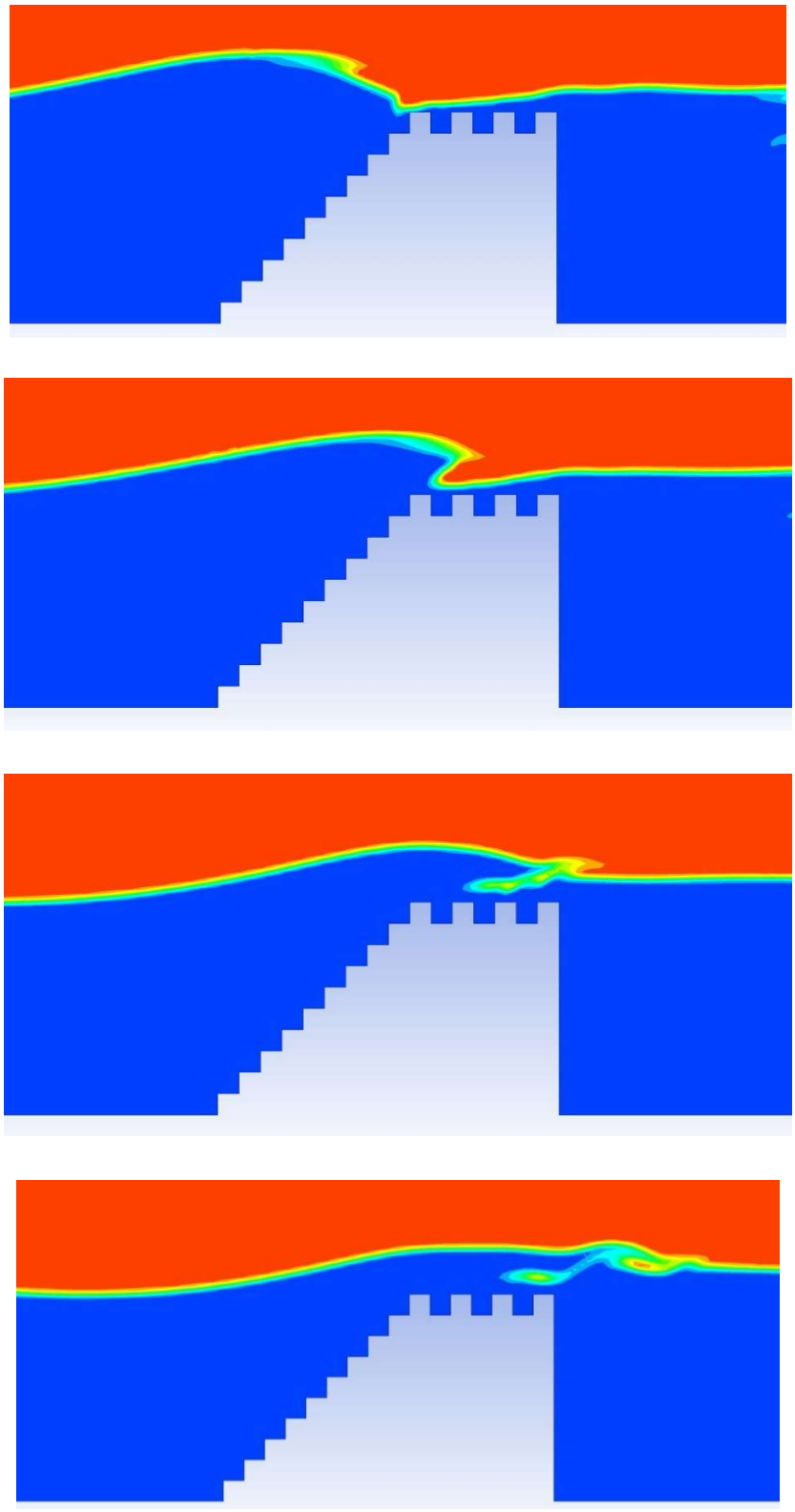

Figure (6.39) Wave breaking through the breakwater face

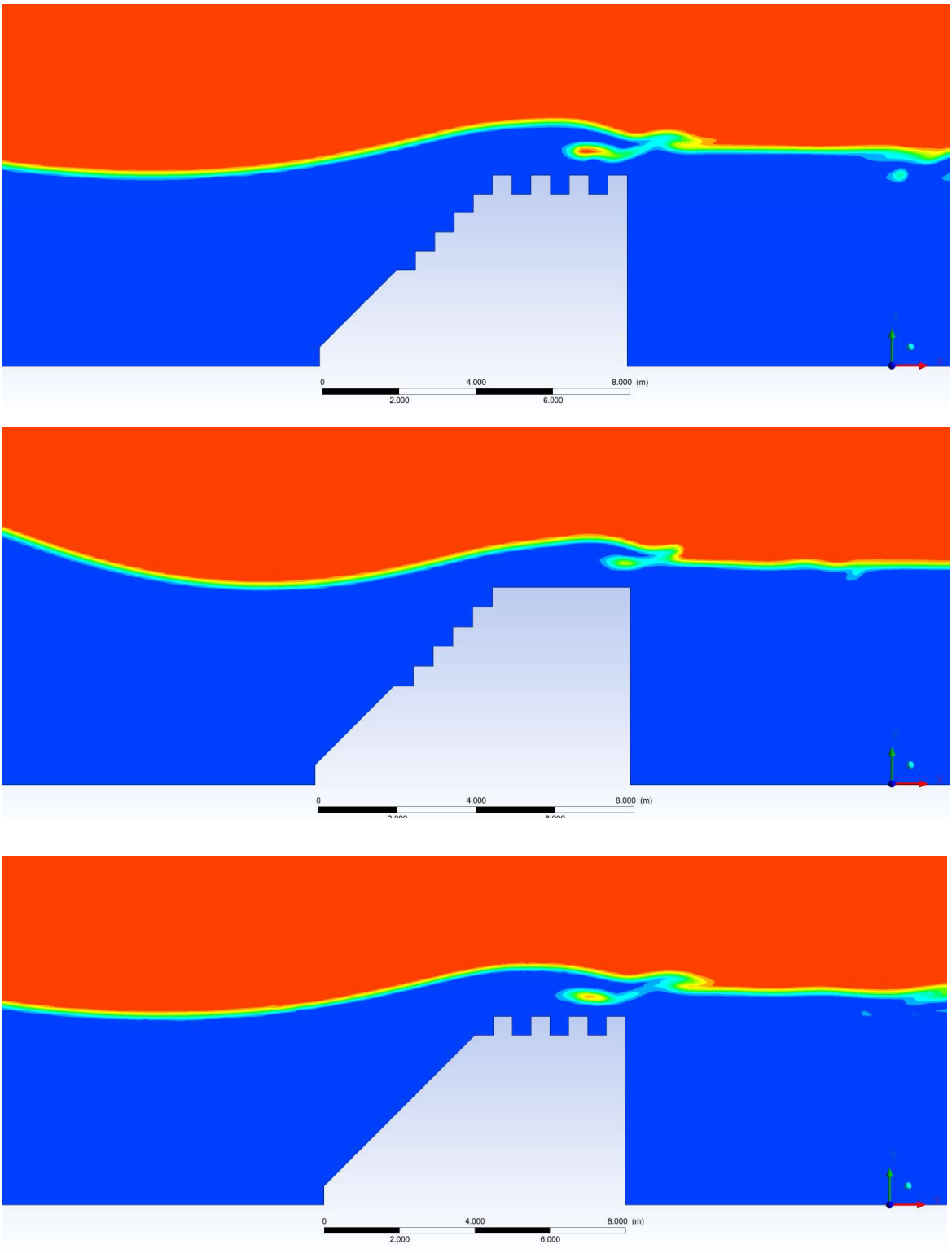

Figure (6.40) wave breaking through different breakwater (MD2, MD3, MD4)

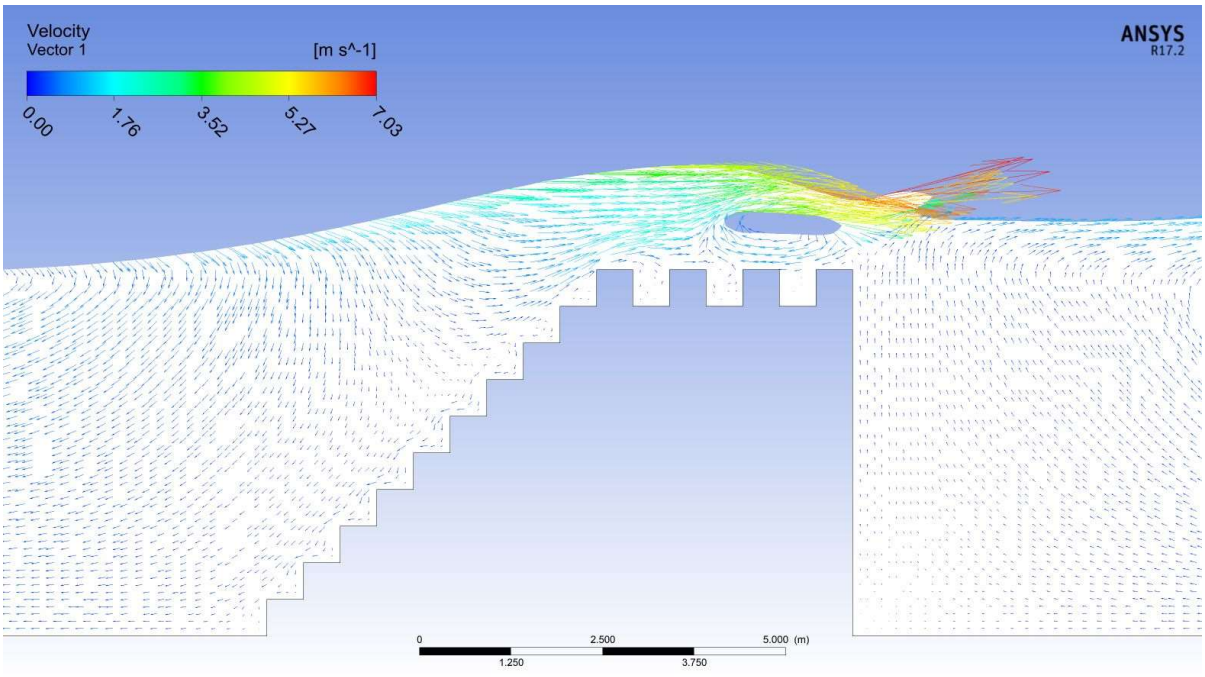

Figure (6.41) flow vectors color by velocity of wave

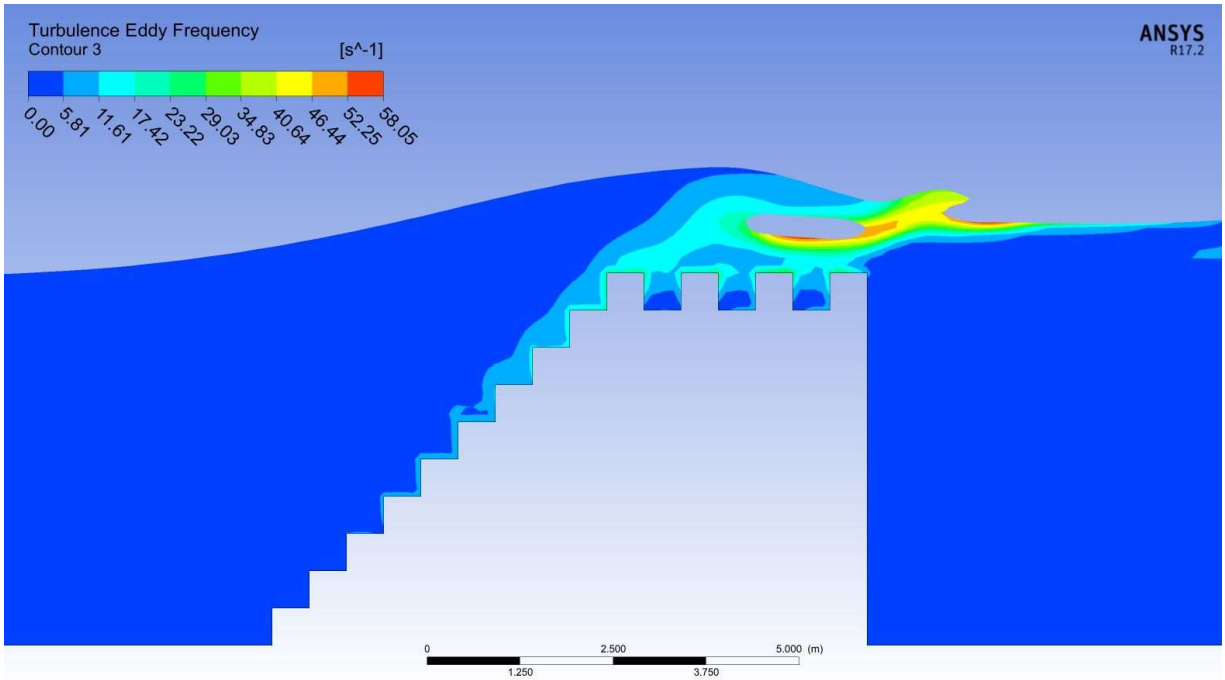

Figure (6.42) turbulence eddy frequency for wave breaking through MD1 model

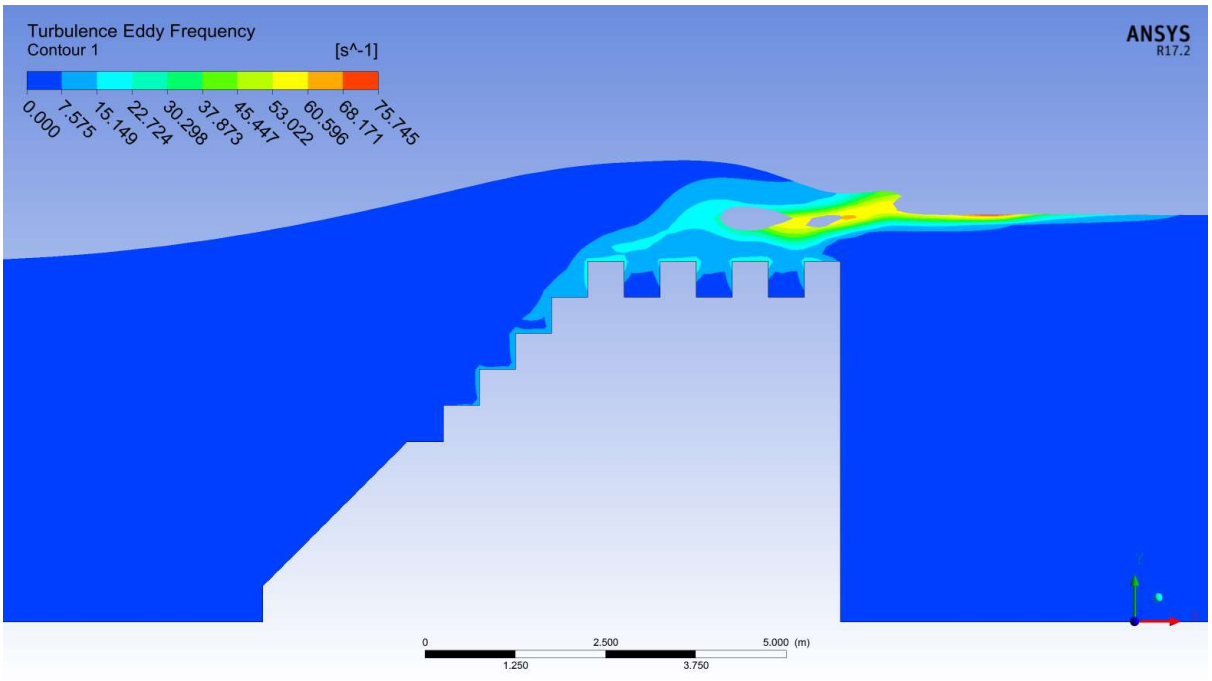

Figure (6.43) turbulence eddy frequency for wave breaking through MD2 model

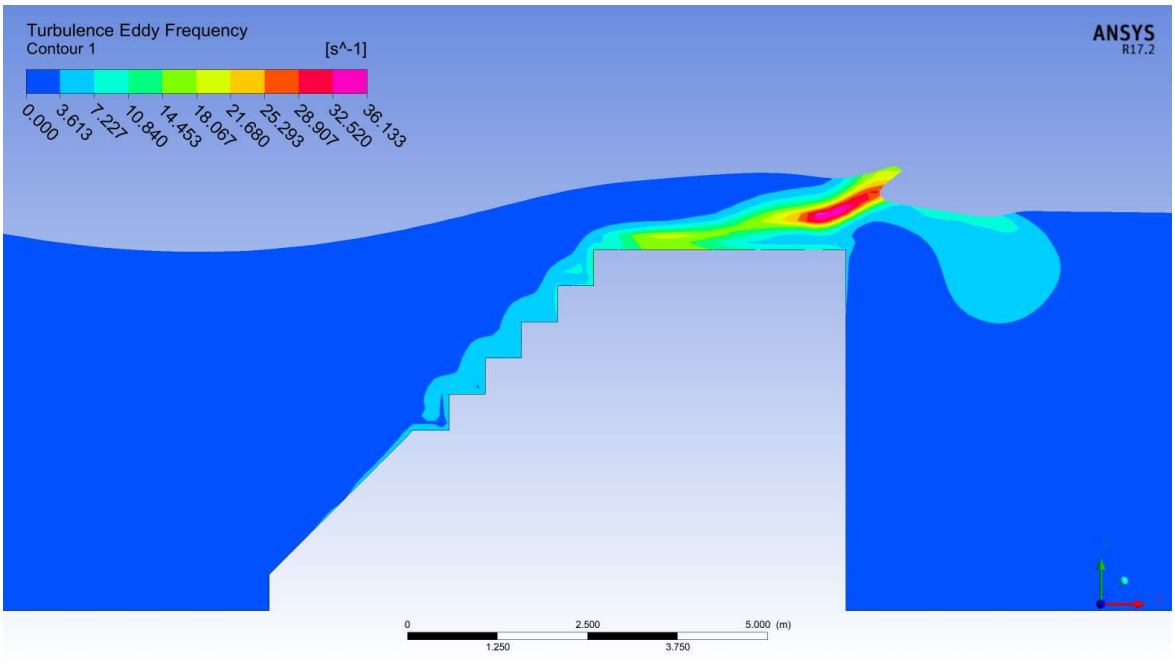

Figure (6.44) turbulence eddy frequency for wave breaking through MD3 model

6.8 Inclination of Breakwater

The lateral slope of the breakwater is an essential part of the design of the mitigation structures, as explained earlier in the chapter three of the outputs of the dimensional analysis equation. In this part, four values of the lateral inclination of The Breakwater were tested to clarify the extent of the influence of lateral inclination on the values of energy dispersion. The following table (6.12) shows the values of the transmissions wave coefficient depending on the values of the lateral slope.

Table (6.12) values of the transmissions wave coefficient depending on the values of the lateral flat slope.

Inclination (degree)	Incident wave (m)	Transmission wave (m)	Transmission coefficient (Ct)	Energy dissipation coefficient (1-Ct)
30	1.4	0.42	0.3	0.7
37	1.4	0.42	0.3	0.7
40	1.4	0.44	0.31	0.69
45	1.4	0.51	0.36	0.64
50	1.4	0.51	0.36	0.64
60	1.4	0.55	0.39	0.61

Table (6.13) values of the transmissions wave coefficient depending on the values of the lateral stepped slope.

Inclination (degree)	Incident wave (m)	Transmission wave (m)	Transmission coefficient (Ct)	Energy dissipation coefficient (1-Ct)
30	1.4	0.27	0.192	0.8
37	1.4	0.27	0.192	0.8
40	1.4	0.3	0.21	0.79
45	1.4	0.32	0.23	0.77
50	1.4	0.37	0.265	0.73
60	1.4	0.40	0.285	0.71

It is noticeable that the values of the slope of the breaker surface are affected in a very simple way compared to the surface roughness, as shown in the tables above

Chapter Seven

Conclusions and Recommendations

Chapter Seven

Conclusions and Recommendations

7.1 Conclusions

The outputs and results of this study will be divided into two-part A, and B. The first part will be concerned with laboratory study and CFD model. The second part will deal with the outputs and results of the case study.

Part A: Experimental and CFD Results

The experimental results, in comparison with the numerical results, showed that the flume dimension (15*0.45*0.3) m used can be relied upon to represent the different breakwater models, in addition it is possible to avoid reflection of wave from faraway boundary through the use of a wave absorber at the downstream side. It is essential to use (UDF) to describe the regular physical behaviour of the wave before reaching the breaker to ensure that no energy is lost from the wave before reaching breaker zone. Mesh independent solution is reached with a minimum of 240 grids per wave-length with a grid size 0.005 m and aspect ratio 1. The increase in the surface area of the breakwater (steps breakwater) leads to an increase in the dissipations of the incident wave energy through the generation of turbulence and vortices at the front of the breaker. As a result, an in brief:

- The highest value for energy dissipations (1 - Ct) % are received for zero submerged depth in model of sloped steps model (M2) is 80 %.
- The minimum energy dissipation (1-Ct) % (maximum transmission coefficient is received for narrow rectangular model M5.

- the surface roughness of the breaker (steps sloped has a limited effect on the dispersion performance depending on the wave height and the submersible depth of the breaker.
- The non-uniformity of the steps located in front of the breakwater structure have oscillatory effect to the dissipation of incident wave energy based on submerged depth with a limited effect not exceeding wave height.
- Wave dissipations process goes through three stages, starting from the front of the breakwater with a distance not exceeding the wavelength, where the breaker begins to affect the behavior of the wave from this area, then when the wave reaches the breakwater body, the breaker acts as a barrier to the passage of the wave. The irregularity of the breaker surface (Roughness of surface), here it plays as an auxiliary factor for the dispersion of energy on the lateral slope and the upper breaker surface.

Part B: Case study Results

Given the limited amount of knowledge on numerical modelling of the wave field in lake or shallow reservoirs, the current study was conducted on plain sallow water depression of Najaf sea using the **MIKE21 SW** model.

- The amount of variation between the simulated wave heights and those calculated using an empirical equation is less than 9%. As a result, the MIKE21 SW model can simulate wind-generated waves in simple sallow water lakes.
- **3** scenarios were tested for the best location of the breaker according to the topography of the study area. The first scenario was the best in terms of the extent of the impact on the largest area and longest shore line protection according to transmission coefficient Ct behind the breaker.

- In the simulation, three of breakwaters with a variety of settings for their orientation and placement were used. The results of **Scheme 1 Figure (6.24)** indicated that it was the most successful at reducing the wave height and covered the most area (1.19 km2) along the coast line of the target region. The findings make it abundantly evident that waves breaking close to shore are greatly influenced by bathymetric data. This highlights how important it is to have good bathymetric measurements of the waters near the beach.
- It is also noticeable that the best scenario of the breaker is achieved when the wave direction (315^{o}) is perpendicular to the axis of the breaker (315^{o}- 90^{o}).
- The best cross-section of the breaker was achieved by the **MD1** and **MD2** figure (6.28) and (6.29) models and the criterion in the measurement was the amount of energy dispersion (1-Ct) equal to 80 %. In both models, there were two main parts in the dispersion process, the first is the upper part of the breaker, which acts as a stilling Basin, and the second is the progressive front part of the breaker, which works to create a turbulent environment for the incident wave before it reaches the breaker.
- In summary, based on the analysis of wave characteristics and the variation of wave parameters at specific points ($P_{1\text{-}8}$) of interest, it is evident that the implementation of the proposed project would result in a considerable reduction in wave height behind the breakwater compared to the pre-project conditions. Furthermore, Scheme 1 exhibits a more pronounced enhancement in wave conditions.

7.2 Recommendation for Further Studies

For the scientific benefit of future researchers, the following are some points that can be adopted.

- It is possible to test a new type of Breakwater, namely floating Breakwater, which provide a healthier environment in the seas by not separating the movement between the front of the breaker and its rear.
- Air barriers, also one of the new topics on the dispersion of energy by Breakwaters through making the air babbles as a turbulence maker.
- The study area is exposed to a lot of flood waves resulting from the recharging of the underground basins surrounding the area, it is possible that the study will be more comprehensive by introducing hydrological variables in the study.

References

References

- A.V. Mahalingaiah, B. R. Tayade, N. V. Gokhale, M. D. Kudale; Design of Submerged Offshore Reefs for the Coastal Protection Measures. Science Direct, Aquatic Procedia, Elsevier Journal Publication, ISSN: 2214-241X, Volume 4, pp. 198-205, March 2015. https://doi.org/10.1016/j.aqpro.2015.02.027
- Abdul Khader, M. Ii, and S. P. Rai. "A study of submerged breakwaters." Journal of Hydraulic Research 18, no. 2 (1980): 113-121. https://doi.org/10.1080/00221688009499555
- Ali Mohsen Hayder, (2020). "Modeling of Stream Flow and Sediment Yield for Some Watersheds of Tigris and Euphrates Rivers by Using SWAT". Ph.D. Thesis, University of Technology. (unpublished).
- ANSYS. Fluent, "Ansys fluent theory guide 17.0," Inc, Canonsburg, PA, 2015.
- ANSYS, Inc. ANSYS FLUENT. Release 20.0: Theory guide
- ANSYS. ANSYS FLUENT 16.0 Meshing Help. ANSYS Inc., release 12.1 editions, November 2018c.
- AW the Arab weekly, E-Internet Page Site (2020) http://theaeabweekly.com/ieaq-eyes-economic-dividends-monumental-breakwater-faw-port.
- Ayat, B., 2013. Wave power atlas of eastern media terranean and Aegean seas. Energy 54, 251e262. https://doi.org/10.1016/j.energy.2013.02.060
- Battjes, J. A. (1974). Surf similarity. In *Coastal Engineering 1974* (pp. 466-480). https://doi.org/10.1061/9780872621138.029

- Bi, F., Song, J., Wu, K., Xu, Y., 2015. Evaluation of the simulation capability of the WaveWatch III model for Pacific Ocean wave. Acta Oceanol. Sin. 34(9), 43e57. https://doi.org/10.1007/s13131-015-0737-1
- Board, B. E. (1940). *A model study of the effect of submerged breakwaters on wave action*. Tech. Memo. 1.
- Bilici, Ç. (2014). "A model study on wave transmission through pile breakwaters "A thesis submitted to the graduate schools of natural and applied science of middle east technical university. https://doi.org/10.9753/icce.v34.posters.18
- Buckler, W.R., Winters, H.A. (1983), Lake Michigan bluff recession. Annals of the Association of American Geographers, 73(1), 89-110. https://doi.org/10.1111/j.1467-8306.1983.tb01398.x
- Chanson, H. (2004). Hydraulics of open channel flow. Book Elsevier.
- Seabrook S. R. and Hall K. R., "Wave Transmission at Submerged Rubble Mound Breakwaters", COASTAL ENGINEERING, CHAPTER, (1998).
- Suh, K.D., Jung, H.Y., Pyun, C.K., 2007. Wave reflection and transmission by curtainwall-pile breakwaters using circular piles. Ocean Eng. 34(14e15), 2100e2106. https://doi.org/10.1016/j.oceaneng.2007.02.007
- Dean, R. G., & Dalrymple, R. A. (1991). Water wave mechanics for engineers and scientists (Vol. 2). world scientific publishing company. https://doi.org/10.1142/1232
- Dean, Robert G., and Robert A. Dalrymple. Water wave mechanics for engineers and scientists. Vol. 2. world scientific publishing company, 1991. https://doi.org/10.1142/1232

- DHI, M. (2017). MIKE 21 Spectral Wave Module, Scientific Documentation. Hørsholm, Denmark: DHI Water Environment Health.
- Dick T. M., and Brebner A., "Solid and Permeable Submerged Breakwaters", COASTAL ENGINEERING, CHAPTER 72, (1968). https://doi.org/10.9753/icce.v11.72
- Dick, T. Milne, and A. Brebner. "Solid and permeable submerged breakwaters." In Coastal Engineering 1968, pp. 1141-1158. 1968. https://doi.org/10.1061/9780872620131.072
- Douglass S. L. and Krolak J., "Highways in The Coastal Environment", Hydraulic Engineering Circular 25, Second Edition, department of Civil Engineering University of South Alabama 307 University Boulevard Mobile, Alabama 36688, (2008).
- Duan, X.; Mao, P.; Mao, C. Research on the status of seawall along the southeast coast (Fujian Province). Ocean. Eng. 1996, 14, 41–49. (In Chinese). https://doi.org/10.3390/jmse10121809
- Farhan, A. A., & Abed, B. S. (2021). Estimation of surface runoff to Bahr Al-Najaf. Journal of Engineering, 27(9), 51–63 https://doi.org/10.31026/j.eng.2021.09.05
- G. Jarlan, "A Perforated Vertical Wall Breakwater," The Dock and Harbour Authority, vol. 41, no. 486, pp. 394-398, 1961
- Garrison, Tom S. *Essentials of oceanography*. Fifth Edition Cengage Learning, 2014.
- Goda, Y. and Suzuki, Y. (1976). Estimation of incident and reflected waves in random wave experiments. Proc. 15th Int. Conf. Coastal Engineering, Hawaii. https://doi.org/10.9753/icce.v15.47

- Gou, He, Feng Luo, Ruijie Li, Xiaotian Dong, and Yifeng Zhang. "Modeling study on the hydrodynamic environmental impact caused by the sea for regional construction near the Yanwo Island in Zhoushan, China." *Water* 11, no. 8 (2019): 1674.
- Gomes, A., Pinho, J. L., Valente, T., Antunes do Carmo, J. S., & V. Hegde, A. (2020). Performance assessment of a semi-circular breakwater through CFD modelling. *Journal of Marine Science and Engineering*, *8*(3), 226. https://doi.org/10.3390/jmse8030226
- Hara M., Yasuda T. and Sakakibara Y., "Characteristics of A Solitary Wave Breaking Caused by A Submerged Obstacle", COASTAL ENGINEERING, CHAPTER 18, (1991). https://doi.org/10.1061/9780872627765.072
- Harris, Lucy. "MPM study of water wave interaction with porous seawalls." PhD diss., University of Cambridge, 2020.
- Hanson, J. L., & Jensen, R. E. (2004, November). Wave system diagnostics for numerical wave models. In 8th International Workshop on Wave Hindcasting and Forecasting, Oahu, Hawaii (pp. 231-238).
- Hoque, M. A., Perrie, W., & Solomon, S. M. (2020). Application of SWAN model for storm generated wave simulation in the Canadian Beaufort Sea. *Journal of Ocean Engineering and Science*, *5*(1), 19-34.
- Holthuijsen, L.H. Waves in Oceanic and Coastal Waters, 1st ed.; Cambridge University Press: Cambridge, UK, 2010; 404p
- http://www.gebco.net/data_and_products/gridded_bathymetry_data/.
- https://apps.sentinel-hub.com/eo-browser.
- Hughes, S. A. (1993). Physical models and laboratory techniques in coastal engineering. Singapore; River Edge, NJ: World Scientific.

https://doi.org/10.1142/2154

- Itô, K., & Henry Jr, P. (1996). *Diffusion processes and their sample paths: Reprint of the 1974 edition*. Springer Science & Business Media. https://doi.org/10.1007/978-3-642-62025-6
- Mettam, J. D., & Berry, J. G. (1982). Factors of safety for the design of breakwaters. In *Coastal Engineering 1982* (pp. 2097-2106). https://doi.org/10.1061/9780872623736.125
- Mathewson, P. R. (2011). The evaluation of shore protection structures used for erosion control at Lake Pukaki, New Zealand.
- Kamphuis, J. W. (2020). Introduction to coastal engineering and management (Vol. 48). World Scientific. https://doi.org/10.1142/11491
- Komar, P.D. Beach Processes and Sedimentation, 2nd ed.; Prentice Hall: Upper Saddle River, NJ, USA, 1998; 544p.
- Krogstad, H. E., Arntsen, o. A., 2003. Linear Wave description and Theory. Norwegian University of Science and Technology.
- Le Méhauté, B., & Le Méhauté, B. (1976). An introduction to water waves. An introduction to hydrodynamics and water waves, 197-211. https://doi.org/10.1007/978-3-642-85567-2_15
- Li, J.F., Qi, Y.X., Sun, J., 2006. The primary discussion on calculation method of reservoir crest super elevation in the plain area. J. Northwest Hydroelectric. Power 22(5), 41e43 (in Chinese).
- Li, Y., Huang, Z., Zhang, J.F., Wu, W.J., Zhang, C.F., Zhao, Q.F., 2014. Application and verification of sea wave forecast by WAVEWATCH III model in the Bohai Sea of China. J. Meteorol. Environ. 30(1), 23e29 (in Chinese). https://doi.org/10.3969/j.issn.1673-503X.2014.01.004.

- Lin, P. (2008). Numerical modeling of water waves. CRC Press. Taylor & Francis Routledge
- Liu, P.-F., Lin, P., Chang, K.-A., and Sakakiyama, T. (1999). Numerical modeling of wave interaction with porous structures. Journal of Waterway, Port, Coastal and Ocean Engineering, 125(6):322–330 https://doi.org/10.1061/(ASCE)0733-950X(1999)125:6(322)
- Mathewson, P. R. (2011). The evaluation of shore protection structures used for erosion control at Lake Pukaki, New Zealand. MSC thesis. Department of Geography University of Canterbury.
- Mc.Feeters, S. K. (1996). The use of the Normalized Difference Water Index (NDWI) in the delineation of open water features. International journal of remote sensing, 17(7), 1425-1432.
- Mettam, J. D., & Berry, J. G. (1982). Factors of safety for the design of breakwaters. In *Coastal Engineering 1982* (pp. 2097-2106). https://doi.org/10.1061/9780872623736.125
- Noujas, V., Thomas, K.V., Ajeesh, N.R., 2017. (Shoreline management plan for a protected but eroding coast along the southwest coast of India). J. Sediment. Res. 32, 495e505. https://doi.org/10.1016/j.ijsrc.2017.02.004
- Novak P., Guinot V., Jeffrey A. and Reeve D. E., "Hydraulic Modelling an Introduction", Principles, methods and applications, ISBN 0-203-86162-0, Taylor & Francis e-Library, (2010).
- Omran, H. A., Mahmood, M. S., & Abbas, A. (2014). Quantity and Distribution of The Current Sur-Face and Ground Water Resources in Bahr An-Najaf In Iraq.

- Rafael E. Vasquez1, Carl D. Crane, I., Correa, J. C., 2014. Analysis of a planar tensegrity mechanism for ocean wave energy harvesting. journal of mechanics and robotics 6 (3), 12. https://doi.org/10.1115/1.4027703
- Roelvink, D., Reniers, A., 2012. A guide to modeling Coastal Morphology. World Scientific. https://doi.org/10.1142/7712
- Reniers, A. J. H. M., Ranasinghe, R. W. M. R. J. B., Roelvink, J. A., & Ruessink, B. G. (2012). On bar growth and decay during interannual net offshore migration. *Coastal Engineering*, *60*, 190-200. https://doi.org/10.1016/j.coastaleng.2011.10.002
- Rusu, E. Strategies in using numerical wave models in ocean/coastal applications. J. Mar. Sci. Technol.-Taiwan. 2011, 19, pp. 58–73. https://doi.org/10.51400/2709-6998.2138
- R. G. Dean and R. A. Dalrymple, Water wave mechanics for engineers and scientists. World Scientific Publishing Company, 1991, vol. 2.
- Ringe, S. (2020). Designing of One Directional Wave Tank. project report, Uppsala University.
- Sakakiyama, T. and Liu, P. L. F. (2001). Laboratory experiments for wave motions and turbulence flows in front of a breakwater. Coastal Engineering, pages 117–139. https://doi.org/10.1016/S0378-3839(01)00027-8
- Stucky, A., Bonnard, D. (1937). Contribution to the experimental study of marine rock fill dikes. *Bull. Technique de la Suizze Romande*.
- Takahashi, Shigeo. "Design of vertical breakwaters." PHRI reference document nr. 34 (2002).

- Van Der Meer J. W. and Daemen I. F. R., "Stability and Wave Transmission at Low-Crested Rubble-Mound Structures", J. Waterway, Port, Coastal, Ocean Eng. 120:1-19, (1994). https://doi.org/10.1061/(ASCE)0733-950X(1994)120:1(1)
- Weggel J. R., "Maximum Breaker Height for Design", COASTAL ENGINEERING, CHAPTER 21, (1972). https://doi.org/10.9753/icce.v13.21
- Wang, S.; Li, R.; Ji, M.; Dong, X.; Zhu, W. Combined application of SWAN and CGWAVE model in calculation of design wave parameters. J. Waterw. Harb. 2015, 4, 308–312.
- Xiana, Fu, Z., Meng, Y., Zhang, K., & Cheng, Z. (2019). Analysis of wave clipping effects of plain reservoir artificial islands based on MIKE21 SW model. Water Science and Engineering, 12(3), 179–187. https://doi.org/10.1016/j.wse.2019.08.002
- Yan Xiang, Zhi-min Fu, Ying Meng, Kai Zhang, Zheng-fei Cheng. (2019). Analysis of wave clipping effects of plain reservoir artificial islands based on MIKE21 SW model. Water Science and Engineering 2019, 12(3): 179e187. https://doi.org/10.1016/j.wse.2019.08.002
- Yang, X.C., Zhang, Q.H., 2013. Joint probability distribution of winds and waves from wave simulation of 20 years (1989-2008) in Bohai Bay. Water Sci. Eng. 6(3), 296e307.
- Yuwono N, Sriyana I. Wave Transmission and Energy Dissipation in a Box Culvert-Type Slotted Breakwater. Advances in Technology Innovation. 2022 Aug 5;7(4):270. https://doi.org/10.46604/aiti.2022.9080

- Zhang, W. Study on the Suspension Flux of Substance in Nearshore and Its Application in Jiangsu Sea Area. Ph.D. Thesis, Hohai University, Nanjing, China, June 2013.
- Zheng, D.X., Zhou, R.X., Jin, R.Q., Zheng, L., 2009. Discussion on the calculation method of plain reservoir wave run-up. Yellow River 3, 86e87 (in Chinese).
- Miles, J. W. (1962). Transient gravity wave response to an oscillating pressure. *Journal of Fluid Mechanics*, *13*(1), 145-150.
  https://www.usgs.gov/landsat-missions/landsat-8

Appendix-A

(UDF)

Appendix-A

Ansys Fluent Solver (UDF)

In this appendix, the C++ program language are used to defined UDF (user define function) to described the flap type motion of wave maker motors.

Note that: this code is repeated for each run according to specific water depth in flume e.g. (0.22 ,0.25, 0.27, 0.3)

Appendix A. UDF Code

Code made for wavemaker in Microsoft Visual.

```
include "udf.h"
#include "dynamesh_tools.h"

static real period = 1;
static real amplitude = 2;
static real pi = 3.14159265358979323846;
static real depth = 0.22;

DEFINE_CG_MOTION(oscillate,dt,vel,omega,time,dtime)
{
        /* define the variables */
        Thread *t;
        face_t f;
        real dv, ang_freq;
        NV_S(vel, =, 0.0);
        NV_S(omega, =, 0.0);

/* get the thread pointer for which this motion is defined */
        t = DT_THREAD(dt);
        ang_freq = 2 * pi / period;

/* loop over each face in the zone to create an array of data */
        begin_f_loop(f,t)
        {
                /* set x-component of velocity */
                omega[1] = amplitude * cos(ang_freq * time) ;
        }
        end_f_loop(f,t)

        Message("time = %f, x_vel = %f\n", time, omega[1]);
}
```

المستخلص

الأمواج الناتجة من الرياح هي الأكثر شيوعا بالمقارنة مع مصادر الامواج الاخرى في البحار. بالنظر إلى محدودية المعرفة في مجال النمذجة الرياضية للامواج التي تسببها الرياح في المياه الضحلة او البحيرات،وكونها محل اهتمام الباحثين. تم دراسة هذا النوع من الامواج وكيفية تشكلها في منطقة منخفض بحر النجف كحالة دراسية بالاظافة الى بعض الخصائص الاخرى الخاصة الامواج المتولدة نتيجة للرياح .

تم اعتماد نموذج رياضي عددي غير منتظم التقسيم لدراسة خصائص الموجة المتولدة (MIKE21)، يعتمد هذا الموديل على قاعدة توازن الكتلة وتم توضيف هذا النموذج لايجاد افضل موقع لمشتتات الطاقة بالقرب من المنشات الحيوية التي تتاثر بارتفاع الموجة في منطقة الدراسة . ان مقدار الفرق مابين قيم ارتفاع الموجة الناتجة من الموديل الرياضي والمعادلات الوضعية كان اقل من 9% . ثلاثة سيناريوهات للكاسرتم اعتمادها لايجاد افضل موقع واتجاه للمنشأ.

اوضحت النتائج التي تم الحصول عليها تفاوتا بقيم ارتفاع الموجة العابرة وموقع الكاسر والمساحة التي يغطيها الكاسر تبعا للسيناريوهات الثلاثة المعتمدة في الدارسة . السيناريو الاول اعطى قيم للمساحة التي يغطيها الكاسر تقترب من 1.19 كم مربع ، السيناريو الثاني 0.889 كم مربع ، والثالث يغطي مساحة تقترب من 1.11 كم مربع . أظهرت هذه الدراسة أن ارتفاع الموجات في المنطقة الأمامية والخلفية للكاسرفي منطقة الدراسة وتبعا لنقاط محددة للقياس مابين 0.35 و 0.7 متر في المقدمة والمؤخرة للمنشأ. هذا يعني انخفاضًا بنسبة حوالي 40٪ إلى 60٪ بالمقارنة مع الأرتفاعات الأصلية التي كانت تتراوح بين 1.25 إلى 0.9 متر. جميع السيناريوهات المستخدمة جيدة إلى حد ما في تشتيت الطاقة عن طريق كسر النمط الوحيد للموجة بمعدلات قد تصل إلى 50٪ من ارتفاع الموجة الواصلة ، وكان السيناريو الأول هو الأفضل والأكثر كفاءة من حيث تشتيت الطاقة.

من جهة اخرى ، تم دراسة الأداء الهيدروليكي لشكل جديد من الكواسر من خلال دراسة مختبرية مدعومة بنموذج رياضي رقمي CFD لفحص أشكال النماذج المختلفة اعتمادًا على معامل الموجة العابرة Ct. تم تحديد نمط موجات مختلفة من خلال ملف UDF لنموذج CFD لتثبيت الموجة القادمة Hi بنفس الخصائص. تم دراسة أداء الكاسر المختلفة على أساس تشتيت الطاقة من خلال اختبار نماذج مختلفة تحت ظروف موجات مختلفة وعمق الماء والعمق الغاطس النسبي. أظهرت نتائج هذه الدراسة ايظا أن معامل الانتقال يزداد مع زيادة ارتفاع الموجة المندفعة لجميع أنواع نماذج الكاسر، وبالنسبة لجميع نماذج الأرصفة، يزداد ارتفاع موجة

الانتقال (Ht) مع زيادة العمق الغاطس النسبي (Hs/Hi). تم تسجيل أعلى قيمة لتشتيت الطاقة (Ct - 1)% لعمق غاطس صفري في نموذج تدرج مائل بالرمز(M2) وهي 80%. تم اعتماد برنامج Ansys Fluent لنمذجة موجة ثابته الخصائص مع شبكة ديناميكية لتمثيل نوع حركة االرياح لتوليد الموجات. تلعب الشواطئ الرقمية دورًا مهمًا في نموذج CFD لمنع انعكاس الموجة في الجانب الآخر من الحاجز وتمثيل الشاطئ رياضيا لمحاكاة واقع الظاهرة الفعلي . تم اختيار 240 شبكة لكل طول موجة للحصول على حل مستقر والحصول على نتائج مقبولة مقارنة بالتجربة.

.

جمهورية العراق
وزارة التعليم العالي والبحث العلمي
جامعة بابل
كلية الهندسة
قسم الهندسة المدنية

منشآت تشتيت الأمواج السطحية ، حالة تطبيقية، بحر النجف وسط العراق

إطروحة
مقدمة الى كلية الهندسة / جامعة بابل
وهي جزء من متطلبات نيل درجة الدكتوراه فلسفة في الهندسة / الهندسة المدنية / موارد مائية

من قبل
عدي عبد الصاحب محمد حسن الطرفي

بإشراف
أ. د. عبد الحسن خضير الشكر

1445 هـ

2023 م